UNIVERSITY OF OKLAHOMA

GRADUATE COLLEGE

EVALUATION OF HOLLOW-CORE-FRP-CONCRETE-STEEL COLUMN AND FOOTING CONNECTION

A THESIS

SUBMITTED TO THE GRADUATE FACULTY

in partial fulfillment of the requirements for the

Degree of

MASTER OF SCIENCE

By

OMAR YADAK

Norman, Oklahoma

2024

EVALUATION OF HOLLOW-CORE-FRP-CONCRETE-STEEL COLUMN AND FOOTING CONNECTION

A THESIS APPROVED FOR THE
SCHOOL OF CIVIL ENGINEERING AND ENVIRONMENTAL SCIENCE

BY THE COMMITTEE CONSISTING OF

Dr. Royce W. Floyd, Chair

Dr. Jeffery S. Volz

Dr. P. Scott Harvey

Acknowledgment

I would like to express my gratitude and deep appreciation to my advisor Dr. Floyd for his continuous support, patience and guidance throughout my master's research. I have gained a lot of knowledge and understanding of best practices in research conduction, especially in experimental research and data analysis. I am certainly grateful for the privilege of learning and fostering my growth as a researcher from such a dedicated mentor like Dr. Floyd, and the way he inspired me to continue further and pursue my Ph.D.

I want to thank the rest of my committee members, Dr. Jeffery Volz and Dr. Scott Harvey, for their feedback and contributions to improve the thesis. I also would like to thank our Fears Lab manager John Bullock for his dedication and help with building my specimens.

During my research, I had the opportunity to work with incredible fellow graduate and undergraduate students who helped me complete my research including Zach Tiry, Bruno Siri, Jake Choate, Dip Banik, Mujtaba Ahmadi, Dylan Becerra, Cade Harris, Steve Roswurm, Jacob Starks, and Jackson Milner.

Last but not least, I truly appreciate my family and friends for their continuous support and even for their help in lab sometimes throughout my master's research. They made it possible to complete my degree and I am extremely grateful to all of them.

Abstract

Accelerated bridge construction (ABC) has recently gained popularity among state departments of transportation to minimize construction costs, time and waste, and optimize the use of materials. This research focused on the connection details between hollow-core fiber-reinforced polymer-concrete-steel columns (HC-FCS) and their foundations. The column consists of a concrete core sandwiched between an outer fiber-reinforced polymer (FRP) tube and an inner steel tube. Two foundation anchorage details were tested with multiple embedment lengths into the footing to evaluate the connection's capability to transfer axial load and bending moment and achieve the ultimate column flexural and shear capacities. Seven column-footing specimens were cast and tested to failure to study the effect of embedment length, diameter-to-thickness ratio, compressive strength of the concrete footing, and end-of-column anchorage on monolithically cast connection capacity. Two specimens utilizing a socketed connection filled with ultra-high-performance concrete (UHPC) designed to represent connection of precast elements were cast and tested to failure. The specimens were designed to be tested as a simply supported beam using a typical load frame by constructing each 2 ft by 2 ft by 4 ft-1 in. footing with a column portion embedded at the desired embedment length at each end of the footing. The column portion of the specimen was in the form of only a steel tube. An 8.625 in. diameter steel pipe with a thickness of 0.219 in. was used for eight specimens, while a 6.625 in. diameter steel pipe with a thickness of 0.25 in. was used for one specimen. Embedment length had a significant effect on the performance of the column-footing connection. The short embedment lengths tested ($1.6D_i$ and $1.68D_i$) were not sufficient to develop the steel pipe flexural strength for the monolithic connection specimens with a normal-strength concrete footing. However, the use of socketed connection with UHPC, high-strength concrete footing, and welding a series of lugs to the embedded pipe prevented the steel

pipe from pulling out to some extent, and local buckling occurred in the steel pipe at a moment greater than the calculated capacity of the steel pipe with an embedment length of $1.6D_i$. The $1.8D_i$ embedment length prevented the steel pipe from pulling out whether using the socketed connection with UHPC, high-strength concrete, or normal-strength concrete. The specimens with this longer embedment length failed after exceeding the flexural strength of the steel pipe, and local buckling occurred in the steel pipe. This suggests that the column-footing connection with a $1.8D_i$ embedment length is potentially sufficient to achieve the flexural strength capacity of the steel pipe.

Table of Contents

List of Figures

List of Tables

1. Introduction

1.1 Background

The Federal Highway Administration (FHWA) and state Departments of Transportation (DOTs) have and are currently sponsoring research studies for new techniques and designs related to Accelerated Bridge Construction (ABC). ABC has several advantages over traditional construction as it reduces the delivery time of a project, provides a safer work zone, and reduces interruption of traffic flow (ElGawady, 2018). While there are many ABC techniques available for bridge superstructures, there are limited techniques for bridge substructures. The best technique to accelerate construction of substructure elements is using precast bridge piers or columns.

Several precast column designs are used for ABC purposes. Some of these include Concrete-Filled Steel Tubes (CFSTs), Concrete-Filled Fiber-reinforced polymer Tubes (CFFTs), and hollow-core concrete columns. Concrete-Filled Tubes (CFTs) generally tend to provide more strength-to-size efficiency and fast construction. Such columns consist of a hollow steel tube or fiber-reinforced polymer (FRP) tube filled with concrete (Stephens et al., 2015).

One of the most recent column designs is a Hollow-Core FRP Concrete Steel (HC-FCS) column or FRP-Concrete-Steel Double-Skin Tubular column. In this thesis, it will be referred to as HC-FCS. This design includes an outer FRP tube and an inner steel tube acting as stay-in-place formwork, and concrete is added between them, creating a concrete shell. HC-FCS columns use 60% - 70% less material than CFT columns and provide better confinement for the concrete (ElGawady, 2018). Most research studies have shown superior behavior of this column design in terms of ductility, flexural strength, and energy absorption compared to the other currently used columns (Teng et al., 2007; Lu Han, 2010; Zhang, 2012; Albitar et al., 2015).

The HC-FCS column design has been investigated for regions susceptible to earthquakes, as the design meets the ductility demands for bridge piers and columns. To meet the higher ductility demand, the design and construction of the column-footing connection for HC-FCS precast columns are crucial. The connection must achieve the strength of HC-FCS columns to ensure the ultimate strength is controlled by the column, provide pullout and slip resistance, and be economical and easy to construct for ABC purposes (ElGawady, 2018).

Previous studies have examined multiple anchorage details for the footing-column connection of conventional and CFST columns, including monolithic, pocket connection, post-tensioning system, and socket connection designs (Moon, 2013; Pentelides and Neupane, 2022). These studies have highlighted the advantages of each connection in developing the required strength of the columns. Several parameters have been investigated, such as the embedment length of the column into the footing, the diameter-to-thickness ratio of the steel tube, the footing compressive strength, and the shear reinforcement of the footing (Moon, 2013; Pantelides and Neupane, 2022).

Recent studies by ElGawady investigated two types of footing-column connection for HC-FCS columns. The results showed that the socket connection develops the full plastic flexural capacity of the column and provides better ductility and energy dissipation compared with the monolithic connection (ElGawady, et al., 2015; ElGawady, et al., 2018).

The research described in this thesis examined connection details between HC-FCS columns and footings to develop foundation anchorage details and find the best embedment length for connecting the column to the footing. The embedment length of the steel tube is crucial to provide the ultimate flexural and shear capacities of HC-FCS columns.

1.2 Objectives and Goal

The overall goal of the research described in this thesis was to develop design procedures and recommendations for HC-FCS column-footing connection. Progress toward this goal was made through three objectives:

i) Evaluate the effect of inner steel tube thicknesses and embedment lengths on the column-footing connection performance.

ii) Identify the required embedment length to achieve the ultimate flexural capacity and shear capacity of the HC-FCS column.

iii) Evaluate the effect of the footing compressive strength concrete and the use of a socket connection with Ultra-High-Performance-Concrete (UHPC) to develop full capacity of the HC-FCS column.

2. Literature Review

2.1 Hollow-Core FRP Concrete-Steel (HC-FCS) Columns

Fiber Reinforced Polymer (FRP) has become more commonly used in the civil engineering industry due to its pronounced advantages in recent decades. It offers excellent strength and superior corrosion resistance when compared to steel. Teng et al. (2007) proposed an innovative column design that incorporates steel, concrete, and FRP, with the concrete core sandwiched between an outer FRP tube and an inner steel tube. This design leverages the strengths of the three materials, resulting in a structural element with significantly greater strength capacity than concrete-filled double-skin steel tubular columns, as suggested by Han (2010). The double-skin steel column has an outer hollow steel tube, an inner hollow steel tube, and concrete is filled in between the tubes. Figure 1 shows a general cross-section view of HC-FCS columns.

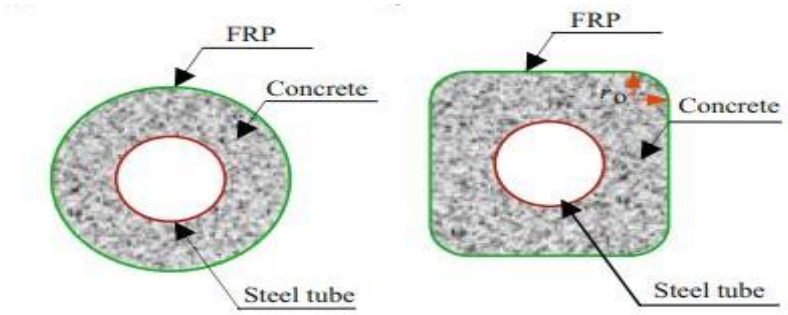

(a) (b)

Figure 1. Cross-section view of (a) circular and (b) square HC-FCS columns (Han, 2010)

Several studies investigated a series of HC-FCS specimens to compare performance of the column design relative to other column types. Han (2010) constructed four circular and four square HC-FCS columns, as shown in Figure 1. All specimens were tested under combined axial load and cyclic lateral load. The cyclic lateral load was applied in the middle of the specimens, and the ends

of each specimen were attached to cylindrical bearings. Figure 2 shows the testing setup used by Han (2010).

Figure 2. Testing setup arrangement used by Han (2010)

The results of these tests showed that HC-FCS columns demonstrated high energy dissipation, and an increase in the number of FRP layers improved the ultimate strength of the column. However, further investigation was suggested to carry out a parametric study and better understand each component of HC-FCS columns (Han, 2010).

Idris and Ozbakkaloglu (2014) investigated the effect of six parameters on the behavior of HC-FCS columns: axial load, concrete strength, the amount of confinement, type of fiber, inner steel tube thickness, and filling the inner steel tube with concrete (Idris and Ozbakkaloglu, 2014). Figure 3 shows a cross-section view of the specimens tested by Idris and Ozbakkaloglu (2014), and Figure 4 shows the side view of the specimens.

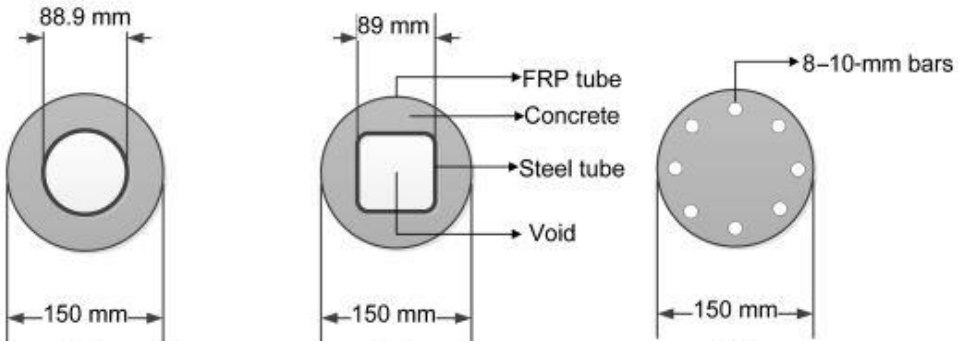

Figure 3. Cross-section view of (a) circular HC-FCS, (b) square HC-FCS, and (c) CFFT columns (Idris and Ozbakkaloglu, 2014)

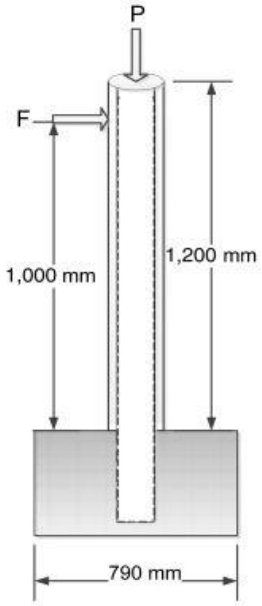

Figure 4. Side view of HC-FCS columns tested by Idris and Ozbakkaloglu (2014)

The test was conducted by applying a combined axial load with cyclic lateral load similar to testing by Han (2010). Increasing the amount of confinement increased the lateral drift capacity, whereas concrete strength and inner steel thickness did not have a significant effect on the lateral drift capacity of the column (Idris and Ozbakkaloglu, 2014).

2.2 Foundation Connections for Circular Concrete-Filled Steel Tubes (CFSTs)

Moon (2013) examined column-footing connections for CFST columns to develop full capacity and avoid pullout of the column from footing. He proposed two connection methods to achieve ultimate ductility in seismic regions while ensuring simplicity and cost-effectiveness for CFST columns. Moon (2013) investigated both direct and recessed connection approaches. The recessed connection involved isolating the reinforcement of the footing from the steel tube using a corrugated steel pipe (CSP) with a larger diameter than the steel pipe. The CSP was removed after casting the footing, and the column was placed. Then, the gap between the footing and the steel tube was filled with high-strength grout. The monolithic connection approach involved anchoring the column to the footing using an annular ring welded to the end of the steel tube, and the footing and column were cast simultaneously (Moon, 2013). Figure 5 illustrates the two types of connections.

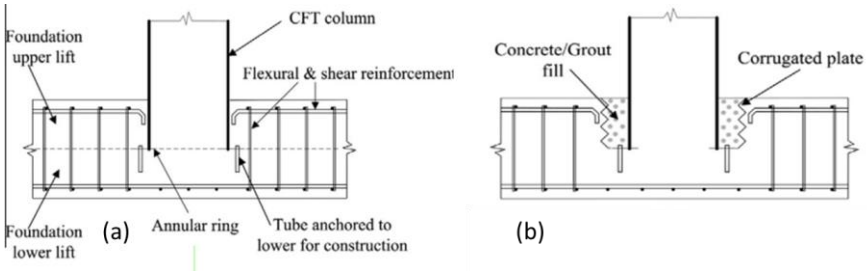

(a) (b)

Figure 5. Footing-column (a) monolithic and (b) socket connections (Moon, 2013)

A series of CFST specimens constructed with a monolithic connection was experimentally tested by evaluating several parameters such as embedment length and shear reinforcement ratio. These specimens were also analyzed with a finite element model to compare the test values with the theoretical ones (Moon, 2013). Table 1 shows the parameters examined for the test specimens.

Table 1. Properties of Specimens Tested by Moon (2013)

Test Specimen	Study Parameter	L_e/D	$f'_{c,CFT}$ (MPa/ksi)	$f'_{c,FT}$ (MPa/ksi)	f_y (MPa/ksi)	f_u (MPa/ksi)
K1	No shear reinforcement	0.6	75.8/11	75.8/11	525.7/76.3	602.2/87.4
K2	Shear reinforcement	0.6	75.8/11	75.8/11	525.7/76.3	602.2/87.4
K3	Embedment depth	0.9	71/10.3	71/10.3	525.7/76.3	602.2/87.4
1-50	Straight welded tube	0.8	59.9/8.7	75.8/11	337.6/49	413.4/60
4-50	Spiral welded tube	0.8	59.3/8.6	74.4/10.8	351.4/51	537.4/78

In order to further investigate the effect of embedment length and other crucial parameters, 56 specimen models were designed to evaluate several parameters by using non-linear finite element analysis of the monolithic connection. The parameters included annular ring size, embedment length, shear reinforcement ratio, concrete compressive strength of the footing, and steel tube diameter-to-thickness ratio. Those parameters were studied to analyze the effect of each one on the connection between the footing and column and understand the behavior of this type of connection (Moon, 2013). Figure 6 shows the components of the finite element model used for each specimen.

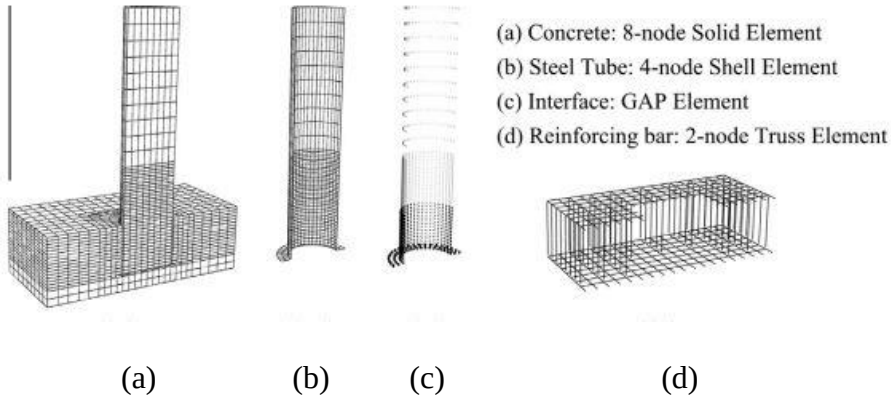

Figure 6. Components of finite element model of specimens examined by Moon (2013)

Two failure modes were observed in this study. Pullout failure occurred when the footing failed to confine the column, and the steel tube slipped out from the footing. Column buckling occurred when the column exceeded its flexural capacity and failed near the interface surface between the column and footing (Moon, 2013). Figure 7 shows the simulation results for the finite element models.

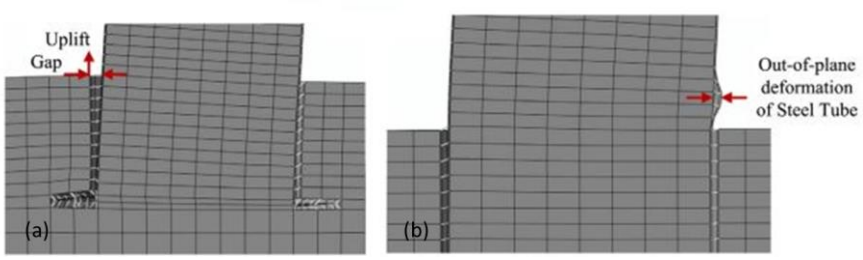

(a) (b)

Figure 7. Finite element model results for (a) pullout failure and (b) column buckling failure (Moon, 2013)

The results showed the significance of those parameters indicated in Table 1 in the connection design to transfer the full deformation demands from column loading to the footing. The embedment depth of the steel tube had the largest effect on the footing-column connection. Two embedment length equations were derived as a function of steel tube diameter and thickness and footing concrete compressive strength based on the finite element analysis and the seismic demands for the studied region (Moon, 2013). Equation 2.2.1 is for low and moderate seismic regions and Equation 2.2.2 is for high seismic regions.

$$\frac{D_i t_s f_u}{l_e^2 + D_i l_e} \leq 0.6\sqrt{f'_{c,FT}}\ MPa \quad (7.2\sqrt{f'_{c,FT}}\ psi) \qquad (2.2.1)$$

$$\frac{D_i t_s f_u}{l_e^2 + D_i l_e} \leq 0.55\sqrt{f'_{c,FT}}\ MPa \quad (6.6\sqrt{f'_{c,FT}}\ psi) \qquad (2.2.2)$$

In these equations, D_i is the steel tube diameter, t_s is the thickness of the steel tube, f_u is the ultimate yielding strength of steel tube, l_e is the embedment length, $f'_{c,FT}$ is the compressive strength of footing.

2.3 Ultra-High Performance Concrete as a Structural and Connection Material

Ultra-High Performance-Concrete (UHPC) is an advanced cementitious composite material with high durability and strength properties exceeding those of conventional concrete. UHPC was developed in the late 20th century and is a product of advancements in superplasticizers, fiber reinforcement, supplementary cementitious materials, and optimized gradation of dry materials (Graybeal 2014). The Federal Highway Administration (FHWA) defines UHPC as a material with compressive strength above 17.5 ksi (124 MPa), pre-and post-cracking tensile strengths above 0.75 ksi (5 MPa), and enhanced durability resulting from its discontinuous pore structure (FHWA, 2022). UHPC has been used in a wide range of structural applications as a material and connection material, including bridge deck connection joints, bridge expansion joints, bridge overlays, precast concrete elements, and high-rise buildings. The combination of strength and durability of UHPC makes it desirable for structural element optimization (Graybeal, 2011).

Multiple research studies have shown that UHPC develops excellent bond with reinforcement and conventional concrete. FHWA (2014) investigated the bond behavior of UHPC with reinforcing rebars. The effect of embedment length, concrete cover, bar spacing, and bar size was studied over 200 direct tension pullout tests. The development length of embedded reinforcing rebars in UHPC can be decreased due to its superior mechanical properties (FHWA, 2014). Soliman (2023) investigated the bond behavior of three UHPC materials. They had different tensile strength properties based on the composition of the cementitious materials in their mix designs. Rebar pullout specimens were tested to evaluate the bond strength between UHPCs and Grade 60 No. 4

reinforcing bars. All specimens demonstrated superior bond strength with a drastic decrease in the development length compared with the conventional concrete bond strength with its required development length (Soliman, 2023). Another study by Alkaysi (2017) investigated factors that affected the bond strength of non-proprietary UHPC with steel reinforcement. These factors include steel fiber content in the UHPC matrix, embedment length of reinforcing bars, and early age characteristics of UHPC (Alkaysi, 2017).

Besides studying the bond strength of UHPC with steel reinforcement, several studies investigated the bond strength between conventional concrete and UHPC in order to use UHPC as a repair material. Valikhani (2019) tested thirty specimens under a bi-surface shear test to evaluate the bond between UHPC and a substrate made of conventional concrete. He studied several parameters, such as substrate roughness degree, mechanical connectors, and bonding agents (Valikhani, 2019). Concrete substrate repaired with UHPC was two times stronger compared to concrete substrate repaired with conventional concrete from literature. The strength was achieved due to an adequate roughness degree of the substrate with and without mechanical connectors, and the failure mode was transferred to the substrate concrete, indicating sufficient bond between the materials (Valikhani, 2019). Due to UHPC's superior bond strength with conventional concrete and impermeability, it has been seen as an attractive material for bridge deck overlays and repair applications. The bond performance between UHPC and conventional concrete was found to be adequate for bridge overlays and other applications. Even though there were several factors investigated that could potentially affect the bond strength, the bond between the two materials was still sufficient to achieve the desired performance (Feng, 2022; Al-Madani, 2022; Munoz, 2013). According to FHWA (2023), UHPC has shown excellent performance in field-cast closure pour or grout material to connect several structural elements on site, especially for connecting

prefabricated elements in the field. Traditional connection solutions have hindered the use of prefabricated elements due to a lack of simplification of the system and/or concerns about long-term durability (FHWA, 2023). Several studies have investigated the durability and effectiveness of UHPC as a grouting material. UHPC has demonstrated its good bonding characteristics for repairing deterioration. Varbel (2020) conducted full-scale testing to evaluate the load-deflection behavior of channel girder assemblages after repairing deteriorated shear keys with UHPC. Results showed that UHPC bonded well with the girders even with minimal surface preparation (Varbel, 2020). UHPC grout and non-shrink grout had similar mechanical performance, however, the non-shrink grout began to deteriorate faster under cyclic loading. Fu (2022) also investigated UHPC as a grouting material but for splice sleeve joints. The results showed that UHPC was suitable to be used as grouting material and provided the required bond strength with the steel interface. This was attributed to the micro and fine particle components within the UHPC composite matrix (Fu, 2022).

2.4 Socket Connection

Multiple studies examined the use of a socket connection instead of a monolithic connection between columns and foundations due to its advantages in terms of durability and fast construction. ElGawady et al. (2018) investigated the seismic behavior of two large-scale HC-FCS columns with two different footing connections: monolithic connection and socket connection. One specimen was cast monolithically with an embedment depth of the column into the footing of $1.6D_i$. The specimen failed due to pullout of the steel tube, indicating insufficient embedment depth and was reused to create a socket connection. The steel tube, with a thickness of 0.25 in., was then reinserted into a newly constructed footing including CSP to create a socket. Another specimen was cast with a socket connection having the same embedment depth as the first socket connection

specimen but using a steel tube with a 0.5 in. thickness. The gap between the columns and sides of the socket for the specimens was filled using a high-strength grout (ElGawady, et al., 2018). The results showed that the column with a socket connection and 0.25 in. thick steel tube achieved the plastic capacity including yielding of the steel tube with minimal damage to the footing. However, the socket connection was not able to develop the ultimate capacity of the column for the 0.5 in. thick steel tube, and pullout failure occurred with severe damage to the footing (ElGawady, 2018).

Another study by Khaleghi (2012) investigated the advantages of a socket connection over monolithic connection method in terms of construction time and construction tolerance for the ABC method. As socket connections are typically used in precast bridge construction to connect precast elements, the study aimed to develop a socket connection that could provide the necessary strength and durability and be easily and quickly constructed on site. The study proposed systems for column-to-footing and column-to-beam connections for ABC and was implemented in Washington. At the base, the column was connected to a spread footing using a socket connection, while at the top, it was connected to the cap beam using bars grouted in ducts (Khaleghi, 2012). The intention to use a socket connection only for the column-footing connection was to provide generous tolerances and fast construction, but the connection design was not as beneficial for use for the column-cap beam connection as it required casting the cap beam in place, which would eliminate the time advantage of prefabrication. (Khaleghi, 2012).

Similarly, Haraldsson (2013) studied a socket connection design for connecting spread footings and precast columns in bridges. For this system, columns were precast and placed in their position, and then footing reinforcement was positioned in place and the footing was cast (Haraldsson, 2013). Figure 8 shows the construction sequence of the socket connection concept.

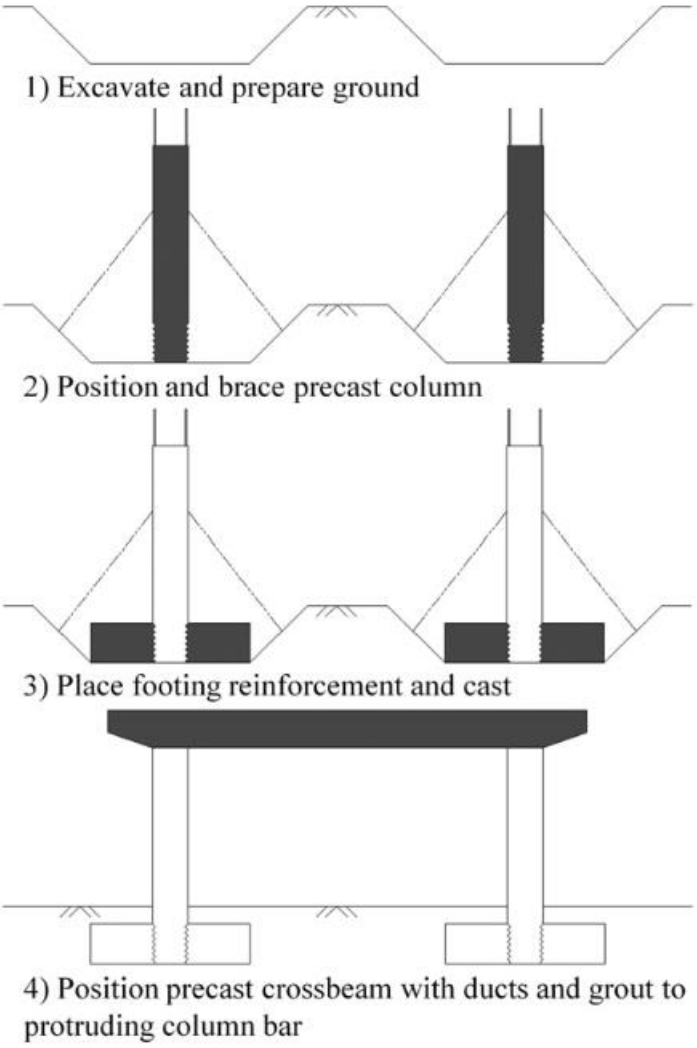

Figure 8. Construction sequence of a typical socket connection by Haraldsson (2013)

The proposed structural details of the connection were modified from the conventional monolithic connection method to avoid having bars cross the column-footing interface and eliminate bending out the longitudinal column reinforcement at the bottom. The longitudinal column bars were straight and were terminated with mechanical anchors (Haraldsson, 2013). By doing that, the resistance to vertical loads depended only on shear friction across the roughened interface between the column and the footing, and the method provided a more direct transfer of internal forces without the need for grout. These bars were straight and terminated with headed anchors, which

simplified transportation and reduced the hazards posed by protruding bars (Haraldsson, 2013). The socket connection design was evaluated by conducting axial load and cyclic lateral load tests on three column-footing connection specimens. Three parameters were studied, including embedment depth of the column into the footing, use of mechanical anchors, and footing diagonal steel and ties, to investigate the strength of the proposed socket connection. The performance of the connection in multiple loading conditions was better than that of a conventional cast-in-place connection system (Haraldsson, 2013). The proposed connection also had several advantages over the conventional method as it allowed generous placement tolerance, did not need grouting, and prevented any potential difficulties with bent rebars (Haraldsson, 2013).

Cheng (2019) examined several parameters that could affect a socket connection design using corrugated steel pipe (CSP) to create a socket. Eight specimens were constructed to evaluate the side shear strength in preformed socket connections with three types of surface textures for the embedded portion of the column and CSP-to-embedded member clearance. High-strength grout with a compressive strength of 8000 psi was used to fill the gap between the column and footing (Cheng, 2019). The specimens were subjected to uniaxial compression force at the top of the column segments, with cyclic axial loading applied only to four specimens. The results showed that all specimens, except the one with a smooth column surface, provided significant side shear strength against the axial load applied to the column segments. The gap between the column segments and CSP affected the performance of the socket connection. The fixity of the connection was less for specimens with a larger gap due to potentially having a bonding issue between surfaces and discontinuity of load transfer. Thus, exposed aggregate for embedded member surface preparation, a standard pattern of corrugation for CSP, and high-strength grout were recommended for better performance of socket connections (Cheng, 2019; He, 2021).

Similarly, White (2016) investigated the performance of socket connections using grout in the gap between the column and footing. The socket connection provided a good seismic response after being subjected to biaxial quasi-static cyclic loading. The results of the socket connection tests in terms of energy dissipation and ductility were comparable to those of a conventional monolithic connection (White, 2016). However, significant damage to the column occurred with the socket connection design such as spalling of concrete and buckling of longitudinal reinforcement.

Zhang (2023) investigated the seismic performance of three different connections of double-column piers: monolithic connection, UHPC grouted corrugated duct connection, and UHPC socket connection. UHPC grouting helped to ensure a rigid connection and reliability for the socket connection and grouted corrugated duct connection. It provided good adhesion at the interface surfaces between the column and footing. All connections had comparable levels of energy dissipation and ductility, but the residual displacement of the socket connection specimen was significantly smaller than the other specimens, indicating its excellent seismic resistance and self-resetting ability (Zhang, 2023, Zhang 2021).

2.5 The Knowledge Gap in Socket Connection

Socket connection has several advantages over the conventional connection methods in column-footing connections. It improves the seismic performance of structures, reduces construction time, and simplifies construction processes, which aligns well with the concept of Accelerated Bridge Construction. However, there is a lack of knowledge about the best practices and implementation of this kind of connection since there is limited research on evaluating the performance of socket connections. One significant challenge is determining the requirements of the socket connection in terms of the socket's size and shape. This is essential in order to understand the load transfer between the structural elements through the connection. The definition of the socket connection is

vague as some research approaches its design differently than other research studies. This is shown in the design differences between Khalegi (2012), Haraldsson (2013) and ElGawady et al. (2018). Another substantial challenge is the uncertainty about the long-term durability of the socket connection. Since it has not been widely used in construction, the safety and reliability of structures incorporating this kind of connection are difficult to evaluate. Thus, further investigation is required to develop design guidelines and construction practices to help standardize the socket connection design.

3. Approach and Procedure

Small-scale Hollow Core-Fiber Reinforced Polymer-Concrete-Steel (HC-FCS) column-footing connections were designed, constructed, and tested to investigate the connection strength and required embedment length of steel tube for the full-scale column-footing connection. The small-scale column to footing connection specimen was designed to be tested as a simply supported beam using a typical load frame. In this loading condition, the contribution of axial load to the connection was neglected resulting in testing the connection specimens in worst case relative to bending. Three associated failure mechanisms were investigated: pullout failure, flexure failure, and footing failure. The column portion of the specimen was in the form of only a steel tube, and nine specimens were designed following the half-scale HC-FCS columns designed by Milner (2023). The specimens were constructed to evaluate the required embedment length as a function of the diameter and thickness of the steel tube and footing concrete compressive strength. Figure 12 shows the trial specimen after casting.

Three embedment lengths were selected for this research study. Embedment lengths of $1.6D_i$ and $1.8D_i$ were selected based on results of previous studies, where D_i represents the inner steel tube diameter, and an embedment length determined by following Equation 2.2.1 proposed by Moon (2013) in Section 2.2 was also used.

In Equation 2.2.1, t_s is the thickness of the steel tube, F_u is the ultimate yielding strength of steel tube, l_e is the embedment length, and $f'_{c,FT}$ is the compressive strength of footing. Additionally, two different diameter-to-thickness ratios were investigated to evaluate the effect on the footing-column connection. The failure modes investigated included steel tube buckling failure, footing failure, and steel tube pullout failure.

3.1 Column Capacity Calculations

Capacity calculations were conducted for the full HC-FCS columns for use in design of the connection test specimens and testing apparatus following procedures used by ElGawady et al. (2015). Calculations were first conducted on a column from the literature to verify that the methods were applied properly and then were applied to the dimensions of the half-scale HC-FCS column used in this project. Table 2 shows the resulting calculated flexural and shear capacities of the half-scale HC-FCS column design used for this project.

Table 2. Half-scale HC-FCS column capacity

Nominal Bending Moment, M_n (k-ft)	414
Nominal Shear Strength, V_n (kips)	124

3.1.1 Column Flexural Strength Calculations

Flexural strength calculations for the HC-FCS column were conducted following guidance reported by ElGawady (2015). Strain compatibility and Bernoulli-Euler assumptions were considered when calculating the flexural strength of the column. It was assumed that plane sections are plane before the column deforms and remain plane after deformation, and the stress-strain behavior of the HC-FCS column steel tube was assumed to be elastic-perfectly plastic. The stress-strain relationship used for the confined concrete of the HC-FCS column was taken from Yu et al. (2006) and is shown in Equation 3.1.1.1.

$$\sigma_c = f'_{co}\left[\frac{2\varepsilon_c}{\varepsilon_{co}} - \left(\frac{\varepsilon_c}{\varepsilon_{co}}\right)^2\right] \qquad (3.1.1.1)$$

In Equation 2, σ_c is the stress in the confined concrete (psi), ε_c is the strain in the confined concrete (in./in.) taken as 0.003, f'_{co} is the unconfined compressive strength of concrete taken as 4500 psi,

and ε_{co} is the strain corresponding to compressive strength (in./in.). Figure 9 shows the cross section of the column used to calculate flexural strength.

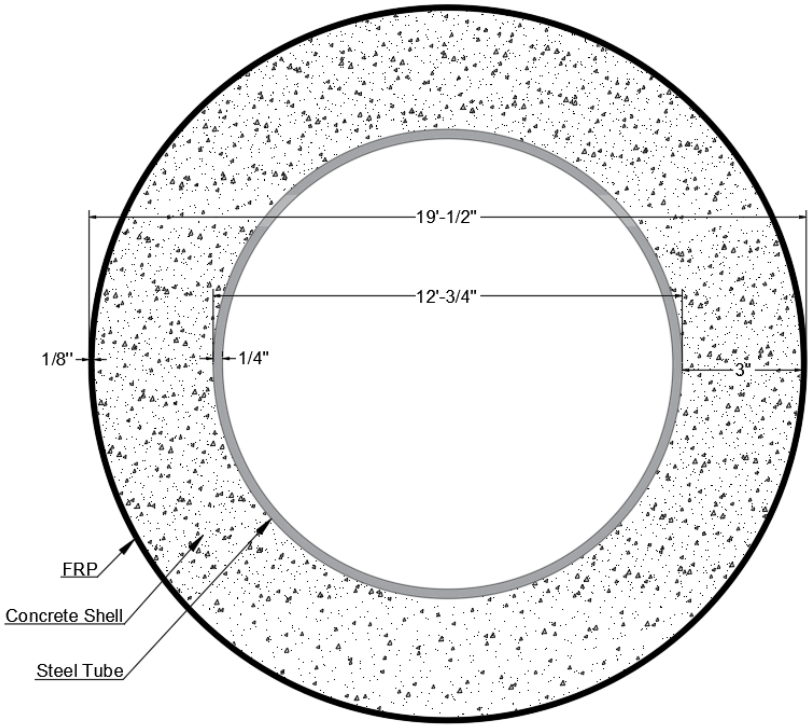

Figure 9. Cross-section of the column used in Milner (2023)

The calculations were performed using a Microsoft Excel spreadsheet. The distance to the neutral axis from the most extreme compression fiber, *c*, was initially assumed, and the compression and tension sides of the column cross-section were divided into 100 segments based on a polar angle (shown in Figure 10). The compressive force in the concrete shell portion of the column was then calculated by summing the resultant compressive forces for each segment considering a solid concrete column, then subtracting the summation of the resultant compressive forces for each segment for a virtual concrete column inside the void.

Angles α_1, α_2, and α_3 (radians) with their corresponding polar angles are shown in Figure 10. Angle α_1 is the angle from the intersection of the neutral axis and column surface to the positive vertical axis considering the column as a solid concrete column, α_2 is the angle from the

intersection of the neutral axis and outer steel tube surface to the positive vertical axis considering virtual concrete column inside the void, and α_3 is the angle from the intersection of the neutral axis and outer steel tube surface to the negative vertical axis of the tension side steel in the steel tube. The polar angles (θ_1, θ_2, θ_3) were calculated using Equation 3.1.1.2, where n is the number of segments.

$$\theta_1 = \frac{\alpha_1}{n} \ , \theta_2 = \frac{\alpha_2}{n} \ , \theta_3 = \frac{\alpha_3}{n} \qquad (3.1.1.2)$$

The shape of the segments was assumed to be rectangular in order to efficiently calculate the area of each segment. The corresponding strain and stress for each segment were then calculated based on the strain compatibility assumption, Hooke's law, and Equation 2, and used with the area to calculate the concrete and steel compressive forces and steel tension force. Hooke's law was used throughout the steel elastic range, where the steel strain was below yielding strain, but steel yielding stress was used once the steel yield strain was exceeded. The steel compressive and tension forces for each segment were summed to obtain the total forces for the column.

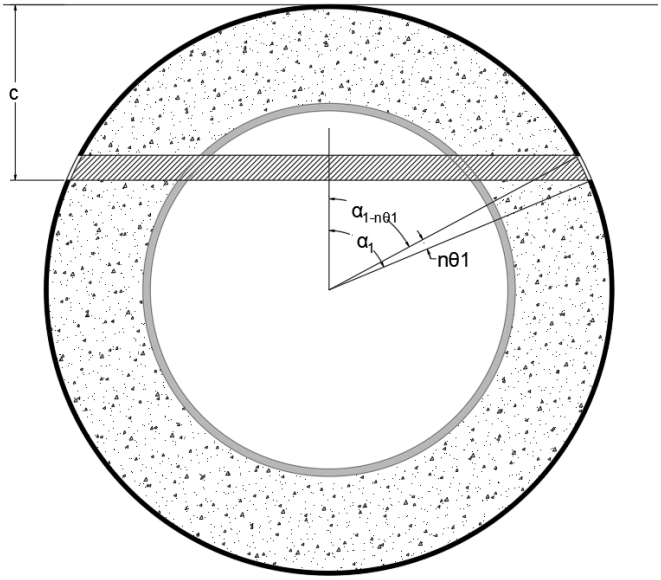

(a)

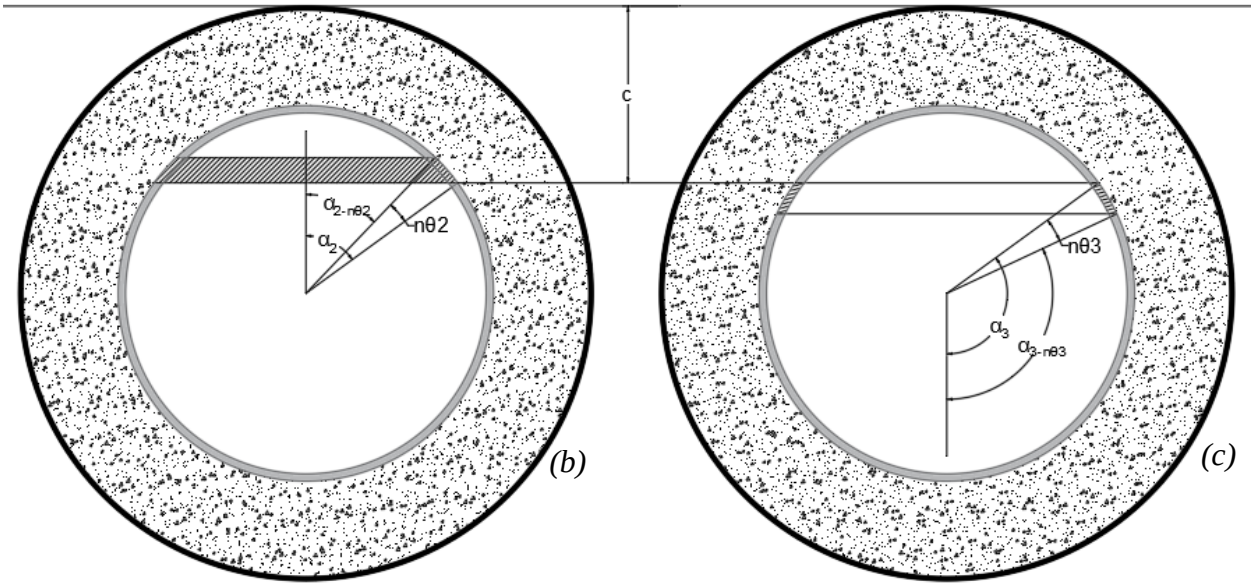

(b) (c)

Figure 10. Cross-section of the column for a segment to calculate compressive and tension forces in (a) assumed solid concrete in compression, (b) virtual concrete and steel in compression, and (c) steel in tension

Multiple iterations were done until force equilibrium $\sum F_x = 0$ was obtained for the compression and tension forces, based on varying the depth to neutral axis *c*. Accordingly, the internal bending moment was then computed about the centroid of the HC-FCS column cross-section. Figure 11 shows the cross-sectional analysis, including the strain and concrete stress profiles. The strain and stress for the solid column for each segment were denoted by $\varepsilon_{s-n\theta 1}$ and $\theta_{s-n\theta 1}$, and the strain and stress for the virtual column for each segment were denoted by $\varepsilon_{v-n\theta 2}$ and $\theta_{v-n\theta 2}$. Steel strains are shown as $\varepsilon_{cst-n\theta 2}$ and $\varepsilon_{tst-n\theta 3}$ for the compressive steel and tension steel, respectively.

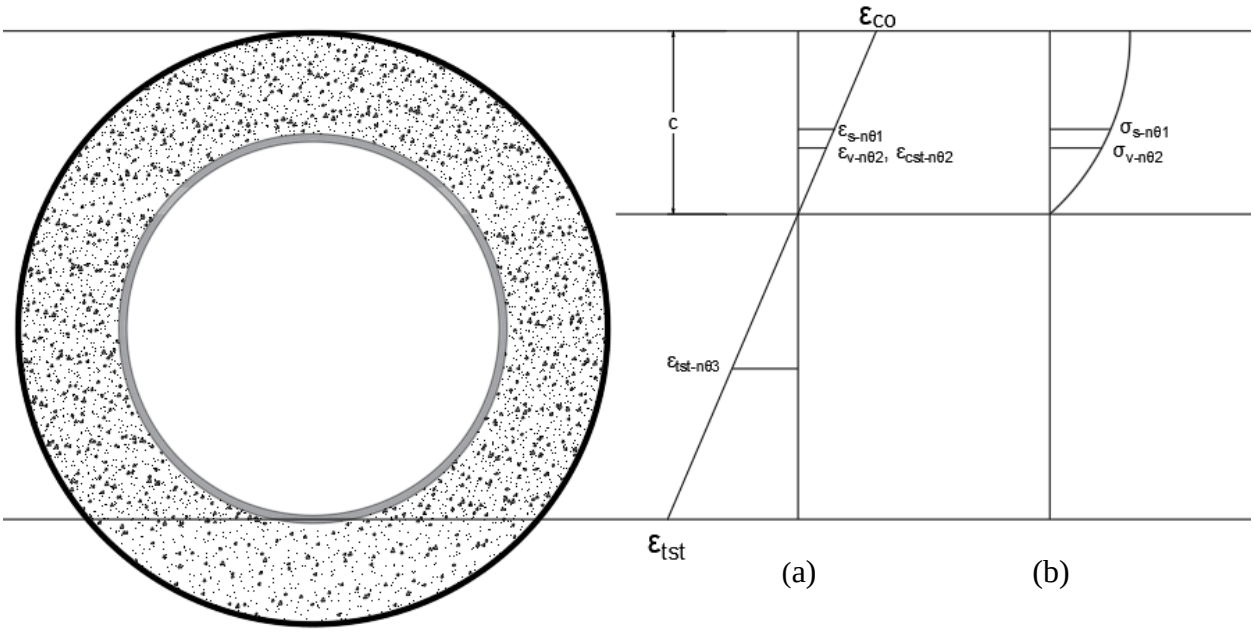

Figure 11. Cross-sectional analysis of the column showing the (a) strain profile for the column and (b) stress profile for the concrete

3.1.2 Column Shear Capacity Calculations

The shear capacity of the HC-FCS column depends primarily on the steel tube capacity where the FRP tube provides additional shear resistance (Yu et. al., 2006). The shear strength of the steel round hollow structural section was determined based on the American Institute of Steel Construction (AISC) Manual. Section G6 provides guidance for calculating the nominal shear

strength, V_n (kips), according to the limit states of shear yielding and shear buckling (AISC, 2011 edition). Equation 3.1.2.1 from AISC Manual (2011) was used to calculate V_n.

$$V_n = \frac{F_{cr} \times A_g}{2} \qquad (3.1.2.1)$$

F_{cr} in Equation 3.1.2.1 is the larger of Equations 3.1.2.2 and 3.1.2.3 but shall not exceed $0.6F_y$:

$$F_{cr} = \frac{1.6E}{\sqrt{\frac{L_v}{D}}\left(\frac{D}{t}\right)^{\frac{5}{4}}} \qquad (3.1.2.2)$$

$$F_{cr} = \frac{0.78E}{\left(\frac{D}{t}\right)^{\frac{3}{2}}} \qquad (3.1.2.3)$$

In Equation 6, F_{cr} is the critical stress (ksi), E is Young's modulus of steel (ksi), L_v is the distance from maximum to zero shear force (in.), A_g is the gross cross-sectional area of the steel tube (in.^{2}), D is the outer diameter of the steel tube (in.), and t is 0.93 times the nominal steel tube thickness (in.).

3.2 Trial Specimen

3.2.1 Column Capacity Calculations and Footing Design

A single trial specimen was constructed as a smaller representation of the test specimens to evaluate the design and testing methods for the small-scale column-footing connection specimens before the primary specimens were constructed. A 5 in. diameter steel pipe was used for the trial specimen chosen due to availability at the Fears Structural Engineering Laboratory. Column capacity calculations were conducted for a column using this pipe diameter following the same procedure used for the half-scale HC-FCS column. Table 3 shows the calculated flexural and shear capacities of the trial HC-FCS column.

Table 3. HC-FCS trial column capacity

Nominal Bending Moment, M_n (k-ft)	49
Nominal Shear Strength, V_n (kips)	47

The concrete footing portion of the trial specimen was designed to support the nominal capacities of the trial HC-FCS column specimen and to ensure failure in the column or the connection. The footing dimensions were 19 in. by 18 in. by 38 in., and the design followed requirements of the AASHTO LRFD Bridge Design Specifications (2017) and ACI Building Code Requirements for Structural Concrete (ACI 318-19).

3.2.2 Casting Procedure, Testing Setup and Results

The footing portion of the trial specimen was cast horizontally using Rapid Set® cement self-consolidating concrete cast in Fears Laboratory with a compressive strength of 7,200 psi. The 5 in. diameter steel pipe was embedded into the footing a length of 1.6*Di* from each end, and the steel pipes were extended 4 ft-2 in. from the interface of the footing to result in a moment large enough to ensure the specimen would fail in flexure or due to pullout of the pipe. Figure 12 shows the trial specimen after casting.

Figure 12. Trial specimen before removing the formwork

The specimen was tested with an 11 ft-6 in. simple span with the ends of the pipe placed on steel supports placed on steel reinforced neoprene bearing pads. A vertical load was applied to the midspan of the footing using a hydraulic cylinder, and a wire potentiometer was placed on each side of the specimen at the load point to measure the vertical deflection of the footing. In addition, a linear variable differential transformer (LVDT) was placed on the end of each steel pipe to measure the vertical deflection resulting from the placement of the steel supports on bearing pads. Figure 13 displays the trial specimen in the testing frame.

Figure 13. Testing setup for the trial footing-column connection specimen

The specimen failed due to pullout of the steel pipe, as intended, with a failure load of 20 kips. At one end of the footing section, there was a vertical separation of approximately 0.125 in. at the interface between the steel pipe and the concrete, while at the other end, the steel pipe pulled out of the footing directly approximately 0.25 in. Figure 14 presents the pullout failure mechanisms at each end of the footing.

Figure 14. Pullout connection failure from each end of the footing

The results of the trial specimen test indicated that the specimen concept and testing methods were sufficient for evaluating the connection. No failure of the footing section or supports was observed with all damage localized at the connection.

3.3 Small-scale Column Connection Specimens

3.3.1 Parameter Matrix

Nine small-scale column-footing connection specimens were constructed to evaluate five parameters including steel pipe embedment in the footing, diameter to thickness ratio, footing concrete compressive strength, presence of shear lugs on the steel pipe, and use of an ultra-high performance concrete (UHPC) socket connection. An 8.625 in. diameter steel pipe with a thickness of 0.219 in. was chosen for eight specimens, while a 6.625 in. diameter steel pipe with a thickness of 0.25 in. was selected for one specimen. In five specimens, the 8.625 in. diameter steel pipe was embedded into a 2 ft by 2 ft by 4 ft-1 in. footing at lengths of $1.6D_i$ and $1.8D_i$ from each end and using the minimum embedment length equation (Equation 1) from Moon (2013). Two of these specimens had high-strength concrete footings with embedment lengths of $1.6D_i$ and $1.8D_i$. One specimen had the 6.625 in. diameter steel pipe, resulting in a different diameter/thickness ratio.

Another specimen had shear lugs welded to the end of the steel pipe. The steel pipes in both the smaller diameter pipe and shear lug specimens were embedded into a footing made with normal-strength concrete at an embedment length of $1.6D_i$. Two specimens were cast with a socket connection using UHPC at embedment lengths of $1.4D_i$ and $1.8D_i$. Table 4 summarizes the parameter matrix for the small-scale column connection specimens. In Table 4 and throughout the report CF is used for "column-footing".

Table 4. Parameter matrix of the small-scale column-footing connection specimens

Specimen	Embedment Length (in.)	Diameter/ Thickness (in./in.)	$f'_{c,FT}$ on Testing Day (psi)	Connection Type
CF-1	1.6*D*	8.625/ 0.219	9,910	Monolithic
CF-2	1.8*D*	8.625/ 0.219	9,270	Monolithic
CF-3	1.6*D*	8.625/ 0.219	5,970	Monolithic
CF-4	1.8*D*	8.625/ 0.219	5,270	Monolithic
CF-5	Eq. 1	8.625/ 0.219	5,270	Monolithic
CF-6	1.6*D*	8.625/ 0.219	4,530	Monolithic with shear lugs
CF-7	1.6*D*	6.625/0.25	4,890	Monolithic
CF-8	1.6*D*	8.625/ 0.219	5,500	Socket
CF-9	1.6*D*	8.625/ 0.219	5,400	Socket

3.3.2 Column Capacity Calculations and Footing Design

Column capacity calculations were conducted for the small-scale specimens following the same procedure used for the half-scale HC-FCS column. Table 5 shows the calculated flexural and shear

capacities of the equivalent small-scale HC-FCS column with the same concrete shell thickness used in the half-scale HC-FCS column design.

Table 5. Small-scale HC-FCS column capacity

Nominal Bending Moment, M_n (k-ft)	136
Nominal Shear Strength, V_n (kips)	73

The footing portion of the specimen was designed to support the nominal capacities of the small-scale HC-FCS column and ensure failure in the column or the connection. The footing design followed the AASHTO LRFD Bridge Design Specifications (2017) and ACI Building Code Requirements for Structural Concrete (ACI 318-19). The cross-section of the footing was designed to prevent concrete breakout failure in the footing following guidelines of ACI 318 section 17.7 (ACI 318-19). The breakout strength of the concrete for the chosen dimensions exceeded the anticipated ultimate applied load required to achieve the nominal flexure capacity of the small-scale HC-FCS column. The footing dimensions were 2 ft by 2 ft by 4 ft-1 in. with rebar reinforcement as shown in Figure 15 and Figure 16. The footings were reinforced with four No. 6 bars top and bottom and No. 3 bars for shear reinforcement and confinement.

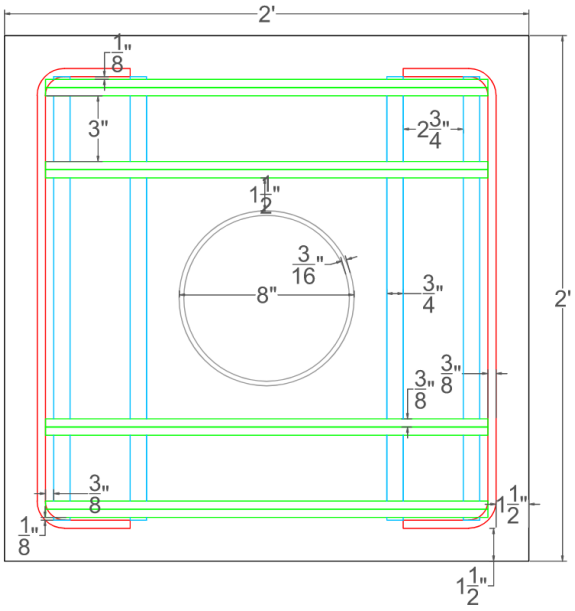
2'
1/8"
3"
2 3/4"
1 1/2"
3/16"
8"
3/4"
2'
3/8"
3/8"
3/8"
1/8"
1 1/2"
1 1/2"

(a)

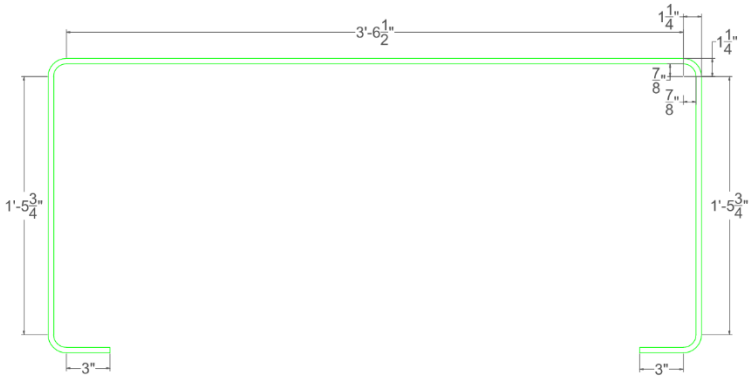
3'-6 1/2"
1 1/4"
1 1/4"
7/8"
7/8"
1'-5 3/4"
1'-5 3/4"
3"
3"

(b)

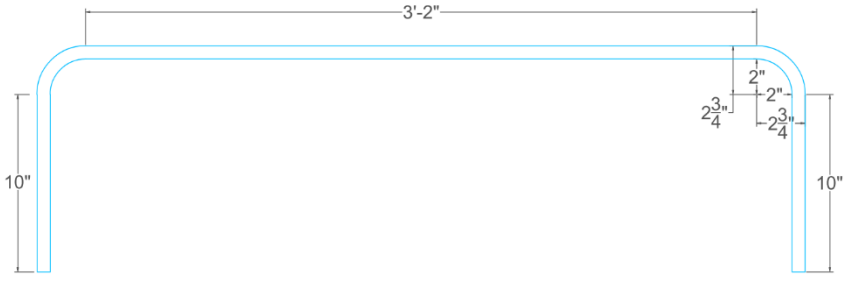
3'-2"
2"
2"
2 3/4"
2 3/4"
10"
10"

(c)

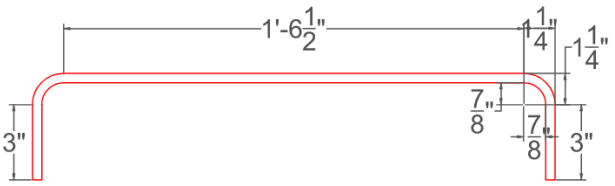

(d)

Figure 15. (a) Footing cross-sectional view, (b) No. 3 rebar, (c) No. 6 rebar, and (d) No. 3 stirrups

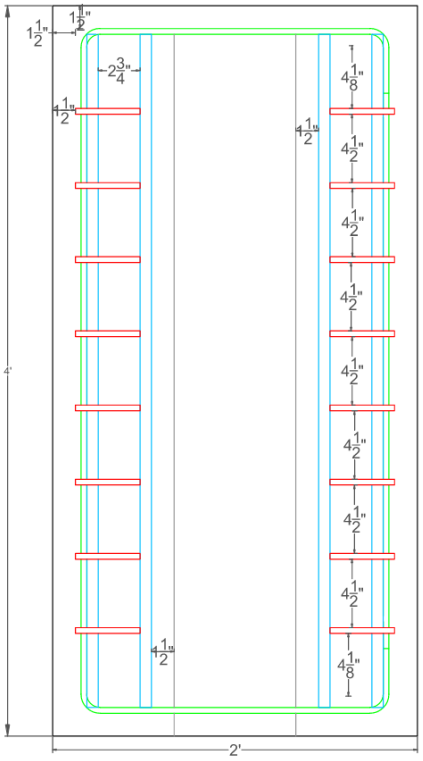

(a)

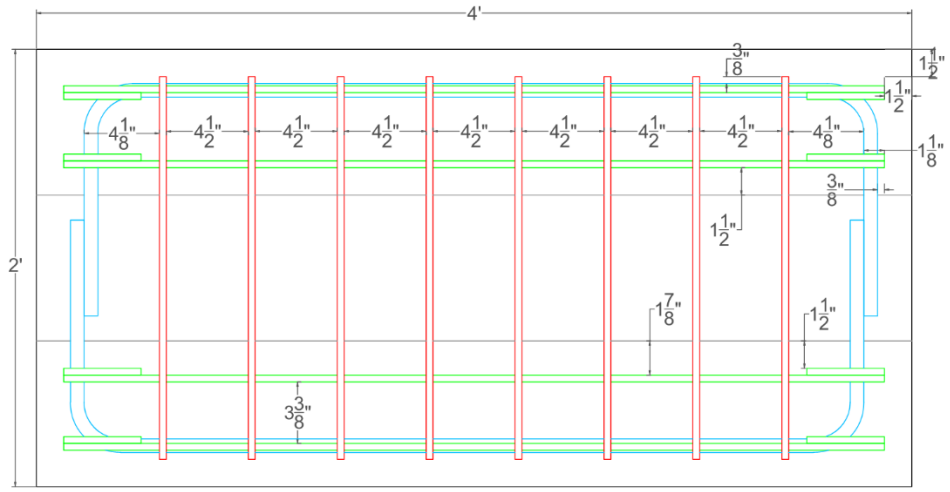

(b)

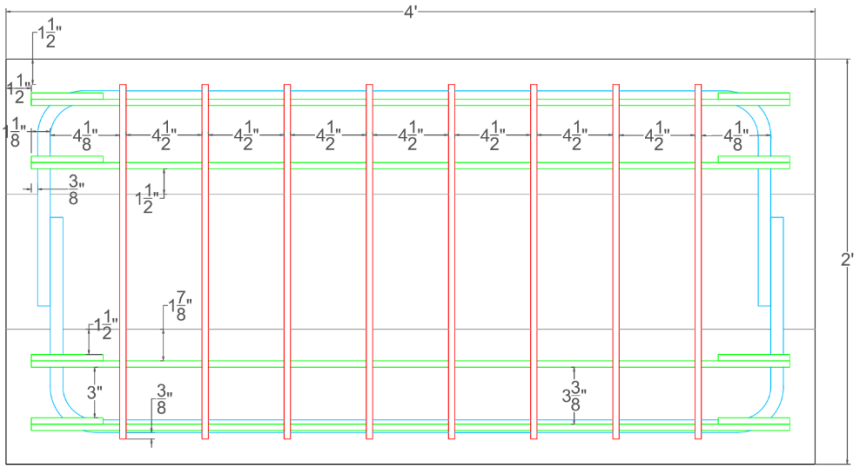

(c)

Figure 16. Footing reinforcement (a) top view, (b) left-side view, and (c) right-side view

3.4 Specimen Construction

3.4.1 Monolithic Column Connection Specimens

Specimens 1, 2, 3, 4, and 5 followed the same construction procedure. Two 2 ft by 2 ft formwork end plates were cut, each with an 8.625 in. diameter circular hole at the center to ensure a proper fit for the steel pipe. Figure 17-a shows a completed end plate. The footing formwork walls and end plates were placed on a 4 ft by 5 ft plywood base and secured in place using wood screws. The

joints along the sides of the formwork were sealed using caulk, as shown in Figure 17-b. Caulk was allowed to set for 24 hours, and then concrete form release agent was applied on the formwork surfaces. Subsequently, the footing reinforcing steel cage was placed inside the formwork, as illustrated in Figure 17-c. Steel pipes were cut at lengths of 102 in. and 104 in. for $1.6D_i$ and $1.8D_i$ specimens, respectively, for each end of the specimen. As the footing was cast horizontally, an insulation foam plug was sealed inside each pipe at the required embedment length in order to prevent concrete filling the pipe outside of the footing surface. The pipes were then carefully pushed inside the formwork until the same embedment length was achieved on both ends, as shown in Figure 17-d. Caulk was applied around the pipe and was allowed 24 hours to set.

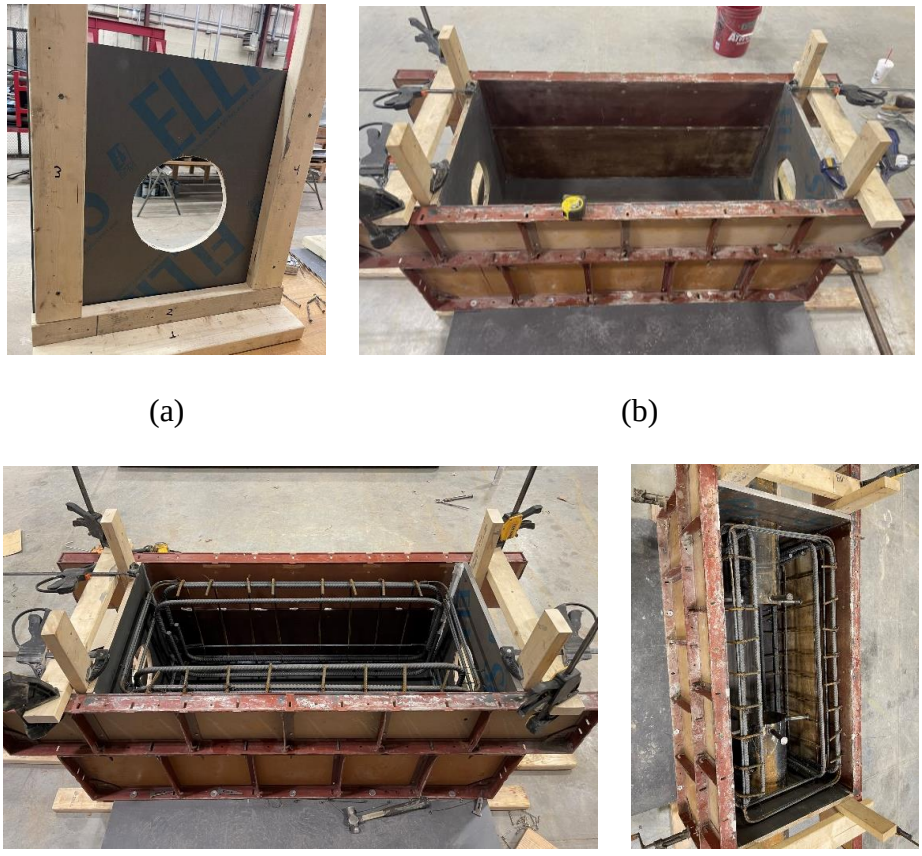

(a) (b)

(c) (d)

Figure 17. Formwork (a) end plate (b) before placing steel cage (c) after placing steel cage and (d) after placing the steel pipes

After the placement of the steel pipes, the insulation foam plug inside each pipe was supported by a wooden plug attached to a piece of 2 in. by 4 in. lumber. The lumber extended out of the pipe and was held in place horizontally by a concrete block. Figure 18 presents a complete view of the formwork for a small-scale column connection specimen.

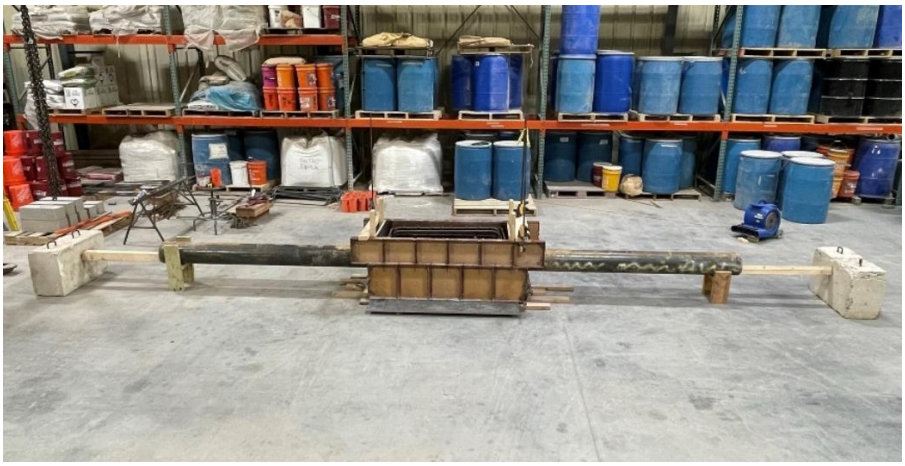

Figure 18. Complete formwork of a small-scale HC-FCS column connection specimen

Two concrete mix designs were used for casting the specimens. A conventional concrete mix design with a water-cement ratio (*w*/*c*) of 0.48, ¾ in. nominal maximum size limestone coarse aggregate, and a targeted slump of 8 in. was used for casting normal-strength concrete footings. The two specimens with high-strength concrete utilized a self-consolidating concrete (SCC) mix design with a *w*/*c* = 0.35, ½ in. nominal maximum size limestone coarse aggregate, and a 25 in. slump flow. A high-range water reducing (HRWR) admixture was added to achieve the desired slump and slump flow for the conventional concrete and SCC mixes. Table 6 presents the mix designs used for casting the small-scale column connection specimens. All concrete was mixed at Fears Laboratory using a large stationary concrete and all castings were carried out inside of Fears Laboratory. Concrete was transferred to the mixer utilizing a concrete transfer bucket and overhead crane and was placed into the center of the formwork to avoid displacing the pipes. Conventional

concrete specimens were consolidated using a concrete vibrator, and the SCC specimens were allowed to consolidate under the weight of the concrete only.

Table 6. Concrete mix designs in SSD

Mix Proportion	Conventional Concrete	Self-Consolidating Concrete
Sand (lb/yd^3)	1219	1476
5/8 in. Coarse Aggregate (lb/yd^3)	-	1445
3/4 in. Coarse Aggregate (lb/yd^3)	1725	-
Cement (lb/yd^3)	682	825
Water (lb/yd^3)	327	289
Adva Cast 575 fHRWR Admixture (fl oz./cwt)	-	7-10
Glenium 7920 HRWR Admixture (fl oz./cwt)	1-2	-

All specimens were covered with plastic sheeting to facilitate a wet condition before the removal of formwork. They were then covered with wet burlap after the concrete reached final set and were cured for seven days after casting. Compressive strength tests were conducted at 7 days, 28 days, and on testing day for each footing. Figure 19 shows column footing specimen 1 after demolding at 7 days of age.

Figure 19. Column footing specimen 1 at 7 days of age

3.4.2 Monolithic Column Connection Specimen with Welded Shear Lugs

Specimen 6 was cast with shear lugs welded to the embedded end of each steel pipe. The design of the shear lugs in this specimen followed the guidelines outlined in ACI Section 22.9.4 (ACI 318-19), ensuring a sufficient number of studs to prevent pullout failure of the steel pipe. The shear stud chosen had a diameter of 0.75 in. and was 5.25 in. long. Studs were welded to the steel pipe by the Fears Lab technician. The adequacy of the weld connection between the stud and steel pipe was validated by using a simple bend test taking the stud more than 30 degrees from vertical. Figure 20 demonstrates the deformation of the trial shear stud without causing a failure in the connection.

Figure 20. Result of stud bending test

Five shear studs were welded at a distance of 1.5 in. from the end of each steel pipe for the column-footing specimen. They were spaced at 5.5 in. around the circumference of the pipe, as displayed in Figure 21-a and Figure 21-b. The formwork was assembled after the studs were welded and the pipes put in place, following the same procedure used for the monolithic specimens. Figure 21-c and Figure 21-d portray the steel pipes inside the formwork and the complete formwork for specimen 6, respectively.

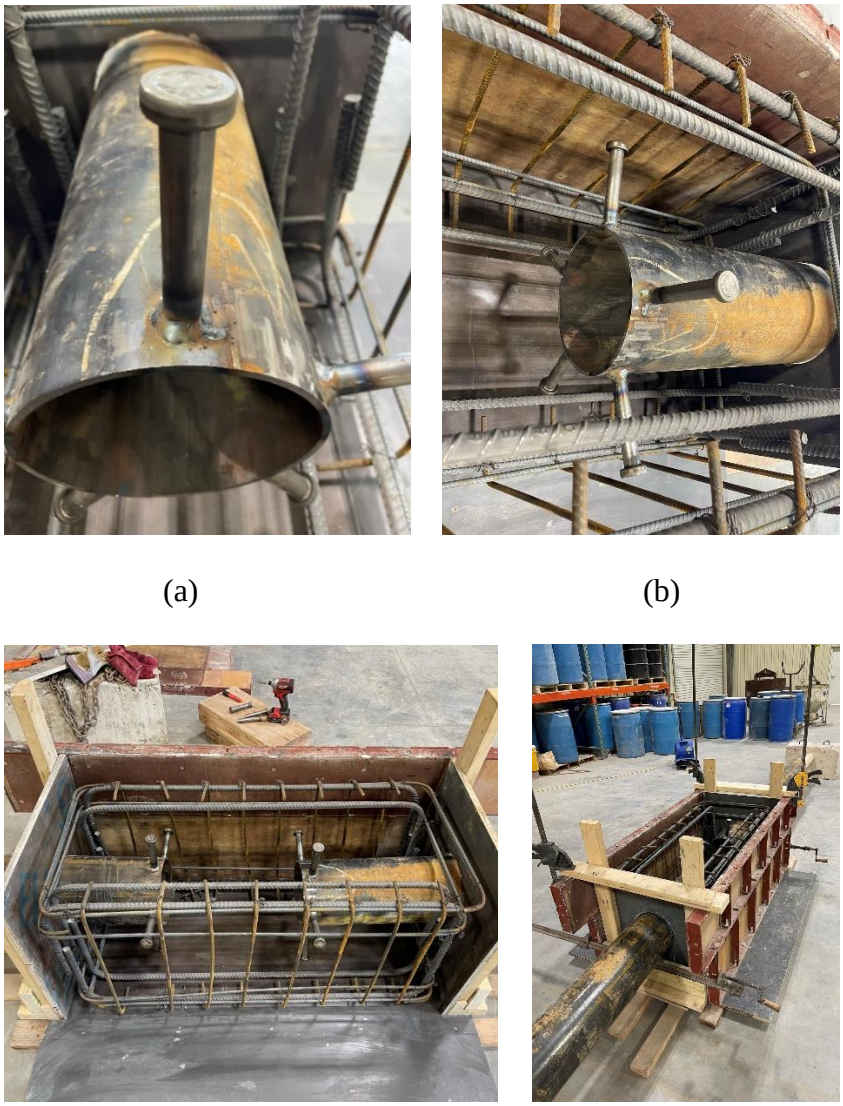

(a) (b)

(c) (d)

Figure 21. (a) Close-up view of a shear stud, (b) shear studs welded at the end of the steel pipe, (c) placement of the steel pipes after welding, and (d) complete formwork for specimen 6

The specimen was covered with plastic sheeting to facilitate a wet condition before the removal of the formwork was cured with wet burlap for 7 days after casting. Compressive strength tests were conducted on 7 days, 28 days, and testing day for the footing.

3.4.3 Socketed Column Connection Specimens

Specimens 8 and 9 were cast using a socketed connection with UHPC between the steel pipe and the concrete footing. Two trial specimens were cast before casting specimens 8 and 9 with the socketed connection evaluate construction methods since the specimens were to be cast horizontally. A 12 in. diameter corrugated steel pipe (CSP) was employed to create the socket. The first trial specimen used a CSP with no modification and was unsuccessful as the CSP could not be easily removed after casting the footing as shown in Figure 22.

(a) (b)

Figure 22. Attempt to remove the CSP from trial specimen 1 showing (a) a portion of the CSP extending from the footing and (b) damage to the CSP and socket caused by attempts to remove the CSP

The second trial specimen included a few modifications to the construction methodology and was successful. For the second trial socketed specimen, the CSP was partially cut along its length, and plastic sheeting was used to cover the CSP and de-bond it from the concrete footing as shown in Figure 23. An insulation foam plug was sealed at the end of the CSP to prevent concrete entering the socket. After the removal of the CSP, a steel pipe section was placed in the socket, a plywood ring was used as formwork to seal the gap, and a trough was constructed at the top of the pipe to

facilitate placement of UHPC. UHPC was successfully cast in the trial socketed connection 2. The J3 UHPC mix design developed by previous research conducted at the University of Oklahoma serves as the baseline mix for this study. The concrete properties and characteristics are outlined in Looney et al. (2019). The composition of J3 UHPC with a 2% steel fiber content by volume is shown in Table 7 (Looney et al. 2019). The mixing procedure used followed that of Looney et al. (2019). The flow of J3 UHPC was measured using ASTM C1856 (2017).

Table 7. Weight ratios of J3 UHPC Composition (Looney, 2019)

Constituent	Mix Proportion
Type I Cement	0.6
Silica Fume	0.1
Slag Cement	0.3
Masonry Sand (1:1 agg/cm)	1.0
w/cm	0.2
Steel Fibers	2% by volume
High Ranger Water Reducer Admixture	18-24 oz/cwt

Figure 24 displays trial socketed connection specimen 2 before and after the CSP was removed from the footing, and Figure 25 shows the complete trial specimen after casting UHPC and demolding the specimen.

Figure 23. CSP covered in plastic sheeting inside formwork for socketed trial specimen 2

(a) (b)

Figure 24. Trial specimen 2 after demolding and removing (a) CSP and (b) plastic sheeting

Figure 25. Complete trial socketed connection specimen

After successfully evaluating the construction method for the socketed connection specimens, the footings for specimens 8 and 9 were cast using a 12 in. diameter CSP. The specimens were constructed following the same footing design and used the same 8.625 in. diameter steel pipe size as the previous specimens. For each specimen, the socket dimensions allowed for approximately 1.5 in. of space on the sides and end of the steel pipe with the desired embedment length of the steel pipe provided in bonded length to the UHPC. The CSP was partially cut along its length from both sides of the specimen, and the CSP was covered with plastic sheeting to de-bond it from the concrete footing, both done to facilitate removal of the CSP from the footing as illustrated in Figure 26-b and Figure 26-c. An insulation foam plug was placed and sealed at the end of the CSP to prevent concrete entering the socket shown in Figure 26-a. Figure 26-d shows the placement of one of the end plates of the formwork with the CSP at the location needed to obtain the required embedment length.

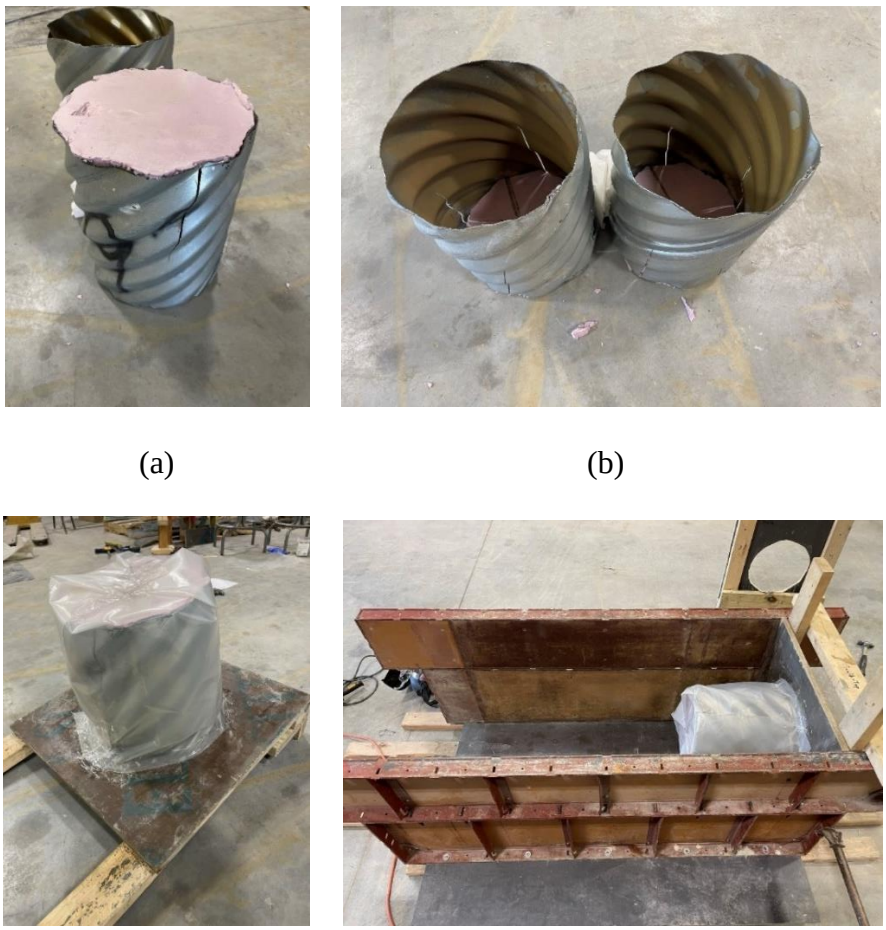

(a) (b)

(c) (d)

Figure 26. The CSP (a) sealed with the insulation foam plug, (b) partially cut along its length, (c) covered with plastic sheeting, and (d) placed in the formwork

Minor changes to the reinforcing bar spacings were required to accommodate the CSP and resulting socket. Once the first end plate was in place the steel reinforcement cage was placed followed by the other end plate with the other CSP. Caulk was used to seal any gaps in the formwork and was allowed to set for 24 hours before casting. Concrete form release agent was applied on the formwork's surfaces. Figure 27 displays the completed formwork for specimen 8 and casting the footing.

(a) (b)

Figure 27. Specimen 8 (a) complete formwork and (b) halfway through casting the footing

The specimens were covered with plastic sheeting to facilitate a wet condition before the removal of formwork and were cured with wet burlap for 7 days after casting. Compressive strength tests were conducted on 7 days, 28 days, and testing day for each footing. Once the formwork was removed, the pieces of CSP were removed and the sockets were sand-blasted to expose the aggregate beneath the surface and create a rough substrate. Figure 28 shows the steps to prepare for casting the socket for specimen 8.

(a) (b)

(c)

Figure 28. Specimen 8 (a) after demolding at 7 days of age, (b) after removing CSP and plastic sheeting, and (c) after sand-blasting the surface of the socket

The steel pipes were cut after the preparation of the sockets was completed. Two 1.5 in. rebar chairs were welded to the end of the pipe to create proper offset from the bottom of the socket, and one was welded on the side to ensure the pipe was centered in the socket, as shown in Figure 29-a. An insulation foam plug was sealed inside each pipe at the required embedment length in order to prevent concrete flowing into the pipe past the end of the footing. The pipes were then carefully pushed inside the socket on each end of the footing at the same embedment length. After the placement of the steel pipes, each foam plug inside the pipes was supported by a wooden plug attached to a 2 in. by 4 in. piece of lumber. The lumber extended out of the pipe and was held in place horizontally by a concrete block. Formwork was constructed around the pipes using a plywood ring, shown in Figure 29-b, cut to match the corrugation of the socket with a plywood tray constructed on the top of the ring to allow for placement of the UHPC as shown in Figure 29-b. Caulk was applied to seal the gaps in the formwork and was allowed to set for 24 hours.

(a) (b)

Figure 29. (a) 1.5-in. rebar chairs welded on the steel pipe and (b) formwork used for the socket cast

Subsequently, the sockets were filled with J3 UHPC to create the connection between the pipe and the footing, with an intended overfill in the formwork to ensure complete filling of the socket. The resulting blocks formed by the tray fill for each end of specimen 8 can be seen in Figure 30-a and Figure 30-b. Figure 30-c shows specimen 8 after casting the socketed connections and demolding the specimen.

(a) (b)

(c)

Figure 30. Specimen 8 (a) north end, (b) south end, and (c) entire specimen after demolding the sockets

3.5 Testing Specimens

3.5.1 Instrumentation and Testing Setup

The nine specimens were tested using the same testing configuration as the trial specimen, but with an 18 ft span length. A vertical load was applied to the midpoint of the footing using a hydraulic cylinder and was measured using a load cell. A wire potentiometer was placed on each side of the specimen at the load point to measure the vertical deflection of the footing. A foil strain gauge was placed on the bottom of the steel pipe 3 in. from the interface with the concrete footing on each side to measure strain in the steel pipe. Two LVDTs were placed on the steel pipe transverse to the end of footing on each side to measure the displacement of the steel pipe relative to the footing. One of the LVDTs was placed close to the neutral axis, and the other was on the extreme tension fiber of the steel pipe. Additionally, an LVDT was placed on the end of each steel pipe at each support to measure the vertical deflection resulting from compression of the neoprene bearing pads used as supports. The bearing pad was placed on a steel frame on top of a concrete block on each end of the steel pipe. The steel frame was provided to restrain lateral movement of the end of the

pipe and neoprene pads were placed between the steel pipe and the vertical portions of the steel support frame. Figure 31 illustrates the placement of the instruments on the specimen.

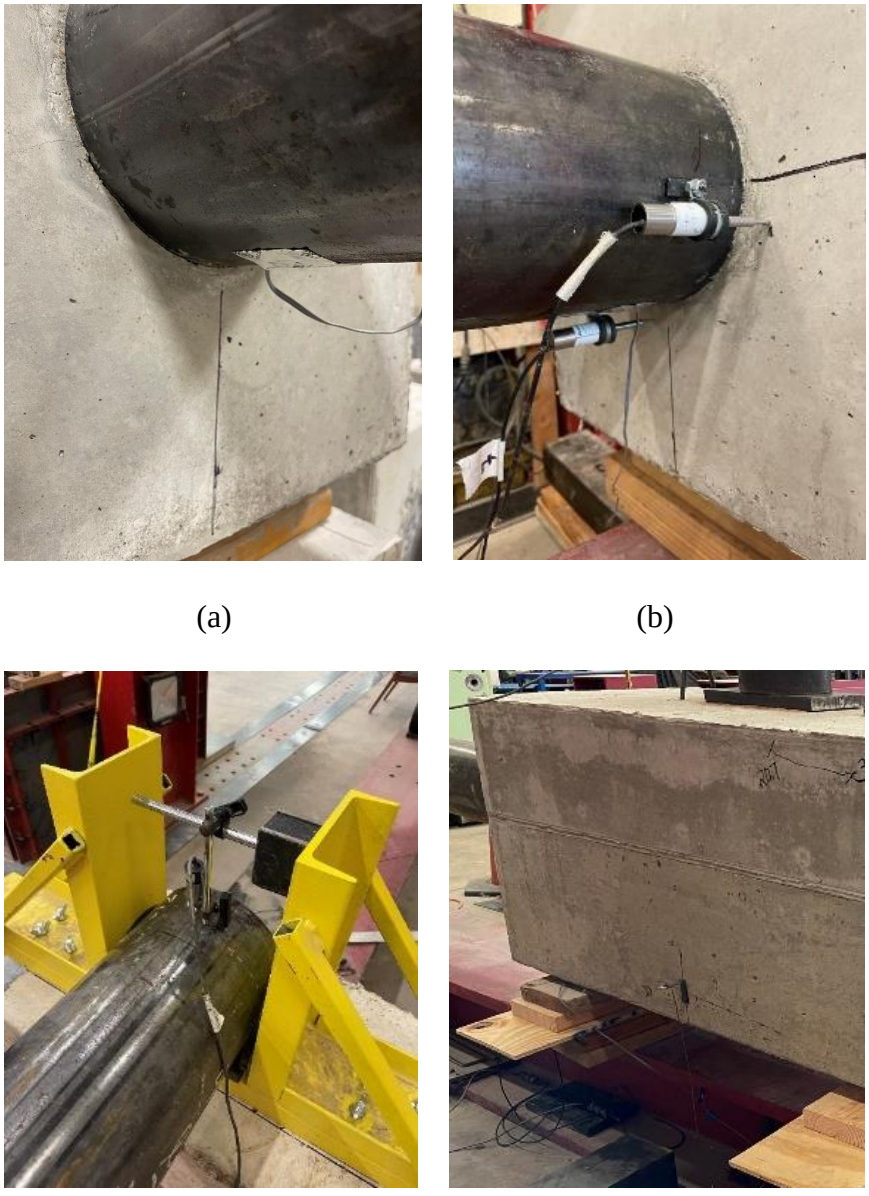

(a) (b)

(c) (d)

Figure 31. Placement of (a) the strain gauge on the bottom of the steel pipe, (b) the two LVDTs placed at each interface, (c) the LVDT used to measure support deflection, and (d) the wire potentiometer

A few modifications were made to the testing setup after testing specimen CF-1 due to large deflections of the bearing pads at the support. The original LVDTs used at the supports for

specimen CF-1 were substituted with longer-stroke LVDTs to ensure sufficient range for measuring vertical deflection resulting from compression of the bearing pads. The unreinforced neoprene bearing pads used for test CF-1, shown in Figure 32-a, were also replaced with stiffer steel reinforced pads to provide better support. Figure 33-a shows the structure of the steel-reinforced bearing pads. Specimen CF-1 also exhibited a significant vertical deflection, and the space underneath the specimen (visible in Figure 32-b) was not sufficient to accommodate this deflection using only the concrete support blocks. Thus, steel blocks were placed on top of each concrete support block to elevate the specimen, allowing for more vertical deflection, as illustrated in Figure 33-b.

(a) (b)

Figure 32. Testing setup for specimen CF-1 showing (a) unreinforced neoprene bearing pad and (b) overall testing setup

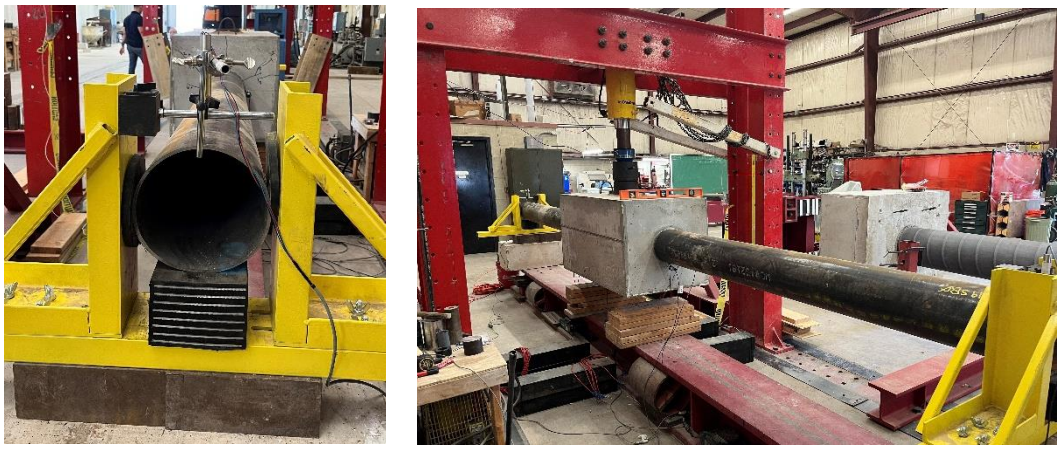

(a) (b)

Figure 33. Testing setup for specimens CF-2 to CF-9 showing (a) steel reinforced neoprene bearing pad and (b) overall testing setup

3.5.2 Procedure

All nine specimens were tested following the same testing procedure. The steel pipes were polished and cleaned for a distance of 6 in. from the interface with the concrete footing. This allowed for easy identification of cracks near the interface and facilitated placement of the strain gauges and LVDTs. Then, the specimen was moved to the testing frame and placed on the supports, as shown in Figure 33. A strain gauge was then placed on the steel pipe at a distance of 3 in. from each interface with the concrete footing. The placement of the strain gauges followed the manufacturer's recommendation and the methodology used on the half-scale HC-FCS columns.

The two LVDTs placed near the interface were attached to steel mounting brackets glued to the steel pipe on each side using a high strength adhesive. The LVDT on the end of the steel pipe at each support was mounted on the steel bracing frame using a magnetic stand. After the placement of the instruments, the specimen was adjusted into the final position for testing, and the load cell and spacers were placed under the hydraulic cylinder. Finally, a steel L-bracket was adhered to

each side of the footing at the midpoint to hook the wire potentiometer for vertical deflection measurements. Figure 34 displays a complete specimen with all instruments placed before testing.

Figure 34. Complete specimen setup before testing

A pre-test was conducted on all instruments to ensure they were functioning properly before testing a specimen. Immediately before application of the load the specimen was rotated by hand until the top surface of the footing was level. The load was then applied in 2 kip increments until failure. Manual vertical deflection measurements and inspection of the specimen for new cracks were conducted after each load increment throughout testing. Additionally, pictures were captured every two load increments to document any changes in the specimen. Notes were made whenever the first crack on the footing or separation at the interface of the steel pipe with the concrete footing was observed. Each test was continued until reaching a vertical deflection of 5 in. or 6 in., depending on the severity of the damage observed during testing. The specimen was then unloaded, the program was stopped, and the final deflection was recorded before removing the instruments.

4. Results

This section presents the results of testing the nine small-scale column footing connection specimens. The failure mechanism of the specimens is evaluated and a comparison between the parameters tested is presented. The self-weight of the footing was not included in the moment calculations, which means that the presented experimental moment capacity is an underestimate of the actual capacity. However, this did not affect the failure mechanism of the specimens and the results were only taken as a comparative study. Five parameters were evaluated including steel pipe embedment length, steel pipe diameter to thickness ratio, connection type, inclusion of shear studs, and compressive strength of the footing. Table 8 and Table 9 show the compressive strength of the footing concrete and UHPC used for the socket connections for each specimen on the testing day, respectively.

Table 8. Compressive strength of footing concrete

Specimen	$f'_{c,FT}$ at testing day (psi)
CF-1	9,910
CF-2	9,270
CF-3	5,970
CF-4	5,270
CF-5	5,270
CF-6	4,530
CF-7	4,890
CF-8	5,500
CF-9	5,400

Table 9. Compressive strength of UHPC

Specimen/Socket	$f'_{c,FT}$ at testing day (psi)
CF-8 North Side	18,130
CF-8 South Side	18,690
CF-9 North Side	17,120
CF-9 South Side	16,600

4.1 Column-Footing Specimen 1

Specimen CF-1 made with high strength concrete and a 1.6D_i embedment was tested as a simple beam with an 18 ft span length as described in Section 3.5.1. Specimen CF-1 specifications and properties are described in Table 4 in Section 3.3.1.

The specimen failed due to the steel pipe buckling locally at a maximum load of 21 kips and was taken to a maximum deflection of 5.6 in., as shown in Figure 35. The moment at the interface corresponding to the maximum load was calculated to be 74 kip-ft, exceeding the calculated flexural strength of the pipe: 68 kip-ft. This indicates that the connection developed the full strength of the pipe with a high-strength concrete footing and an embedment length of 1.6*Di*. Based on the load-displacement curve, the specimen exhibited an initial linear load-displacement behavior, followed by a nonlinear behavior leading to a peak load post-cracking in the footing and ultimately load-sustaining behavior to some extent. It should be noted that the initial stiffness of the specimen from the load-displacement curve may be affected by the deflection from the bearing pads that were placed at the ends of this specific specimen. As loading was continued beyond the maximum load, it was observed that the specimen exhibited some gradual load loss, while vertical deflection continued to increase until the specimen was considered to have failed and the test was

stopped. This load loss may be a result of loading equipment limitations rather than a true representation of behavior.

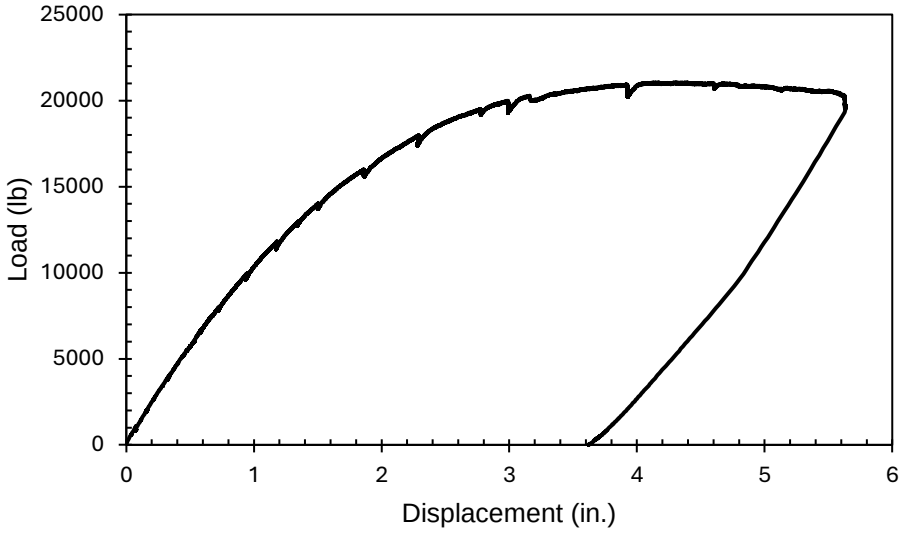

Figure 35. Load vs. displacement curve for specimen CF-1

The failure occurred due to local buckling in the pipe on both sides of the specimen with more evident buckling on the south side as the test continued. The initial crack in the footing concrete was observed at approximately 12 kips, and the initial visible separation at the interface between the steel pipe and footing on the north and south sides of specimen CF-1 started at a load of 8 kips. Figure 36 shows the local buckling of the steel pipe from each side of the footing.

(a) *(b)*

Figure 36. Local buckling of the steel pipe at the (a) north side and (b) south side of the footing for specimen CF-1

The relative horizontal displacement between the footing and the steel pipe on the tension side of the pipe increased significantly on each side of the specimen after the load exceeded approximately 19 kips, as shown in Figure 37. The maximum horizontal displacement, measured by the bottom LVDT, reached 0.19 in. with a corresponding maximum strain of 0.0032 in the steel pipe on the north side of the specimen. On the other hand, the maximum horizontal deflection was 0.14 in. with a maximum strain of 0.022 on the south side. Strain on the tension side of both the north and south side pipes exceeded the theoretical yield strain of the steel pipe, which was determined to be 0.0018. Figure 38 presents the load vs. strain curve for the tension side of the steel pipes on both sides of specimen CF-1. As load continued to be applied after reaching the peak load, the north side exhibited an increase in the horizontal displacement, but the strain remained relatively

constant (fluctuation between 0.0008-0.0009). This suggests a potential discontinuity in the connection on the north side of specimen CF-1. This fluctuation behavior could also indicate that the strain gauge might have been damaged after failure. Although there may have been a loss of bond, the steel pipe on the north side exhibited local buckling as evident in Figure 36-a.

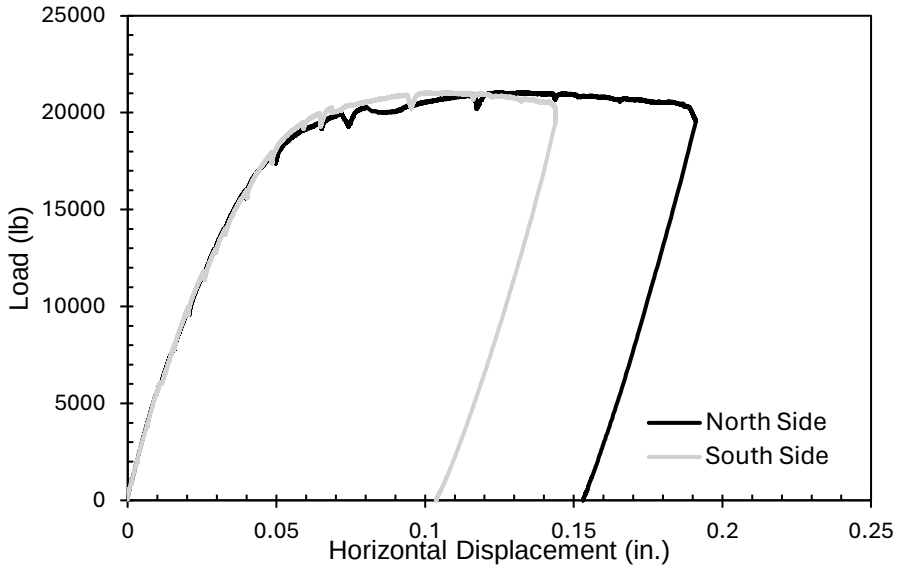

Figure 37. Load vs. tension side horizontal displacement curve for specimen CF-1

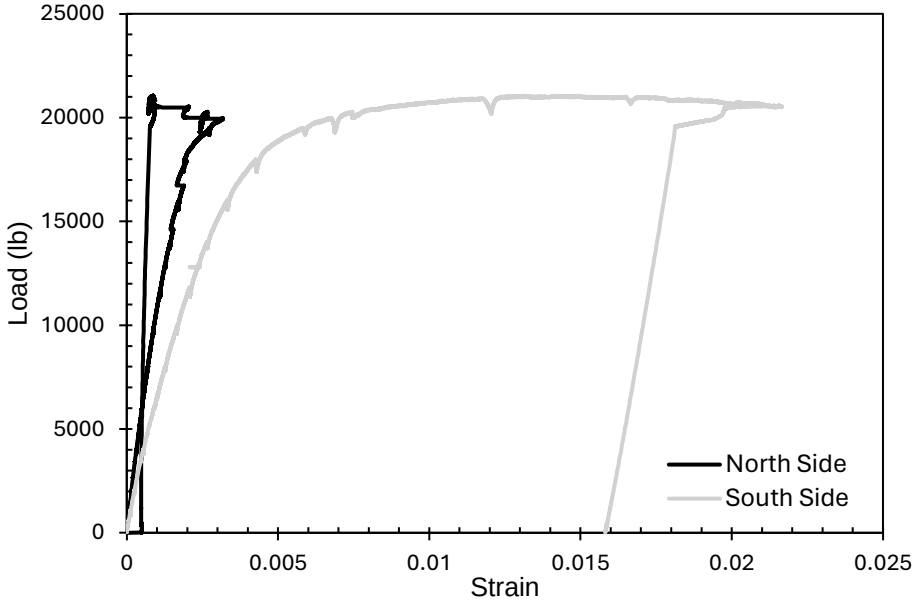

Figure 38. Load vs. strain curve for specimen CF-1

4.2 Column-Footing Specimen 2

Specimen CF-2 made with high strength concrete and a 1.8D_i embedment was tested as a simple beam with an 18 ft span length as described in Section 3.5.1. Specimen CF-2 specifications and properties are described in Table 4 in Section 3.3.1.

The specimen failed due to the steel pipe buckling locally at a maximum load of 22.5 kips and was taken to a maximum deflection of 6 in., as shown in Figure 39. The moment at the interface corresponding to the maximum load was calculated to be 78.4 kip-ft, exceeding the calculated flexural strength of the pipe: 68 kip-ft. This indicates that the connection developed the full strength of the pipe with a high-strength concrete footing and an embedment length of 1.8*Di*. Based on the load-displacement curve, the specimen exhibited an initial linear load-displacement behavior, followed by a nonlinear behavior leading to a peak load post-cracking in the footing and ultimately load-sustaining behavior. As loading was continued beyond the maximum load, it was observed that the specimen exhibited some gradual load loss, while vertical deflection continued to increase until the specimen was considered failed and the test was stopped. This load loss may be a result of loading equipment limitations rather than a true representation of behavior.

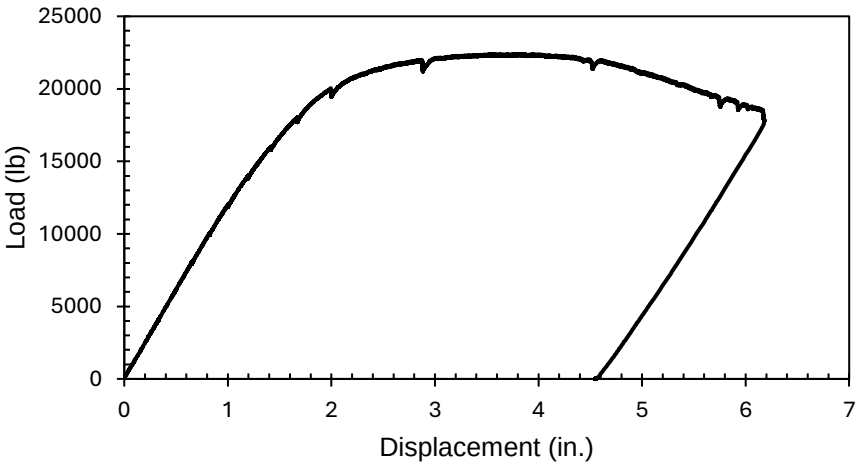

Figure 39. Load vs. displacement curve for specimen CF-2

A local buckling failure occurred in the steel pipe on the south side of the footing, but the same failure was not observed on the north side, as shown in Figure 40. The initial crack in the footing was observed at approximately 8 kips, and the initial visible separation at the interface between the steel pipe and footing on the north and south sides of specimen CF-2 also started at a load of 8 kips.

(a) *(b)*

Figure 40. Steel pipe at the (a) north side and (b) south side of the footing at failure for specimen CF-2

The relative horizontal displacement between the footing and the steel pipe on the tension side of the pipe exhibited different behaviors on the north and south sides of specimen CF-2 after reaching a load of 22.2 kips. The relative horizontal displacement notably increased after reaching that load on the south side. However, on the north side, the relative displacement remained relatively constant until the test was stopped, as illustrated in Figure 41. This indicates that the location of the failure was on the south side of the specimen. The maximum horizontal displacement, measured by the bottom LVDT, reached 0.1 in. with a corresponding maximum strain of 0.022 in

the steel pipe on the north side of the specimen. On the other hand, the maximum horizontal deflection was 0.3 in. with a corresponding maximum strain of 0.031 in the pipe on the south side. Strain on the tension side of both the north and south side pipes exceeded the theoretical yield strain of the steel pipe, which was determined to be 0.0018. Figure 42 presents the load vs. strain curve for both sides of specimen CF-2. As loading was continued after reaching the peak load, the south side exhibited an increase in the horizontal displacement and an increase in the strain up to a load of 20 kips. Then, the strain exhibited a drop from 0.031 to 0.025 which suggests a potential discontinuity in the connection on the south side of specimen CF-2. Although there may have been a loss of bond, the steel pipe on the south side surpassed its theoretical flexural strength, and local buckling failure occurred in the pipe at failure as evident in Figure 40-b. This suggests that the embedment length was sufficient to develop the full strength of the steel pipe and footing despite the fact that the pipe was slipping relative to the footing.

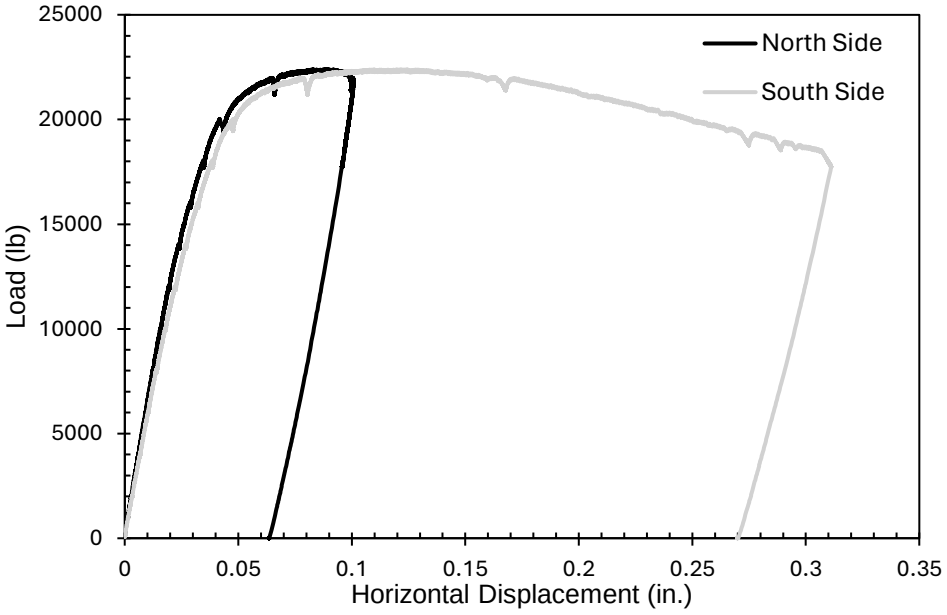

Figure 41. Load vs. horizontal displacement curve for specimen CF-2

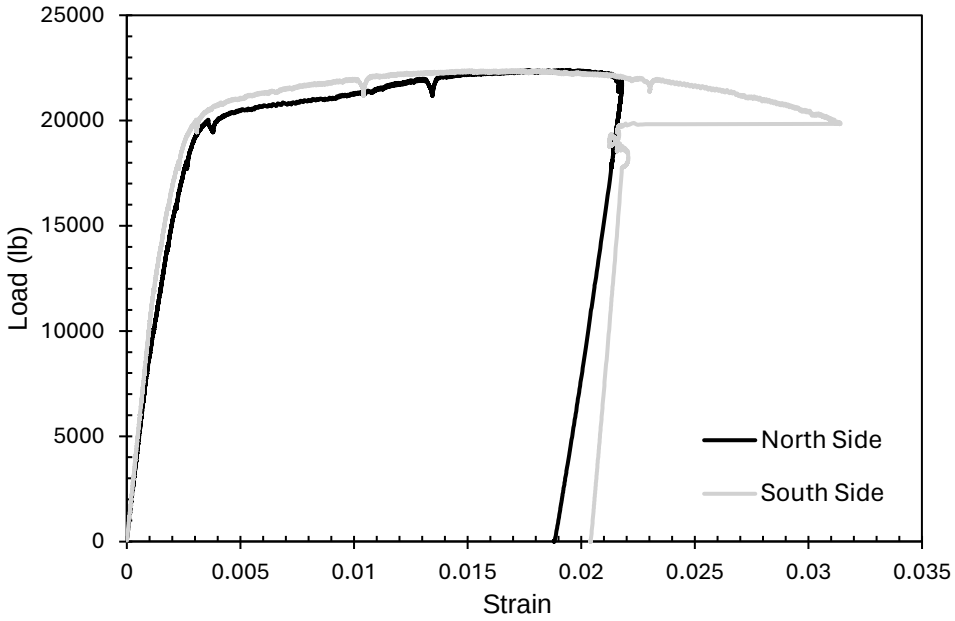

Figure 42. Load vs. strain curve for specimen CF-2

To obtain a closer value of the actual horizontal displacement, the elongation that occurred in the tension side of the pipe was taken into consideration. This elongation was calculated by multiplying the measured strain by the distance to the location of the LVDT on the pipe relative to the surface of the footing. This elongation was then subtracted from the measured horizontal displacement in order to have corrected values of the displacement. Figure 43 presents the load vs. corrected horizontal displacement curve for both sides of specimen CF-2. The north displacement showed a decrease after reaching approximately 20 kips. This decrease suggests that the pipe kept elongating with having a constant measured horizontal displacement. Simultaneously, the trend of the south corrected horizontal displacement was similar to the uncorrected one but with a smaller 0.24 in. maximum displacement. Although the pipe of the south side exhibited local buckling, there was likely a loss of frictional resistance between the pipe and concrete and steel relaxation occurred, as indicated by the horizontal displacement magnitude. The trend of the corrected graphs was similar for this specimen and other specimens compared to their respective original graphs.

Thus, the cleaner original graphs were used to evaluate the failure mechanism instead of the corrected graphs.

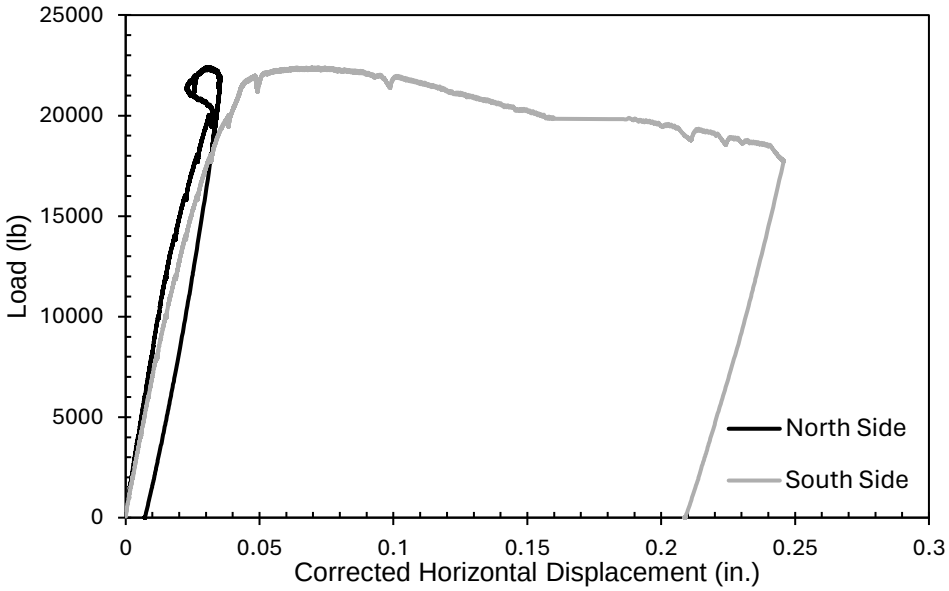

Figure 43. Load vs. corrected horizontal displacement curve for specimen CF-2

The south side strain behavior was further analyzed to understand the significant observed drop in the strain. Since it was not clear how the measured strain and measured horizontal displacements were related, strain vs time and corrected horizontal displacement vs time graphs were created to evaluate the occurrence of events in the specimen response, as shown in Figure 44 and Figure 45. From the graphs, the strain and corrected horizontal displacement increased with time until the strain reached 0.031. Then, the strain dropped to 0.024 in approximately 2 seconds, whereas the displacement continued to increase with time. After that, strain fluctuated (increased and decreased) over time while the displacement increased. This again suggests a potential discontinuity in the connection on the south side of specimen CF-2 or a potential malfunction in the strain gauge.

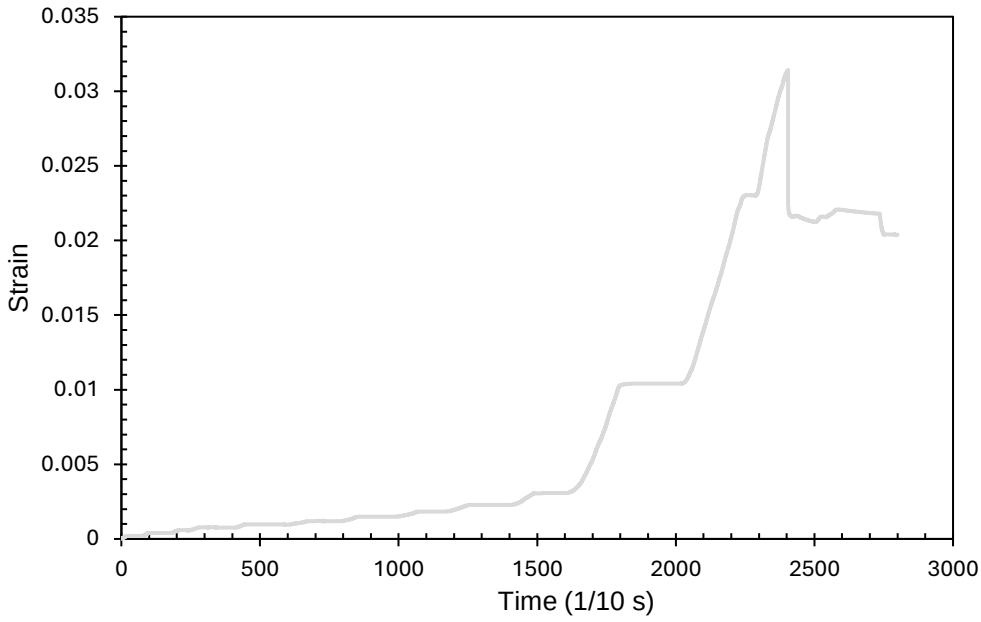

Figure 44. Strain vs. time curve for specimen CF-2

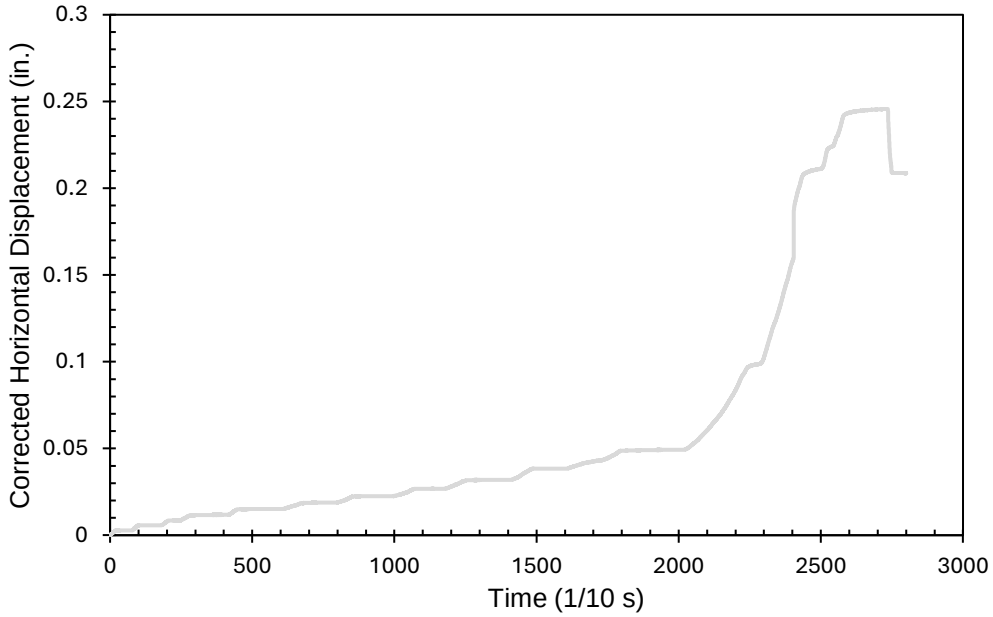

Figure 45. Corrected horizontal displacement vs. time curve for specimen CF-2

4.3 Column-Footing Specimen 3

Specimen CF-3 made with normal strength concrete and a $1.6D_i$ embedment was tested as a simple beam with an 18 ft span length as described in Section 3.5.1. Specimen CF-3 specifications and properties are described in Table 4 in Section 3.3.1.

Specimen CF-3 failed due to the steel pipe pulling out (or slipping) from one side of the footing at a maximum load of approximately 19 kips and the test was stopped at a maximum deflection of 3.7 in., as illustrated in Figure 46. The test was stopped at that deflection instead of going to the same limit as the other specimens due to the severity of the damage to the footing. The moment at the interface corresponding to the maximum load was calculated to be 66.4 kip-ft, which did not exceed the calculated flexural strength of the pipe: 68 kip-ft. This suggests that the connection was not sufficient to develop the full strength of the steel pipe with normal strength concrete at an embedment length of $1.6D_i$. As shown from the load-displacement curve in Figure X5, the specimen exhibited a significant load drop after reaching the maximum load, which is indicative of a pullout failure. The specimen initially exhibited a linear load-displacement behavior, followed by a nonlinear behavior leading to a peak load post-cracking in the footing, and then a sudden significant loss of load carrying capacity. The pullout failure occurred on the north side of the specimen and no damage was observed on the south side, as shown in Figure 47. After the steel pipe started pulling out of the footing, severe damage to the footing occurred on the north side of the specimen corresponding to the location of the pullout failure. The initial crack in the footing was observed at approximately10 kips, and initial visible separation at the interface between the steel pipe and footing on the north and south side of specimen CF-3 was also observed at a load of 10 kips.

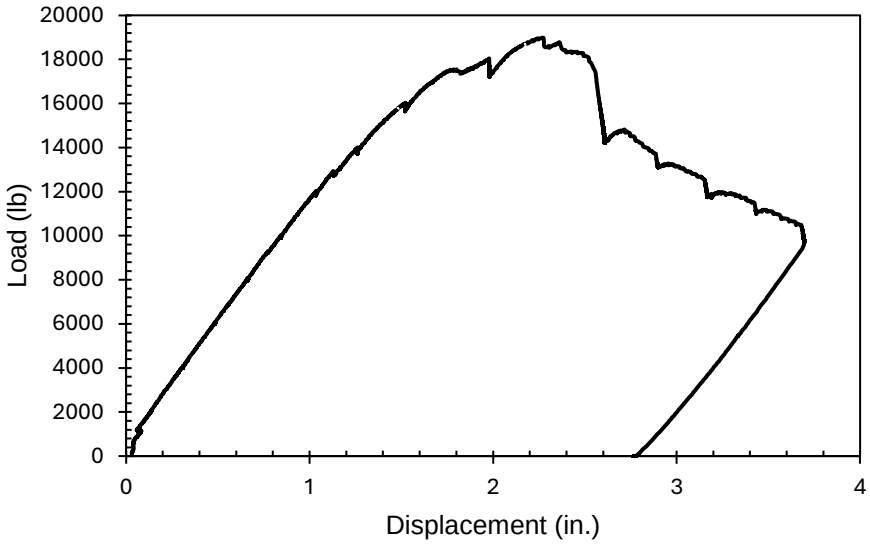

Figure 46. Load vs. displacement curve for specimen CF-3

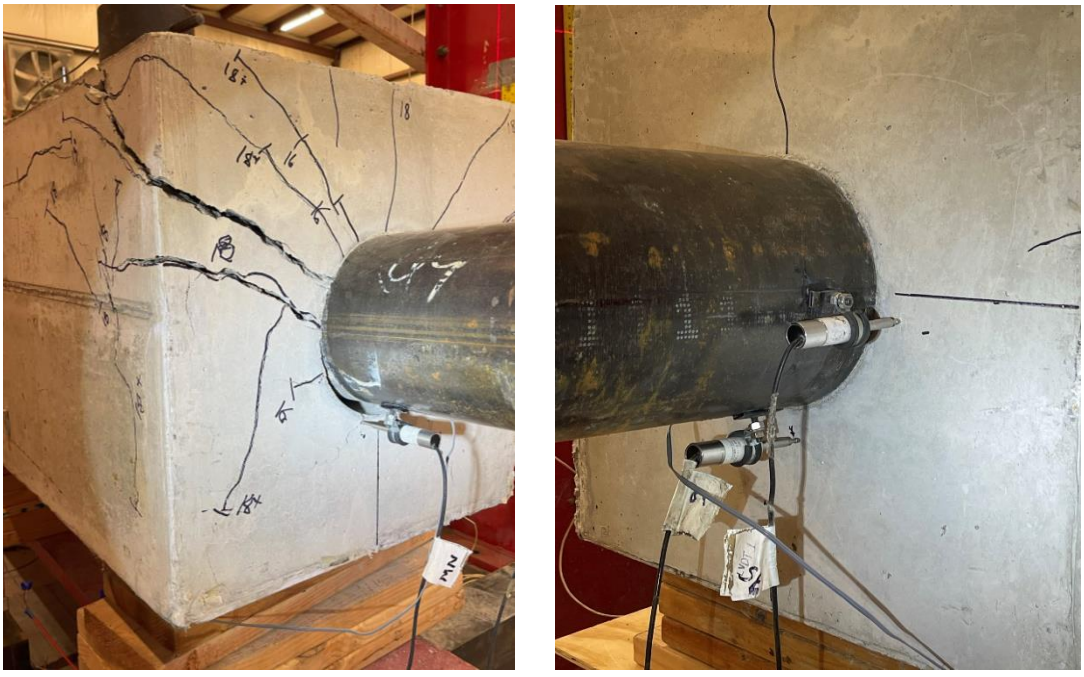

(a) *(b)*

Figure 47. Steel pipe at the (a) north side and (b) south side of the footing at failure for specimen CF-3

The relative horizontal displacement between the footing and steel pipe on the tension side of the pipe exhibited a similar linear behavior on each end of specimen CF-3 until reaching a load of 17 kips. However, the horizontal displacement on each end of specimen CF-3 exhibited different

behaviors after reaching that load. On the south side, the horizontal displacement continued to increase in a linear fashion until peak load, whereas on the north side, the increase in relative displacement was non-linear and notable, as shown in Figure 48. The maximum horizontal displacement on the north side, measured by the bottom LVDT, was 0.5 in. with a corresponding maximum strain of 0.0026 on the tension side of the steel pipe. However, on the south side, the maximum horizontal deflection was 0.05 in. with a maximum strain of 0.0070. Strains on the tension side of both the north and south side pipes exceeded the theoretical yield strain of the steel pipe, determined to be 0.0018. Figure 49 presents the load vs. strain curve for both sides of specimen CF-3. The footing exhibited significant diagonal cracks on the north side of the specimen. This cracking can be attributed to the pullout failure that occurred at the connection. A few cracks started widening as the horizontal displacement increased. Visual inspection at that time indicated that the specimen potentially exhibited concrete breakout failure in the footing after the pullout failure occurred on the north side. The relative horizontal displacement on the north side notably increased after a significant load drop occurred after reaching 17.5 kips. Loading continued with increasing relative horizontal deflection but decrease in measured load, while the strain on the tension side of the steel remained relatively constant until the test was stopped. This implies a discontinuity in load transfer within the structural system which allowed a relaxation of stress in the steel pipe. Simultaneously, the horizontal displacement and strain remained constant on the south side after reaching the peak load, even as loading continued with increasing deflection and decreasing measured load.

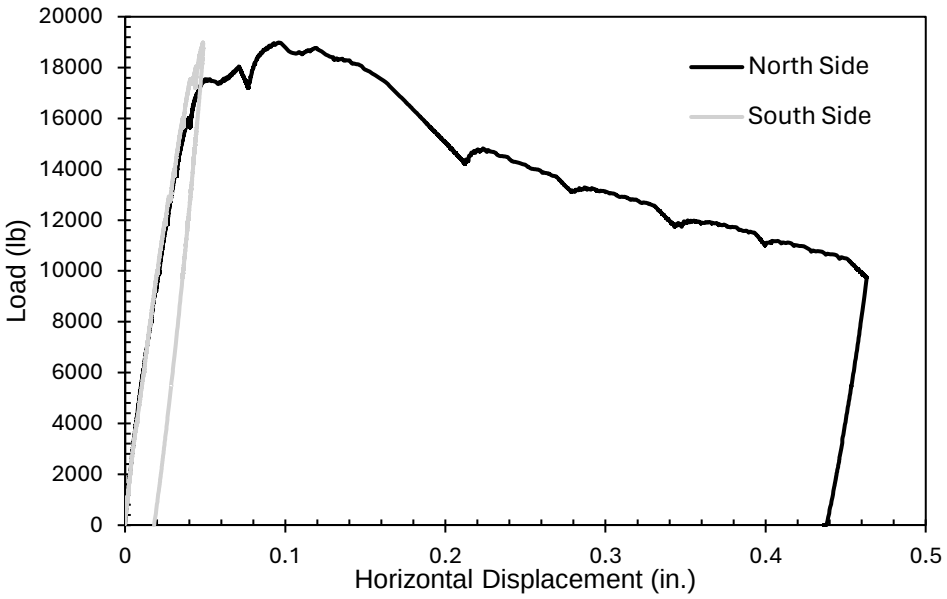

Figure 48. Load vs. horizontal displacement curve for specimen CF-3

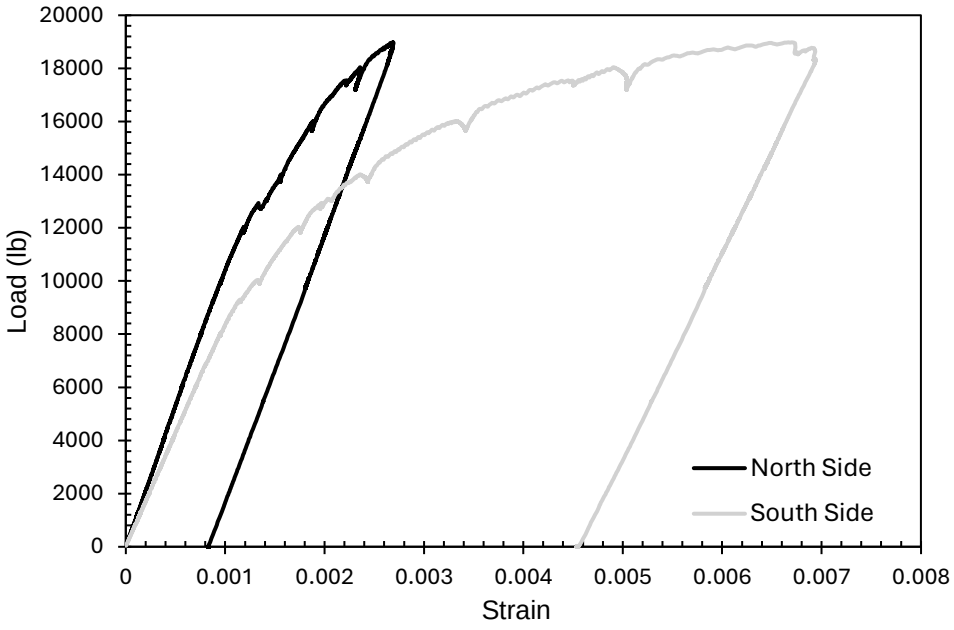

Figure 49. Load vs. strain curve for specimen CF-3

4.4 Column-Footing Specimen 4

Specimen CF-4 made with normal strength concrete and a $1.8D_i$ embedment was tested as a simple beam with an 18 ft span length as described in Section 3.5.1. Specimen CF-3 specifications and properties are described in Table 4 in Section 3.3.1.

The specimen failed due to the steel pipe buckling locally at a maximum load of 21 kips and was taken to a maximum deflection of 5.5 in., as shown in Figure 50. The moment at the interface corresponding to the maximum load was calculated to be 72.5 kip-ft, exceeding the calculated flexural strength of the pipe: 68 kip-ft. This indicates that the connection developed the full strength of the pipe with a normal-strength concrete footing and an embedment length of $1.8D_i$. Based on the load-displacement curve, the specimen exhibited an initial linear load-displacement behavior, followed by a nonlinear behavior leading to a peak load post-cracking in the footing and ultimately load-sustaining behavior. As loading was continued beyond the maximum load, it was observed that the specimen exhibited some gradual load loss, while vertical deflection continued to increase until the specimen was considered failed and the test was stopped. This load loss may be a result of loading equipment limitations rather than a true representation of behavior.

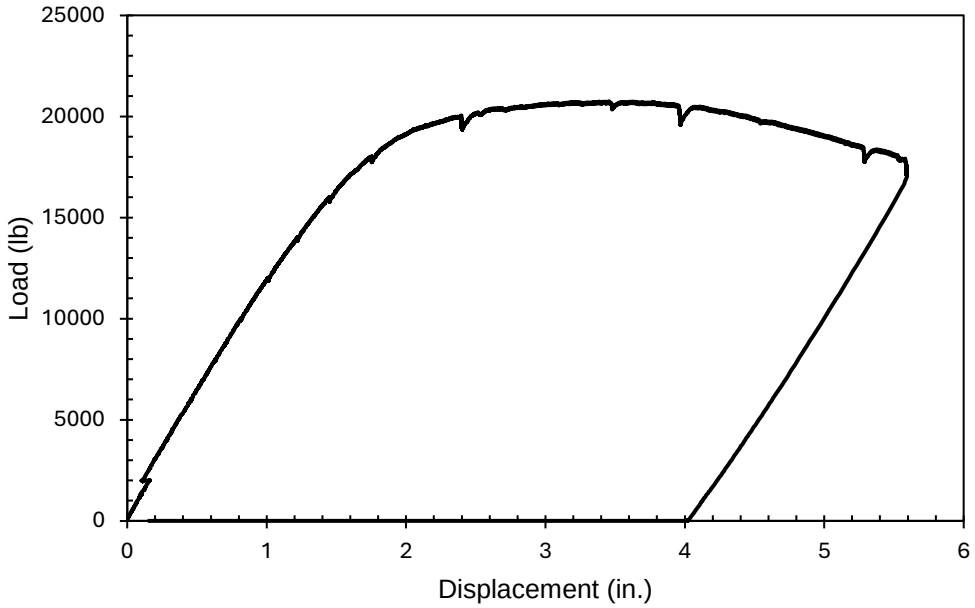

Figure 50. Load vs. displacement curve for specimen CF-4

A local buckling failure occurred in the steel pipe on the north side of the footing, but the same failure was not observed on the south side, as shown in Figure 51. The initial crack in the footing was observed at approximately 10 kips, and the initial visible separation at the interface between the steel pipe and footing on the north and south sides of specimen CF-4 was observed at a load of 6 kips.

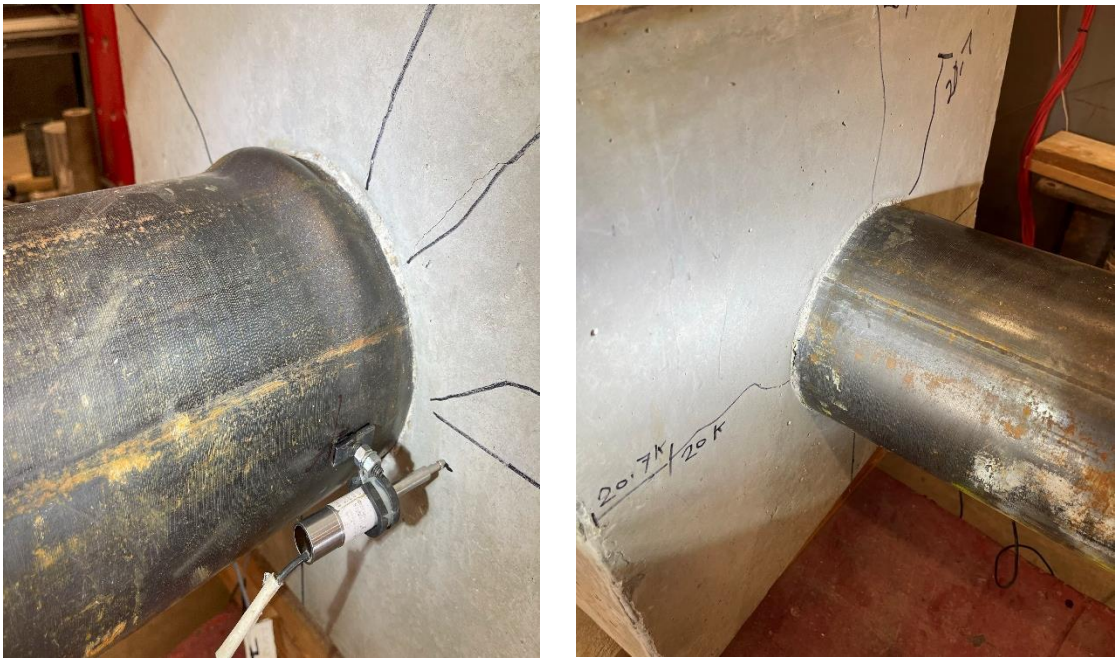

(a) *(b)*

Figure 51. Steel pipe at the (a) north side and (b) south side of the footing at failure for specimen CF-4

The relative horizontal displacement between the footing and steel pipe on the tension side of the pipe exhibited a similar linear behavior on each end of specimen CF-4 until reaching a load of 18 kips, then the horizontal displacement exhibited a notable increase up to 20 kips. However, the horizontal displacement on each end exhibited different behaviors after reaching that load. The relative horizontal displacement increased after reaching that load on the north side but remained relatively constant on the south side, as illustrated in Figure 52. This indicates that the location of the failure was on the north side of the specimen. The LVDT on the tension side of the pipe on the north side fell off the pipe during testing after the specimen reached 5.5 in. of vertical deflection. This resulted in the stopping of data collection for that LVDT, and therefore, an interruption at the end of the curve. The maximum horizontal displacement, measured by the bottom LVDT, reached 0.25 in. with a corresponding maximum strain of 0.031 in the steel pipe on the north side of the specimen. On the other hand, the maximum horizontal deflection was 0.08 in. with a corresponding

maximum strain of 0.012 in the pipe on the south side. Strain on the tension side of both the north and south side pipes exceeded the theoretical yield strain of the steel pipe, which was determined to be 0.0018. Figure 53 presents the load vs. strain curve for both sides of specimen CF-4. As loading was continued after reaching the peak load, the north side exhibited an increase in the horizontal displacement and an increase in the strain. This suggests that the embedment length was sufficient to develop the full strength of the steel pipe and footing despite the fact that the pipe was slipping relative to the footing. The pipe surpassed its theoretical flexural strength, and local buckling failure occurred in the pipe at failure.

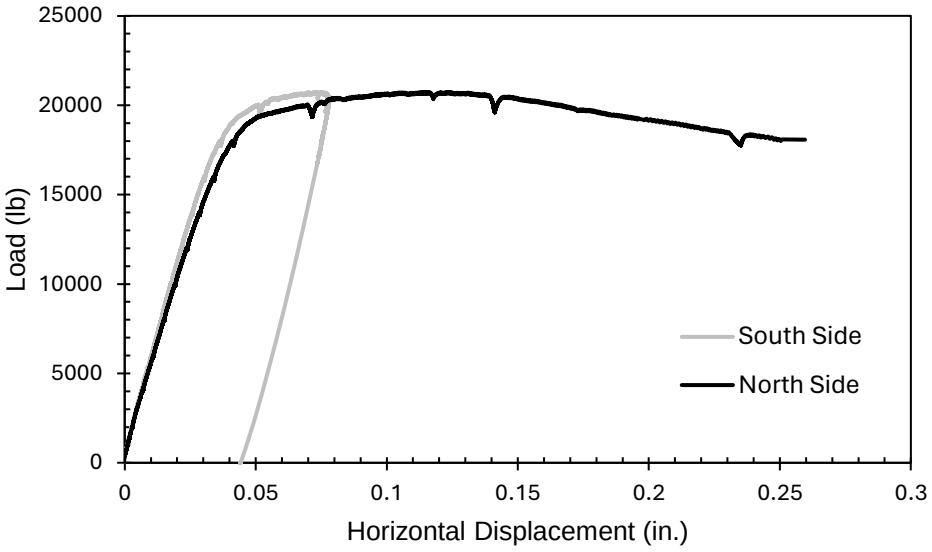

Figure 52. Load vs. horizontal displacement curve for specimen CF-4

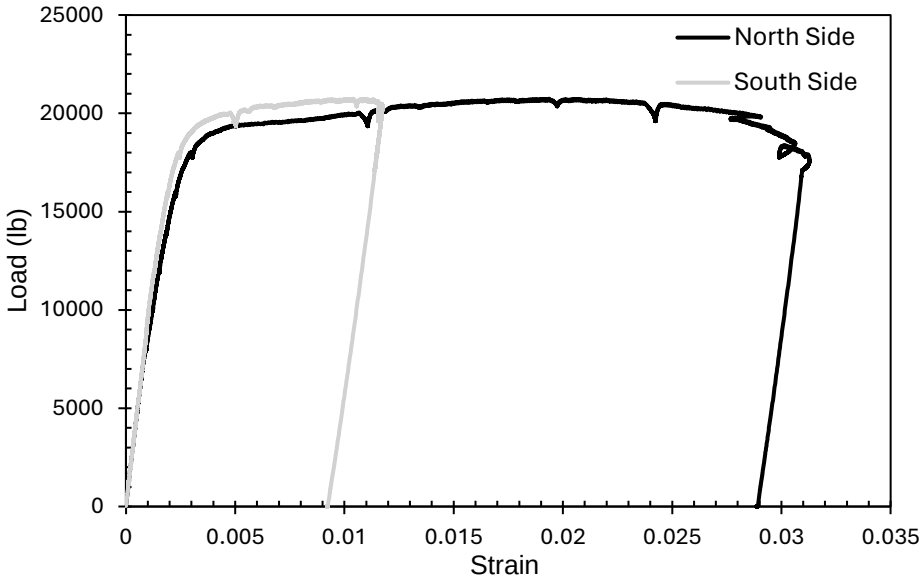

Figure 53. Load-strain curve for specimen CF-4

4.5 Column-Footing Specimen 5

Specimen CF-5 was made with normal-strength concrete and had an embedment length determined using methods identified in the literature review. The embedment length was calculated to be 14.5 in. ($1.68D_i$) using Equation 1, and the specimen was tested as a simple beam with an 18 ft span length as described in Section 3.5.1. Specimen CF-3 specifications and properties are described in Table 4 in Section 3.3.1.

Specimen CF-5 failed due to the steel pipe pulling out (or slipping) from one side of the footing at a maximum load of approximately 18 kips and the test was stopped at a maximum deflection of 5 in., as illustrated in Figure 54. The moment at the interface corresponding to the maximum load was calculated to be 63.4 kip-ft, which did not exceed the calculated flexural strength of the pipe: 68 kip-ft. This suggests that the connection was not sufficient to develop the full strength of the steel pipe with normal strength concrete and an embedment length calculated using Equation 1. As shown from the load-displacement curve in Figure 54, the specimen exhibited a significant load drop after reaching the maximum load, which is indicative of a pullout failure. The specimen

initially exhibited a linear load-displacement behavior, followed by a nonlinear behavior leading to a peak load post-cracking in the footing, and then a sudden significant loss of load carrying capacity. The pullout failure occurred on the south side of the specimen and no damage was observed on the north side, as shown in Figure 55. After the steel pipe started pulling out of the footing, severe damage to the footing occurred on the south side of the specimen corresponding to the location of the pullout failure. The initial crack in the footing was observed at approximately 12 kips, and initial visible separation at the interface between the steel pipe and footing on the north and south side of specimen CF-5 was observed at a load of 10 kips.

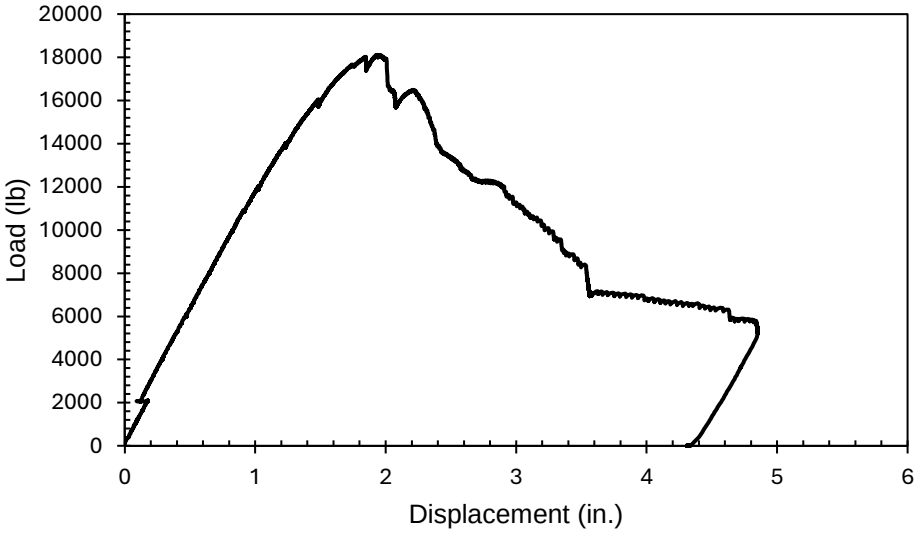

Figure 54. Load vs. displacement curve for specimen CF-5

(a) *(b)*

Figure 55. Steel pipe at the (a) north side and (b) south side of the footing at failure for specimen CF-5

The relative horizontal displacement between the footing and steel pipe on the tension side of the pipe exhibited a similar linear behavior on each end of specimen CF-5 until reaching a load of 16 kips. However, the horizontal displacement on each end of specimen CF-5 exhibited different behaviors after reaching that load. On the north side, the horizontal displacement continued to increase in a linear behavior until peak load, whereas on the south side, the increase in relative displacement was nonlinear and notable, as shown in Figure 56. The LVDT on the tension side of the pipe on the south side was removed for safety of the instrument after the specimen reached 4 in. of vertical deflection. This resulted in the stopping of data collection for that LVDT, and therefore, an interruption at the end of the curve. The maximum horizontal displacement on the south side, measured by the bottom LVDT, was 0.4 in. with a corresponding maximum strain of 0.0047 on the tension side of the steel pipe. However, on the north side, the maximum horizontal displacement was 0.04 in. with a maximum strain of 0.0021. Strains on the tension side of both

the north and south side pipes exceeded the theoretical yield strain of the steel pipe, determined to be 0.0018. Figure 57 presents the load vs. strain curve for both sides of specimen CF-5. The footing exhibited significant diagonal cracks on the south side of the specimen. This cracking can be attributed to the pullout failure that occurred at the connection. A few cracks started widening as the horizontal displacement increased. Visual inspection at that time indicated that the specimen potentially exhibited concrete breakout failure in the footing after the pullout failure occurred on the south side. The relative horizontal displacement on the south side notably increased after a significant load drop occurred upon reaching 18 kips. Loading continued with increasing relative horizontal deflection but decreasing measured load, while the strain on the tension side of the steel remained relatively constant after reaching the peak load. This implies a discontinuity in load transfer within the structural system which allowed a relaxation of stress in the steel pipe. Simultaneously, the horizontal displacement and strain remained relatively constant on the north side after reaching the maximum load, as loading continued with increasing deflection and decreasing measured load. This implies that damage in the specimen mainly concentrated on the south side after reaching 18 kips. This was further confirmed by visual inspection, as the specimen exhibited larger visible vertical deflection on the south side than the north side.

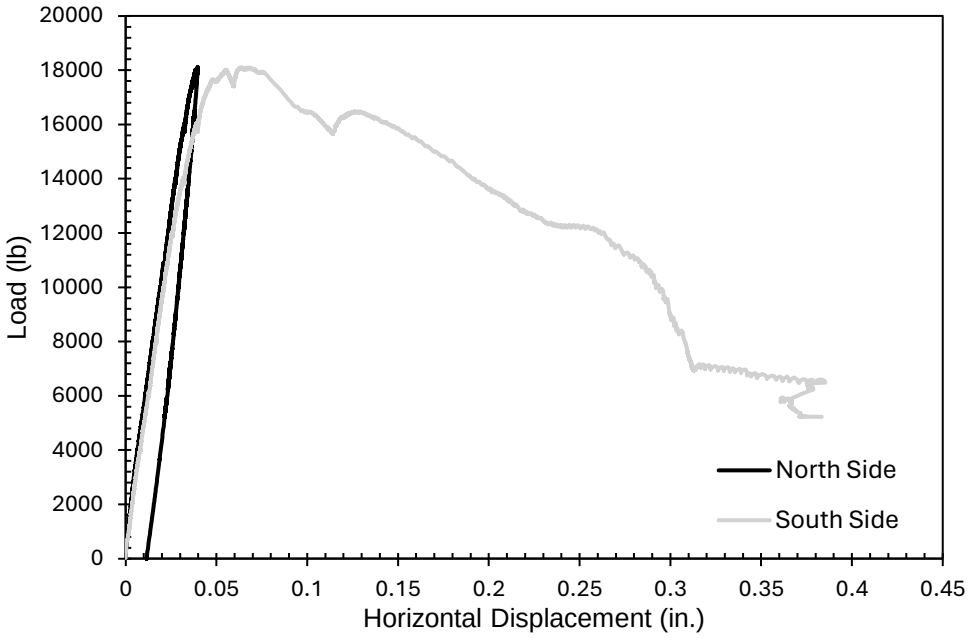

Figure 56. Load vs. horizontal displacement curve for specimen CF-5

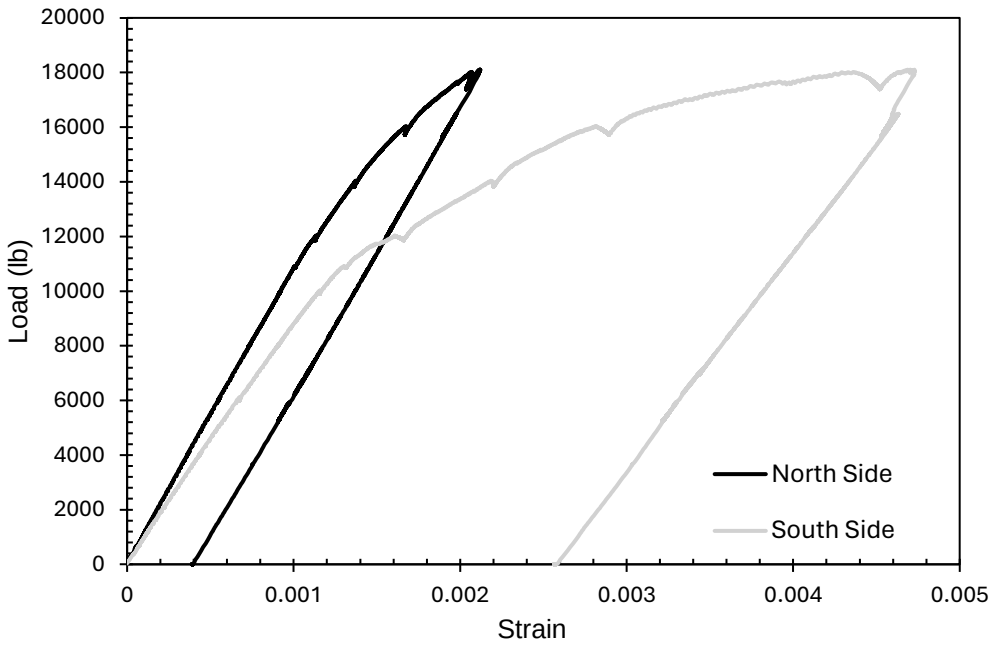

Figure 57. Load vs. strain curve for specimen CF-5

4.6 Column-Footing Specimen 6

Specimen CF-6 was made with normal strength concrete and had an embedment length of $1.6D_i$ with shear lugs welded to the embedded end of each steel pipe. The specimen was tested as a simple beam with an 18 ft span length as described in Section 3.5.1. Specimen CF-3 specifications and properties are described in Table 4 in Section 3.3.1.

Specimen CF-6 failed due to the concrete breaking out in the footing. This then led to the pipe pulling out from one side of the footing at a maximum load of approximately 21 kips and the test was stopped at a maximum deflection of 4.75 in., as illustrated in Figure 58. The test was stopped at that deflection due to the severity of the damage to the footing. The moment at the interface corresponding to the maximum load was calculated to be 74 kip-ft, which exceeded the calculated flexural strength of the pipe: 68 kip-ft. This suggests that the connection was sufficient to develop the full strength of the steel pipe with normal strength concrete and an embedment length of $1.6D_i$ with shear studs welded at the end of each steel pipe. As shown from the load-displacement curve in Figure 58, the specimen exhibited a significant load drop after reaching the maximum load, which corresponds to the concrete breakout failure. The specimen initially exhibited a linear load-displacement behavior followed by a nonlinear behavior leading to a peak load post-cracking in the footing, and then a sudden significant loss of load carrying capacity. The concrete breakout failure occurred on the south side of the specimen and little damage was observed on the north side, as shown in Figure 59. Severe pipe pullout occurred on the south side of the specimen due to concrete breakout failure. The initial crack in the footing was observed at approximately 14 kips, and the initial visible separation at the interface between the steel pipe and footing on the north and south side of specimen CF-6 was observed at a load of 8 kips.

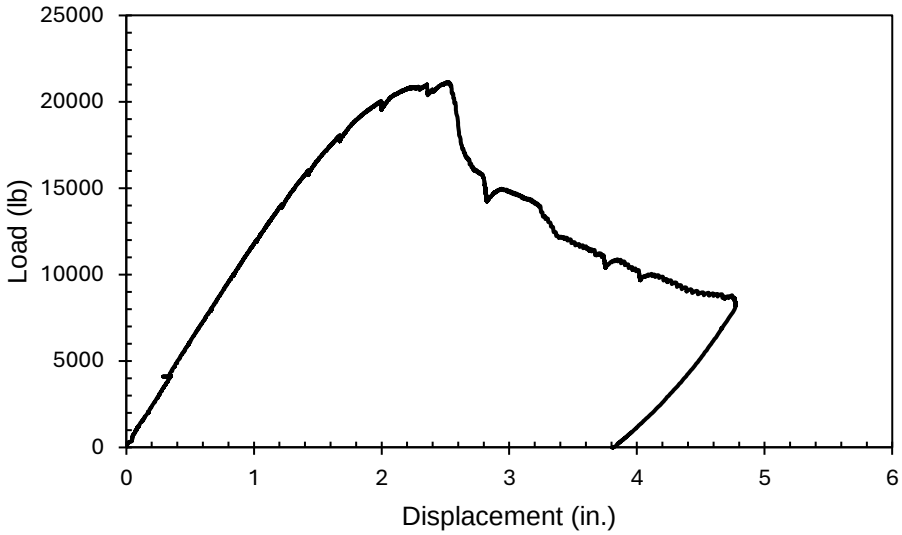

Figure 58. Load vs. displacement curve for specimen CF-6

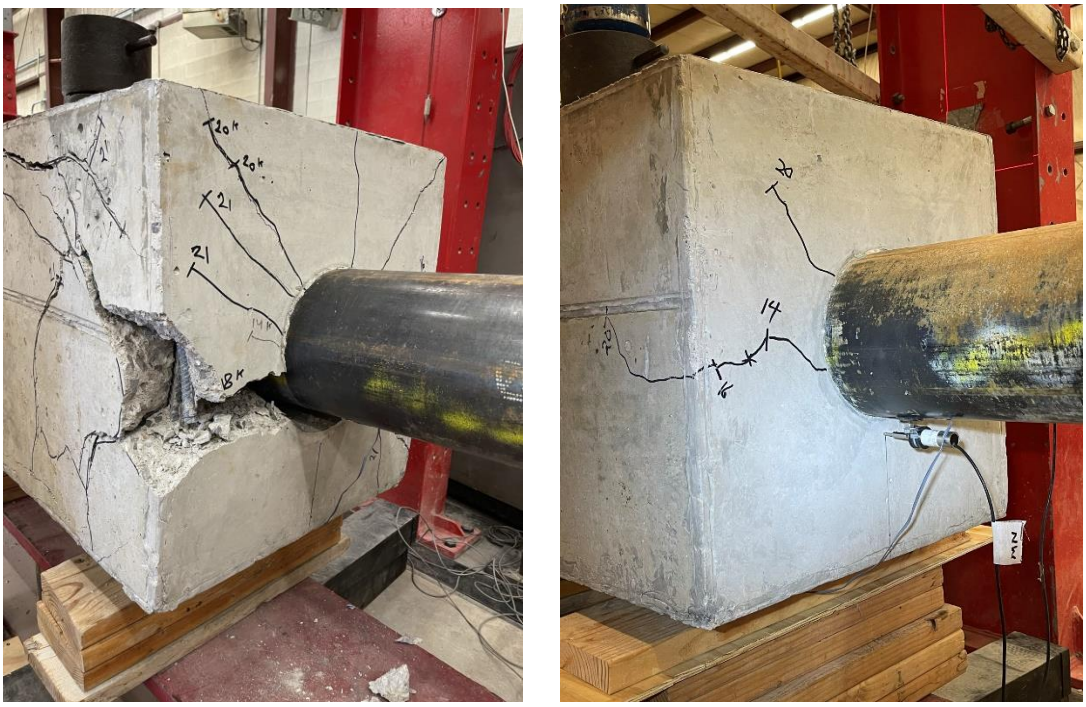

(a) *(b)*

Figure 59. Steel pipe at the (a) north side and (b) south side of the footing at failure for specimen CF-6

The relative horizontal displacement between the footing and steel pipe on the tension side of the pipe exhibited a similar linear behavior on each end of specimen CF-6 until reaching the peak load of 21 kips. However, the relative horizontal displacement significantly increased after reaching

that load on the south side but remained relatively constant on the north side, as illustrated in Figure 60. This indicates that the location of the failure was on the north side of the specimen. The LVDT on the tension side of the pipe on the south side was removed for safety of the instrument after reaching the maximum vertical deflection. This resulted in the stopping of data collection for that LVDT, and therefore, an interruption at the end of the curve. The maximum horizontal displacement, measured by the bottom LVDT, reached 0.064 in. with a corresponding maximum strain of 0.0062 in the steel pipe on the north side of the specimen. On the other hand, the maximum horizontal deflection was 0.70 in. with a corresponding maximum strain of 0.0045 in the pipe on the south side. Strain on the tension side of both the north and south side pipes exceeded the theoretical yield strain of the steel pipe, which was determined to be 0.0018. Figure 61 presents the load vs. strain curve for both sides of specimen CF-6. As loading continued after reaching the peak load, the south side exhibited an increase in the horizontal displacement but a relatively constant strain. This suggests that the pipe was slipping relative to the footing and implies a discontinuity in load transfer within the structural system, which allowed a relaxation of stress in the steel pipe. Although pipe pullout occurred in the specimen after concrete breakout failure occurred, the pipe surpassed its theoretical flexural strength and there was visual evidence of footing failure.

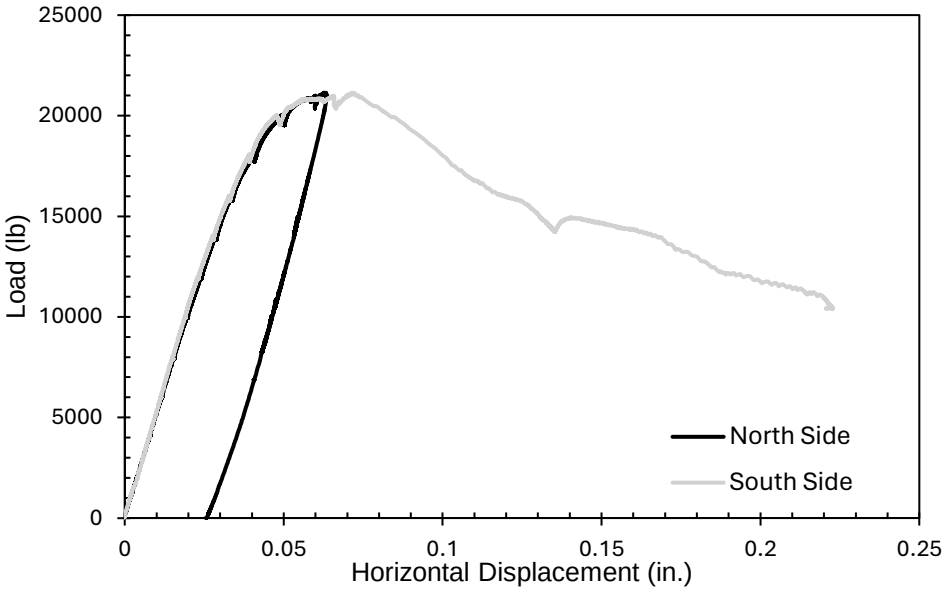

Figure 60. Load vs. horizontal displacement curve for specimen CF-6

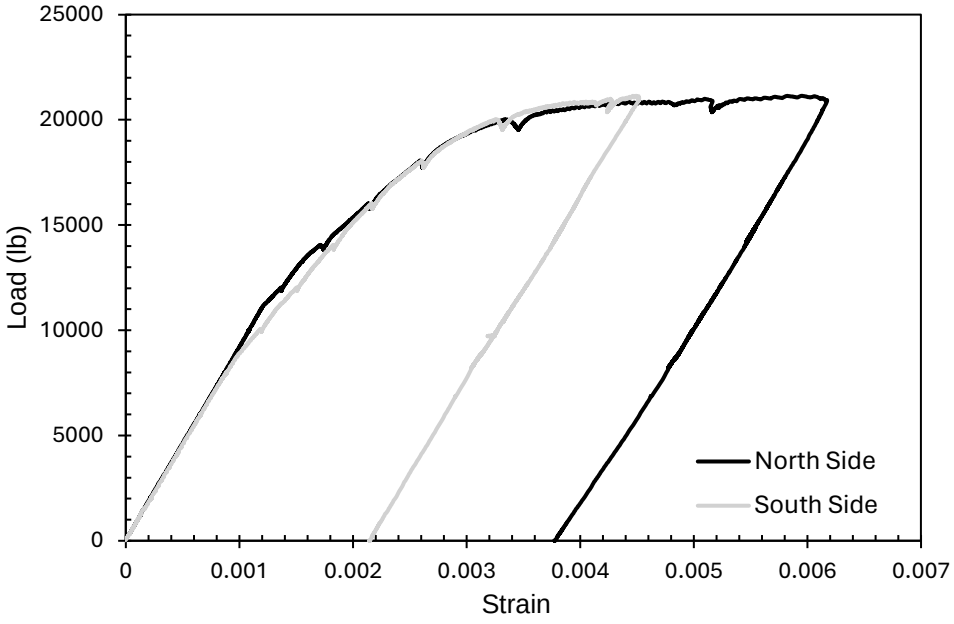

Figure 61. Load vs. strain curve for specimen CF-6

4.7 Column-Footing Specimen 7

Specimen CF-7 was made with normal strength concrete and had an embedment length of $1.6D_i$. The specimen was constructed with a 6.625 in. diameter steel pipe with a 0.25 in. thickness, resulting in a different diameter/thickness ratio compared to the other specimens. It was tested as a simple beam with an 18 ft span length as described in Section 3.5.1. Specimen CF-3 specifications and properties are described in Table 4 in Section 3.3.1.

The specimen failed due to yielding of the steel pipe on one side of the footing at a maximum load of approximately 12 kips and was taken to a maximum deflection of 7 in., as shown in Figure 62. The moment at the interface corresponding to the maximum load was calculated to be 41 kip-ft, exceeding the calculated flexural strength of the pipe: 35 kip-ft. This indicates that the connection developed the full strength of the pipe with a normal-strength concrete footing and an embedment length of $1.6D_i$. Based on the load-displacement curve, the specimen exhibited an initial linear load-displacement behavior, followed by a nonlinear behavior leading to a peak load post-cracking in the footing and ultimately load-sustaining behavior. As loading was continued beyond the maximum load, it was observed that the specimen exhibited minimal load loss while vertical deflection continued to increase until the specimen was considered failed and the test was stopped. The steel pipe yielding failure occurred on the north side of the specimen and no damage to the footing was observed on both sides, as shown in Figure 63. The initial crack in the footing was observed at approximately 10 kips, and the initial visible separation at the interface between the steel pipe and footing on the north and south sides of specimen CF-7 was also observed at a load of 10 kips.

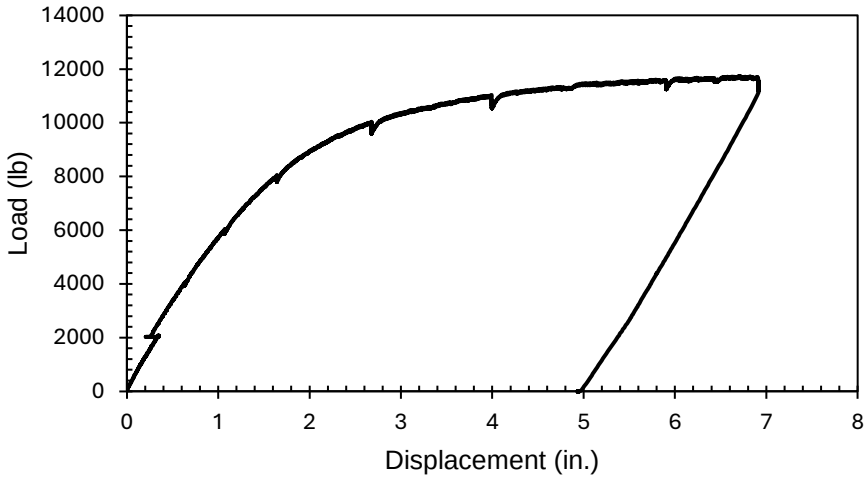

Figure 62. Load vs. displacement curve for specimen CF-7

. *(a).* *(b)*

Figure 63. Steel pipe at the (a) north side and (b) south side of the footing at failure for specimen CF-7

The relative horizontal displacement between the footing and steel pipe on the tension side of the pipe exhibited a similar linear behavior on each end of specimen CF-7 until reaching a load of 9.5

kips, then the horizontal displacement exhibited a notable increase up to the maximum load on each side. However, the magnitude of the horizontal displacement was larger on the north side than the south side, as illustrated in Figure 64. This indicates that the location of the failure was on the north side of specimen CF-7. The maximum horizontal displacement, measured by the bottom LVDT, reached 0.25 in. with a corresponding maximum strain of 0.031 in the steel pipe on the north side of the specimen. On the other hand, the maximum horizontal displacement was 0.08 in. with a corresponding maximum strain of 0.012 in the pipe on the south side. Strain on the tension side of both the north and south side pipes exceeded the theoretical yield strain of the steel pipe, which was determined to be 0.0018. Figure 65 presents the load vs. strain curve for both sides of specimen CF-7. As loading was continued after reaching the peak load, the horizontal displacement and strain on both sides of the specimen remained steady which suggests that the embedment length was sufficient to develop the full strength of the steel pipe and footing despite the fact that the pipe was slipping relative to the footing. The pipe surpassed its theoretical flexural strength with no visible damage to the footing on both sides.

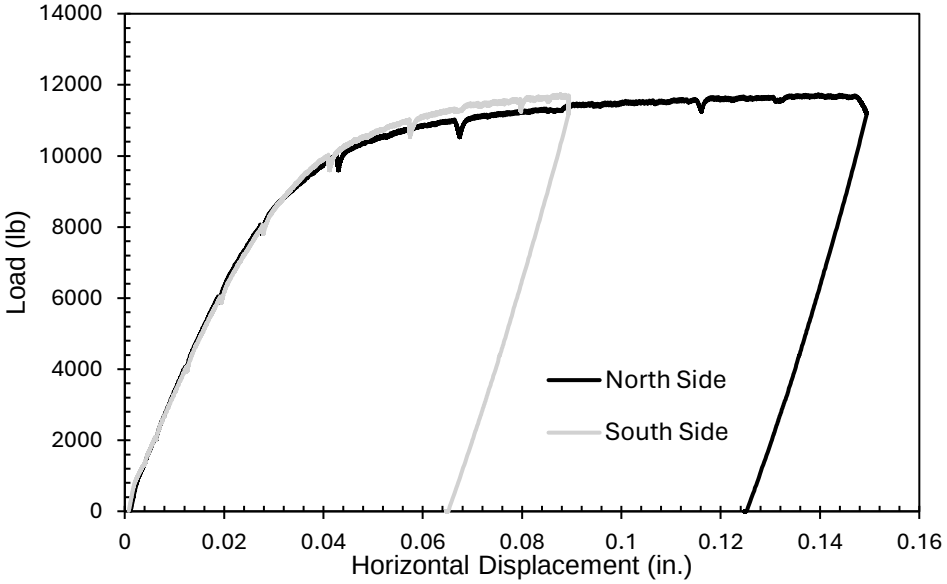

Figure 64. Load vs. horizontal displacement curve for specimen CF-7

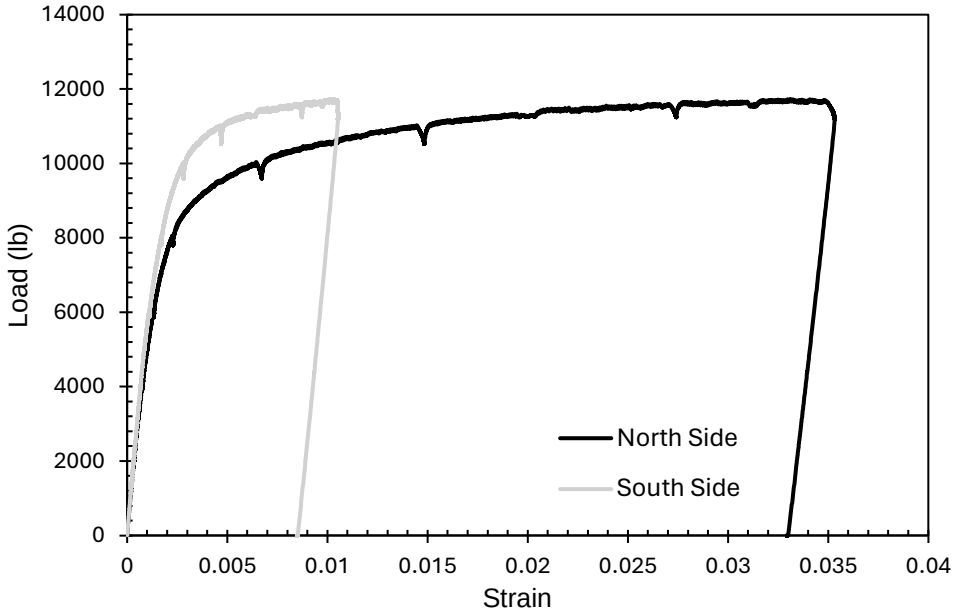

Figure 65. Load vs. strain curve for specimen CF-7

4.8 Column-Footing Specimen 8

Specimen CF-8 was made with normal strength concrete and a 1.4D_i embedment length within a socketed connection made with UHPC between the steel pipe and the concrete footing. The specimen was tested as a simple beam with an 18 ft span length as described in Section 3.5.1. Specimen CF-3 specifications and properties are described in Table 4 in Section 3.3.1.

The specimen failed due to the steel pipe buckling locally at a maximum load of 21 kips and was taken to a maximum deflection of 5.7 in., as shown in Figure 66. The moment at the interface corresponding to the maximum load was calculated to be 72.4 kip-ft, exceeding the calculated flexural strength of the pipe: 68 kip-ft. This indicates that the connection developed the full strength of the pipe with a normal-strength concrete footing, and an embedment length of 1.4D_i, within a UHPC socketed connection. Based on the load-displacement curve, the specimen exhibited an initial linear load-displacement behavior, followed by a nonlinear behavior leading to a peak load post-cracking in the footing and ultimately load-sustaining behavior. As loading was

continued beyond the maximum load, it was observed that the specimen exhibited some gradual load loss, while vertical deflection continued to increase until the specimen was considered failed and the test was stopped. This load loss may be a result of loading equipment limitations rather than a true representation of behavior.

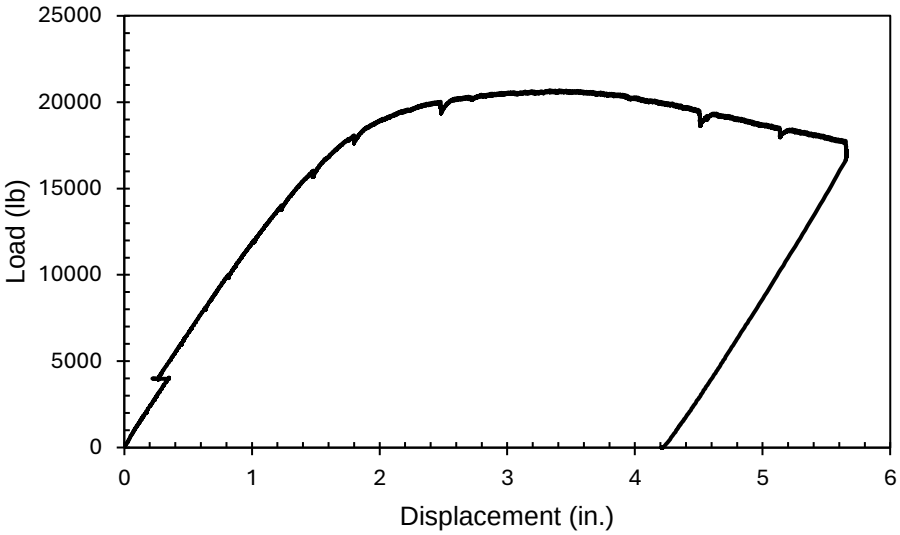

Figure 66. Load vs. displacement curve for specimen CF-8

A local buckling failure occurred in the steel pipe on the south side of the footing, but the same failure was not observed on the north side, as shown in Figure 67. The initial crack in the footing was observed at approximately 14 kips, and the initial visible separation at the interface between the steel pipe and footing on the north and south sides of specimen CF-8 was observed at a load of 10 kips.

. *(a).* *(b)*

Figure 67. Steel pipe at the (a) north side and (b) south side of the footing at failure for specimen CF-8

The relative horizontal displacement between the footing and steel pipe on the tension side of the pipe exhibited a similar linear behavior on each end of specimen CF-8 until reaching a load of 18 kips, then the horizontal displacement exhibited a notable increase up to 20 kips. However, the horizontal displacement on each end exhibited different behaviors after reaching that load. The relative horizontal displacement increased after reaching that load on the south side but remained relatively constant on the north side, as illustrated in Figure 68. This indicates that the location of the failure was on the south side of the specimen. The LVDT on the tension side of the pipe on the south side fell off the pipe during testing after reaching a 5 in. of vertical deflection. This resulted in the stopping of data collection for that LVDT, and therefore, an interruption at the end of the curve. The maximum horizontal displacement, measured by the bottom LVDT, reached 0.08 in. with a corresponding maximum strain of 0.0087 in the steel pipe on the north side of the specimen. On the other hand, the maximum horizontal deflection was 0.35 in. with a corresponding maximum strain of 0.030 in the pipe on the south side. Strain on the tension side of both the north and south

side pipes exceeded the theoretical yield strain of the steel pipe, which was determined to be 0.0018. Figure 69 presents the load vs. strain curve for both sides of specimen CF-8. As loading was continued after reaching the peak load, the south side exhibited an increase in the horizontal displacement and an increase in the strain. The strain dropped from 0.03 to 0.015 after reaching 20 kips which implies a potential discontinuity in the connection on the south side of specimen CF-8. This drop could also indicate that the strain gauge might have been damaged after failure. Although there may have been a loss of bond, the steel pipe on the south side exhibited local buckling as evident in Figure 67-b. The pipe surpassed its theoretical flexural strength, and local buckling failure occurred in the pipe at failure. This suggests that the embedment length was sufficient to develop the full strength of the steel pipe despite the fact that the pipe was slipping relative to the footing.

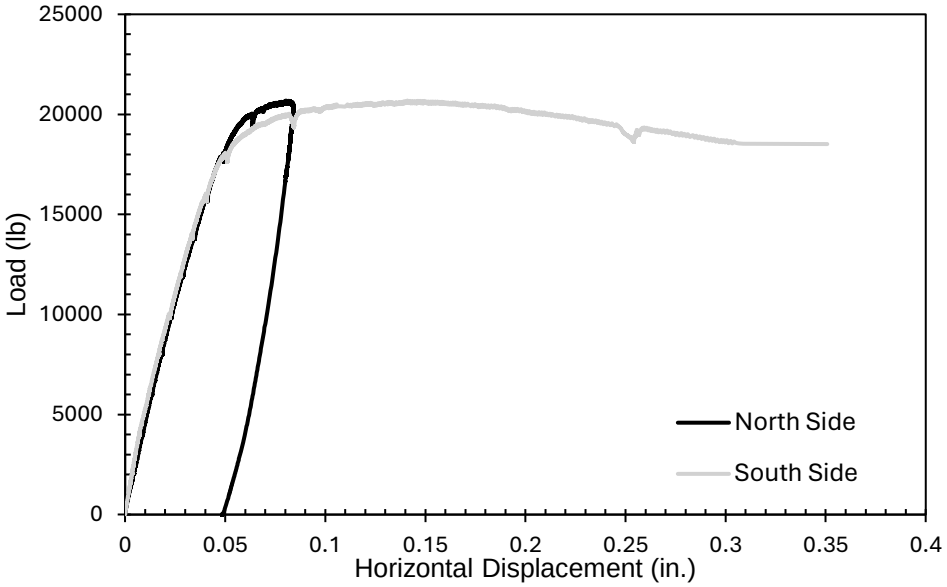

Figure 68. Load vs. horizontal displacement curve for specimen CF-8

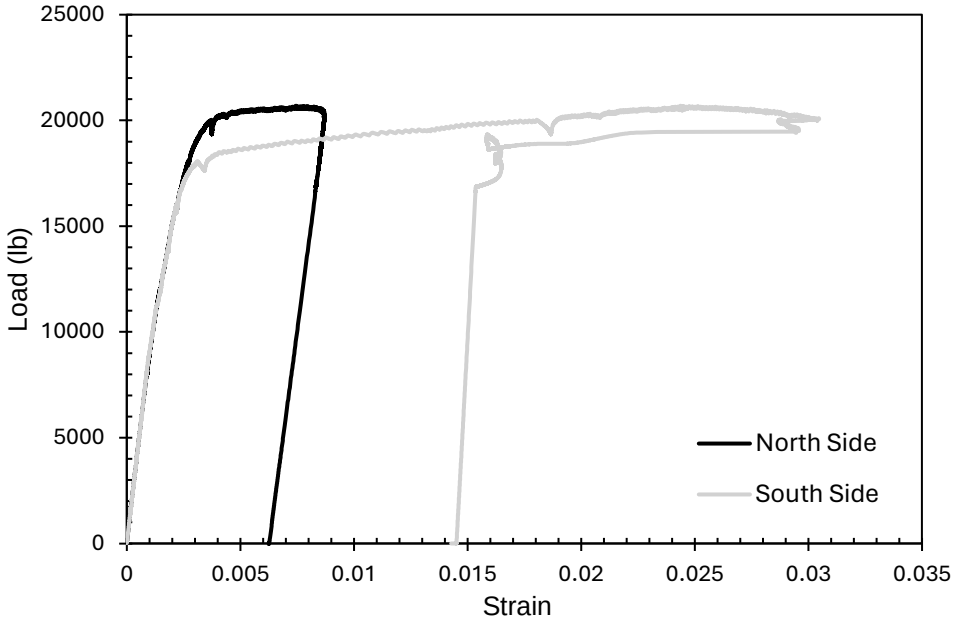

Figure 69. Load vs. strain curve for specimen CF-8

4.9 Column-Footing Specimen 9

Specimen CF-9 was made with normal strength concrete and a 1.8D_i embedment length within a socketed connection made with UHPC between the steel pipe and the concrete footing. The specimen was tested as a simple beam with an 18 ft span length as described in Section 3.5.1. Specimen CF-3 specifications and properties are described in Table 4 in Section 3.3.1.

The specimen failed due to the steel pipe buckling locally at a maximum load of 21 kips and was taken to a maximum deflection of 5.6 in., as shown in Figure 70. The moment at the interface corresponding to the maximum load was calculated to be 74.6 kip-ft, exceeding the calculated flexural strength of the pipe: 68 kip-ft. This indicates that the connection developed the full strength of the pipe with a normal-strength concrete footing, and an embedment length of 1.8D_i, within a UHPC socketed connection. Based on the load-displacement curve, the specimen exhibited an initial linear load-displacement behavior, followed by a nonlinear behavior leading to a peak load post-cracking in the footing and ultimately load-sustaining behavior. As loading was

continued beyond the maximum load, it was observed that the specimen exhibited some gradual load loss, while vertical deflection continued to increase until the specimen was considered failed and the test was stopped. This load loss may be a result of loading equipment limitations rather than a true representation of behavior.

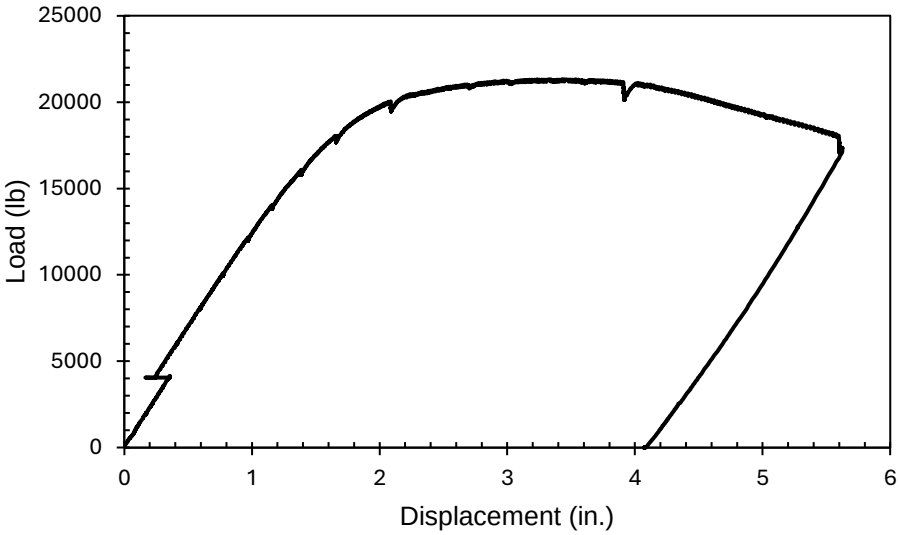

Figure 70. Load vs. displacement curve for specimen CF-9

A local buckling failure occurred in the steel pipe on the south side of the footing, but the same failure was not observed on the north side, as shown in Figure 71. No cracks in the footing were observed throughout testing, and the initial visible separation at the interface between the steel pipe and footing on the north and south sides of specimen CF-9 was observed at a load of 12 kips.

(a) *(b)*

Figure 71. Steel pipe at the (a) north side and (b) south side of the footing at failure for specimen CF-9

The relative horizontal displacement between the footing and steel pipe on the tension side of the pipe exhibited a similar linear behavior on each end of specimen CF-9 until reaching approximately the maximum load. However, the horizontal displacement on each end exhibited different behaviors after reaching approximately the maximum load. The relative horizontal displacement increased after reaching that load on the south side but remained relatively constant on the north side, as illustrated in Figure 72. This indicates that the location of the failure was on the south side of the specimen. The maximum horizontal displacement, measured by the bottom LVDT, reached 0.07 in. with a corresponding maximum strain of 0.023 in the steel pipe on the north side of the specimen. On the other hand, the maximum horizontal deflection was 0.25 in. with a corresponding maximum strain of 0.012 in the pipe on the south side. Strain on the tension side of both the north and south side pipes exceeded the theoretical yield strain of the steel pipe, which was determined to be 0.0018. Figure 73 presents the load vs. strain curve for both sides of specimen CF-9. As loading was continued after reaching the peak load, the south side exhibited

an increase in the horizontal displacement and an increase in the strain. The strain decreased after reaching peak load which implies a potential discontinuity in the connection on the south side of specimen CF-9. This drop could also indicate that the strain gauge might have been damaged after failure. However, it should be noted that unusual behavior was noted in the south side strain data that may be indicative of the gauge being damaged after reaching peak load. Although there may have been a loss of bond, the steel pipe on the south side exhibited local buckling as evident in Figure 71-b. The pipe surpassed its theoretical flexural strength, and local buckling failure occurred in the pipe at failure. This suggests that the embedment length was sufficient to develop the full strength of the steel pipe and footing despite the fact that the pipe was slipping relative to the footing.

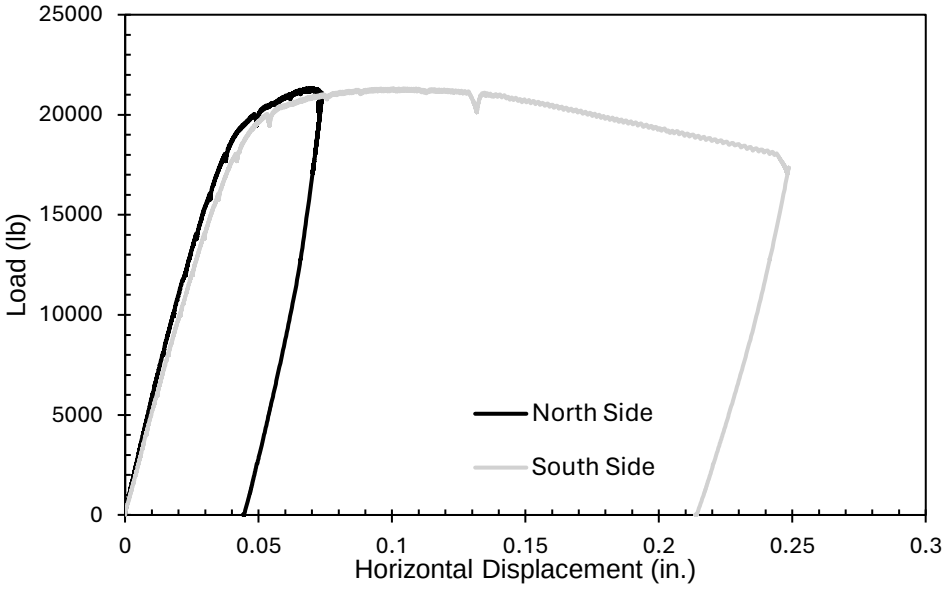

Figure 72. Load vs. horizontal displacement curve for specimen CF-9

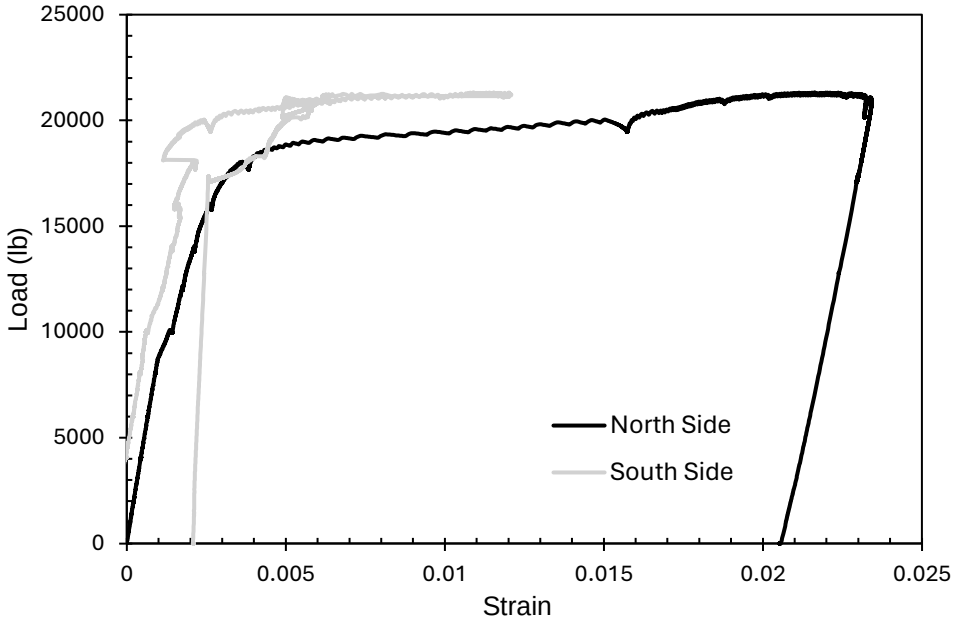

Figure 73. Load vs. strain curve for specimen CF-9

5. Discussion/Comparison

This section provides a summary of the small-scale column footing connection specimen results, as shown in Table 10. It also presents several comparisons based on the respective parameters evaluated in order to suggest HC-FCS column-footing connection design recommendations. Throughout this section, the discussion of horizontal displacement and strain on the tension side of the steel pipes only focuses on the failure sides of the specimens.

Table 10. Results summary for the small-scale column footing connection specimens

Specimen	Maximum Load (lb)	Maximum Moment at Interface, M_{max} (kip-ft)	M_{max}/M_n of the Pipe	Maximum Deflection (in.)	Failure Side	Failure Type
CF-1	21,050	74.0	1.09	5.63	Both	Local buckling
CF-2	22,400	78.0	1.22	6.00	South	Local buckling
CF-3	18,620	66.4	0.98	3.70	North	Pullout
CF-4	20,740	72.5	1.07	5.59	North	Local buckling
CF-5	18,110	63.4	0.93	4.85	South	Pullout
CF-6	21,140	74.0	1.09	4.77	South	Concrete breakout
CF-7	11,730	41.0	1.17	6.92	North	Yielding
CF-8	20,700	72.4	1.06	5.65	South	Local buckling
CF-9	21,320	74.6	1.10	5.62	South	Local buckling

5.1 Specimens CF-3, CF-4 and CF-5

The comparison of specimens CF-3, CF-4, and CF-5 shows the behavior of three specimens with the same diameter pipe and different embedment lengths: $1.6D_i$, $1.8D_i$, and $1.68D_i$ (the minimum embedment length derived from the literature review). These specimens were all cast monolithically with normal-strength concrete. As shown in the load vs. displacement curves in

Figure 74, specimen CF-4 exhibited a load-sustaining behavior after reaching the peak load, while specimens CF-3 and CF-5 experienced a sudden drop in load after reaching their respective peak loads. This implies that the embedment lengths of the steel pipes in specimens CF-3 and CF-5 were not sufficient to develop the load-sustaining behavior exhibited in specimen CF-4. The minimum embedment length derived from the literature review ($1.68D_i$) and $1.6D_i$ resulted in the steel pipe on the south side of the respective specimens pulling out of the footing, leading to a loss of bond between the footing and steel pipe. Specimen CF-5 did not reach the maximum load obtained for specimen CF-3, but the vertical deflection was taken to 4.85 in., with less visual damage to the footing. The maximum load for specimen CF-4 exhibited a more drastic drop compared to the load drop for specimen CF-3.

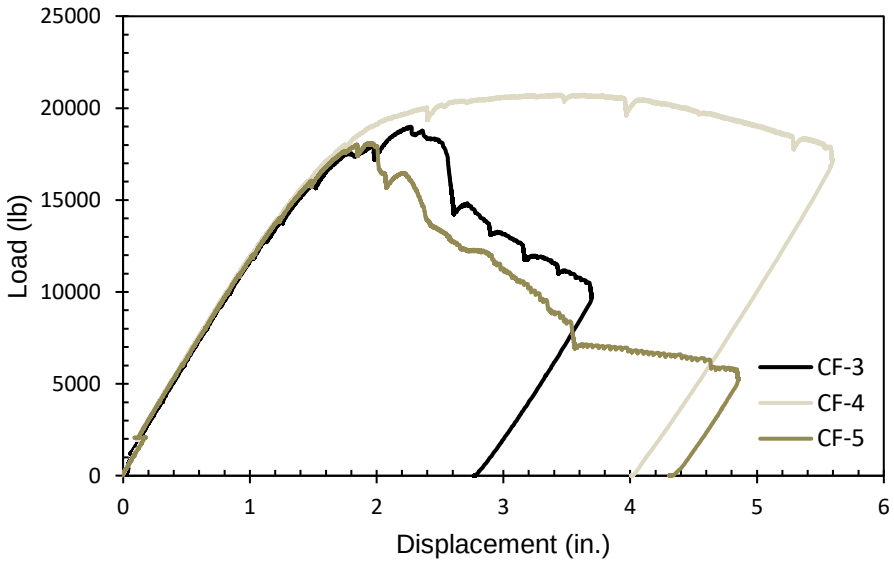

Figure 74. Load vs. displacement curves for specimens CF-3, CF-4, and CF-5

In terms of horizontal displacement, specimens CF-3 and CF-5 exhibited larger displacements than specimen CF-4, as shown in Figure 75. Although the test of specimen CF-3 was stopped at a vertical deflection of 3.70 in., the maximum horizontal displacement was the largest among all the specimens. As observed from the load vs. strain curves in Figure 76, the maximum strain on the

tension side of the steel pipe was 0.0047 and 0.0026 for specimens CF-5 and CF-3, respectively. This higher strain for specimen CF-5 indicates that the column footing connection performed slightly better when compared to specimen CF-3 due to the increase in the embedment length of the steel pipes. When comparing specimen CF-4 to the other two specimens, it was clear that the specimen had an adequate connection between the steel pipe and footing. The embedment length was sufficient to develop the full strength of the steel pipe and footing despite the fact that the pipe was slipping slightly relative to the footing. The pipe surpassed its theoretical flexural strength, and local buckling failure occurred in the pipe at failure as described in Section 4.4.

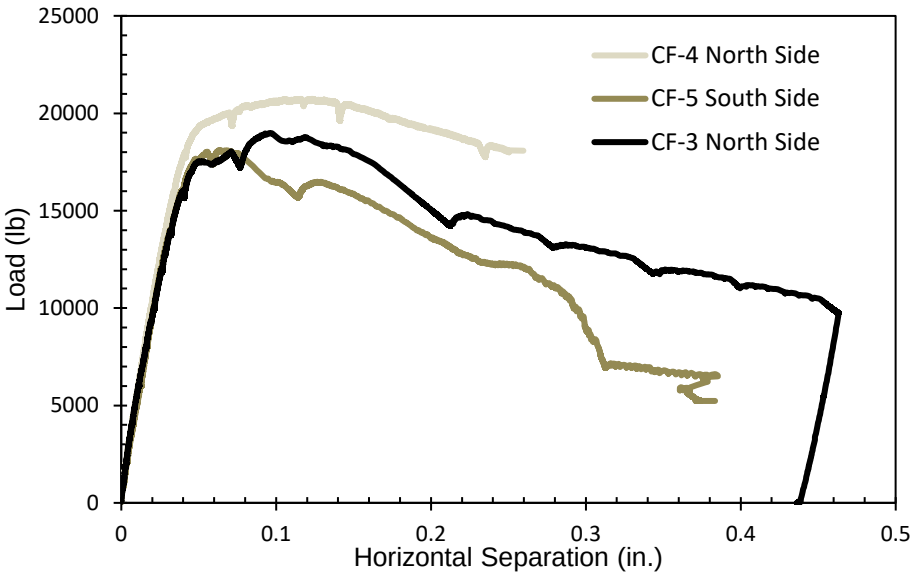

Figure 75. Load vs. horizontal displacement curves for specimens CF-3, CF-4, and CF-5

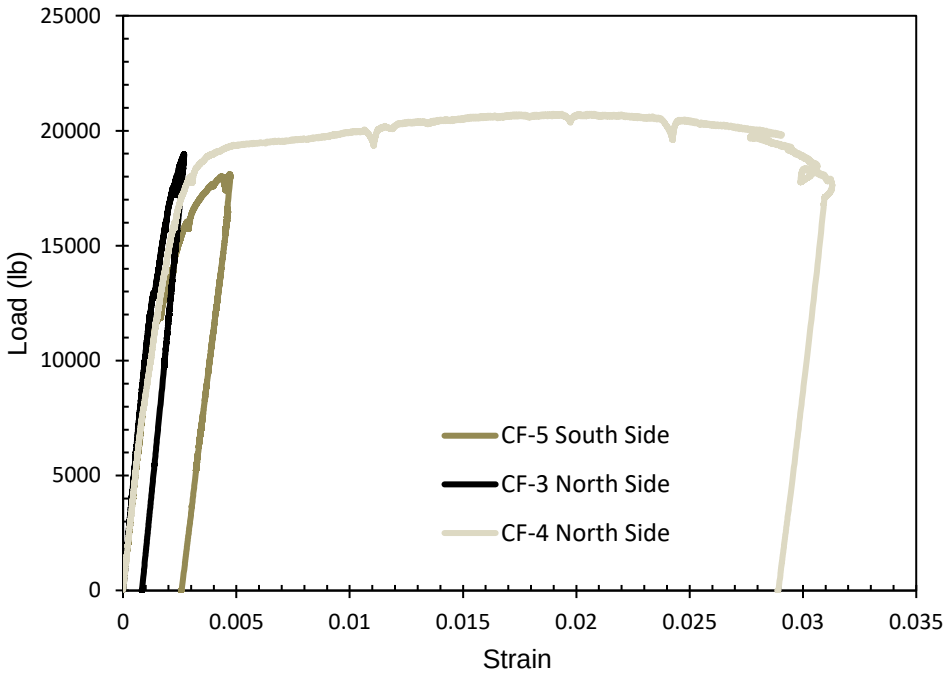

Figure 76. Load vs. strain curves for specimens CF-3, CF-4, and CF-5

5.2 Specimens CF-1 and CF-2

Specimens CF-1 and CF-2 were both cast with high-strength concrete at embedment lengths of $1.6D_i$ and $1.8D_i$, respectively. Both specimens failed due to local buckling of the steel pipes, and minimal damage to the footing was observed. As shown in Figure 77, specimen CF-2 exhibited a higher initial stiffness and failed at a higher maximum load than specimen CF-1, but specimen CF-1 showed a less notable load drop after reaching the maximum load. This can be attributed to the concrete compressive strength of the footing, the failure mechanism of the specimen, and potentially the test setup. Specimen CF-1 had relatively higher concrete compressive strength than specimen CF-2 and exhibited visible local buckling failure on both sides of the specimen. It should be noted that specimen CF-1 was tested using softer rubber bearing pads as supports. Corrections were made to the vertical deflection using the measured pad deflection, but this may have affected

the resulting initial stiffness. On the other hand, local buckling was only visible on one side of specimen CF-2, meaning that the load was better distributed in specimen CF-1.

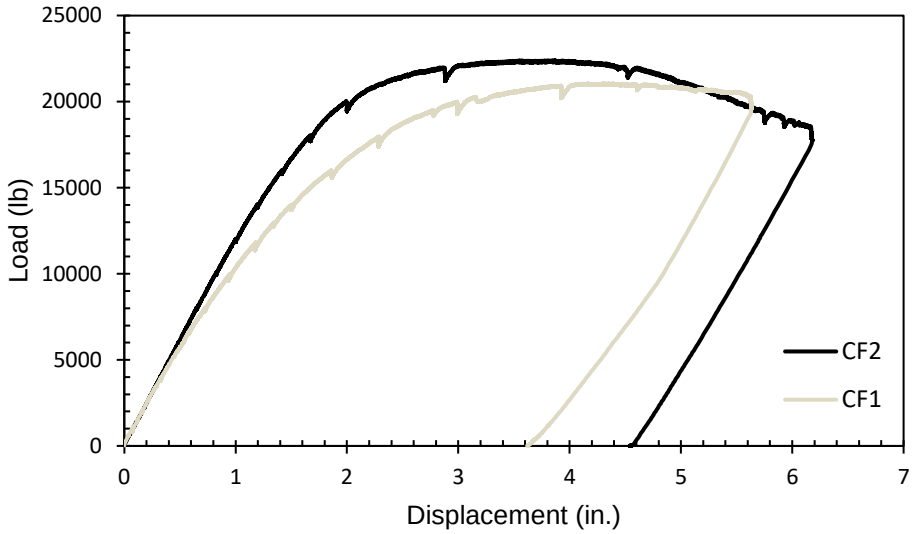

Figure 77. Load vs. displacement curves for specimens CF-3 and CF-2

Although both specimens were tested until reaching a vertical deflection of approximately 6 in., both sides of specimen CF-1 showed significantly less horizontal displacement than the failure side of specimen CF-2, as displayed in Figure 78. This suggests that the column footing connection in specimen CF-1 developed full fixity, where both sides did not have significant slippage of the steel pipe. This also can be indicated by the behavior of the strain on the tension side of the steel pipes. As shown in Figure 79, the decrease in strain after reaching the maximum load was more noticeable on the south side of specimen CF-2 than on the south side of specimen CF-1. This implies that the potential discontinuity in the connection and loss of bond on the south side of specimen CF-2 was more severe despite exhibiting a higher maximum strain in the steel pipe.

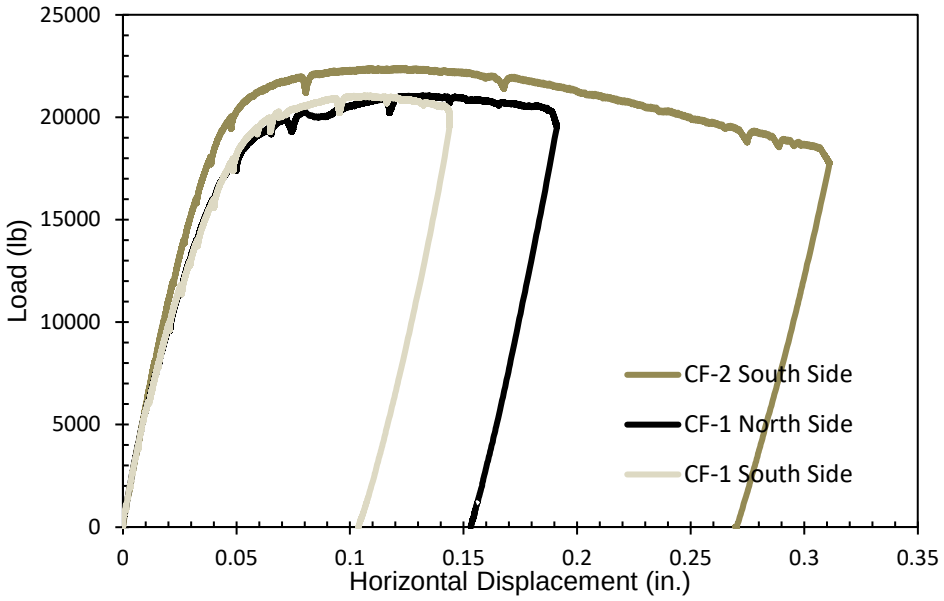

Figure 78. Load vs. horizontal displacement curves for specimens CF-2 and CF-1

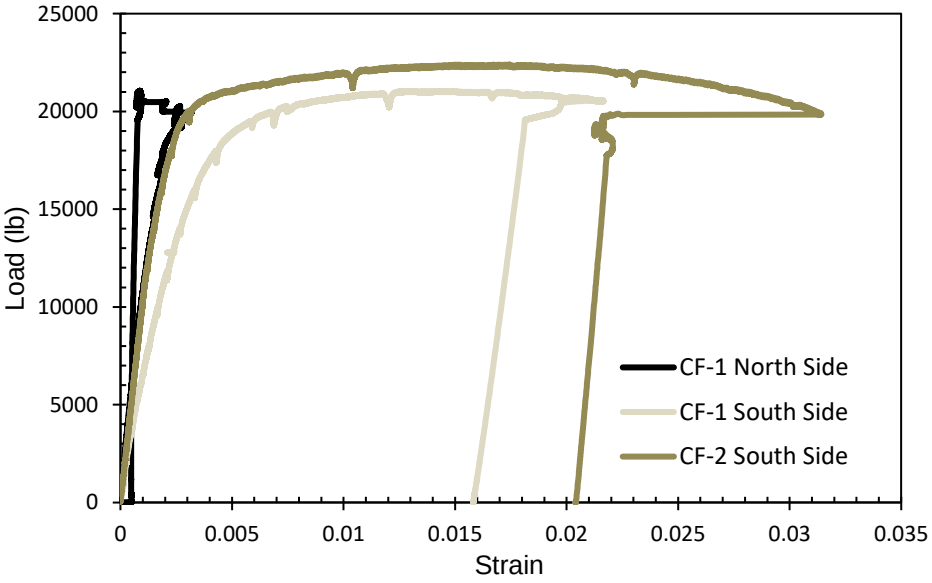

Figure 79. Load vs. strain curves for specimens CF-1 and CF-2

5.3 Specimens CF-3, CF-1, CF-6, CF-7 and CF-8

This comparison shows the behavior of the five specimens with an embedment length of $1.6D_i$, except specimen CF-8, which had an embedment length of $1.4D_i$. As shown in Figure 80, specimens CF-1, CF-7, and CF-8 exhibited load sustaining behavior after reaching the peak load, whereas specimens CF-3 and CF-6 experienced a sudden load decrease after reaching their respective maximum load. The load-sustaining behavior indicates that the column footing connection design was sufficient to achieve the theoretical flexural strength of the steel pipes, and local buckling failure occurred in the pipe at failure. On the other hand, the sudden load decrease for specimens CF-3 and CF-6 implies a discontinuity and a loss of bond between the footing and steel pipe, leading to pullout and concrete breakout failures. The primary difference in behavior between specimen CF-3 and specimen CF-6 was that specimen CF-6 failed at a higher maximum load. Based on visual inspection and maximum horizontal displacement, the order of events in the two failures differed. Specimen CF-6 failed due to footing concrete breaking out before pullout failure occurred, whereas pullout failure occurred first for specimen CF-3. Specimen CF-7 was the only specimen that failed due to the yielding of the steel pipe and failed at a much smaller load which were a function of the smaller diameter of the pipe. No visual local buckling was detected at failure, with minimal damage to the footing.

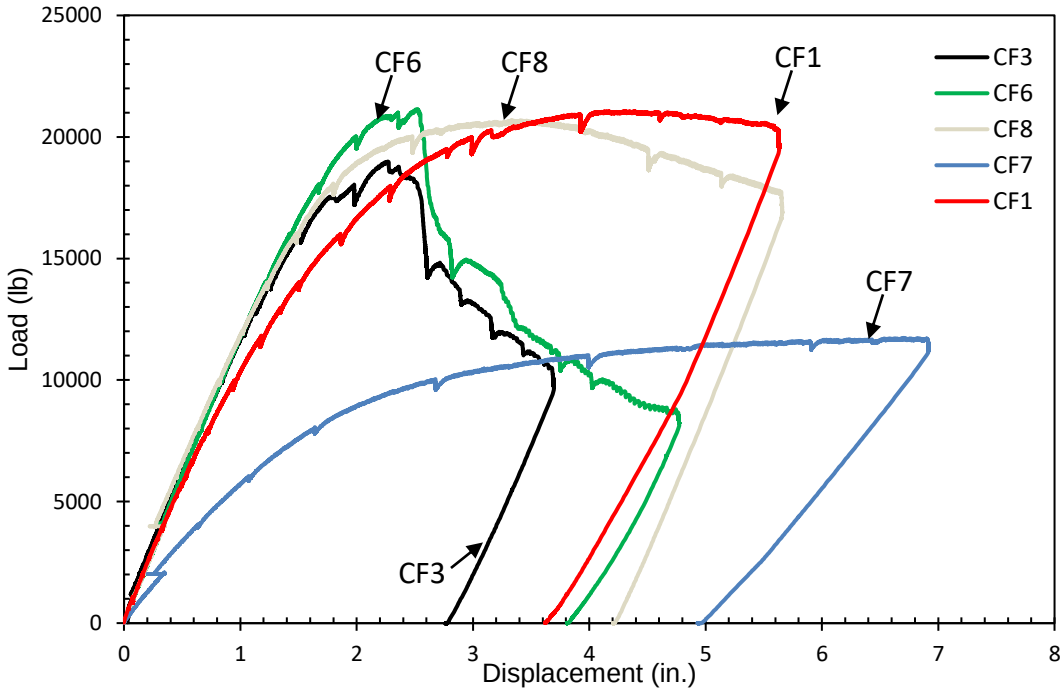

Figure 80. Load vs. displacement curves for specimens CF-1, CF-3, CF-6, CF-7 and CF-8

Figure 81 and Figure 82 present the load vs. horizontal displacement and load vs. strain, respectively, for all the specimens that were embedded at $1.6D_i$ or $1.4D_i$. In terms of horizontal displacement, specimen CF-3 made with normal strength concrete exhibited the most horizontal displacement, which aligns with the theory suggested in the literature review. The literature suggests that a $1.6D_i$ embedment length of the steel pipe is not sufficient to develop the flexural strength of HC-FCS columns. However, the results indicate that a few modifications could be made to the connection design with that embedment length in order to prevent pullout failure. Based on test results, specimen CF-1 (with high-strength concrete) and specimen CF-8 (with a socketed connection using UHPC) developed the steel pipe's flexural strength, and local buckling failure occurred at failure. Specimen CF-6 (with shear lugs welded at the end of the embedded steel pipe) developed the full flexural strength of the steel pipe, but the pipe did not locally buckle and severe damage to the footing occurred. Specimen CF-7 with a smaller diameter to thickness

ratio also developed the full strength of the pipe with limited slip and high strain, but since both the diameter and thickness changed for this specimen, the effect of this parameter is not entirely clear. Therefore, high-strength concrete, smaller diameter to thickness ratio, the use of socketed connection with UHPC, or welding a series of lugs at the end of the steel pipe could potentially improve pullout resistance.

The maximum strain on the tension side of the steel pipe for specimen CF-3 was the lowest of all the specimens, indicating a loss of bond between the footing and steel pipe, which caused a discontinuity in load transfer in the specimen. The strain behavior for specimens CF-1 and CF-8 was similar as it slightly increased after the maximum load but then suddenly decreased. However, the strain in specimen CF-8 was higher than in specimen CF-1, which suggests a better bond between the footing and steel pipe despite its short embedment length. The strain significantly decreased after reaching the peak load for specimen CF-8, whereas specimen CF-1 exhibited less strain decrease. This implies a more notable loss of bond leading to slippage of the steel pipe relative to the footing in specimen CF-8. The strain for specimen CF-6 did not reach the same magnitude as that of specimens CF-1 and CF-8. This can be explained due to the damage that occurred to the footing before the horizontal displacement increased. Then, due to concrete breakout failure, the horizontal displacement got notably larger while the strain stayed relatively constant.

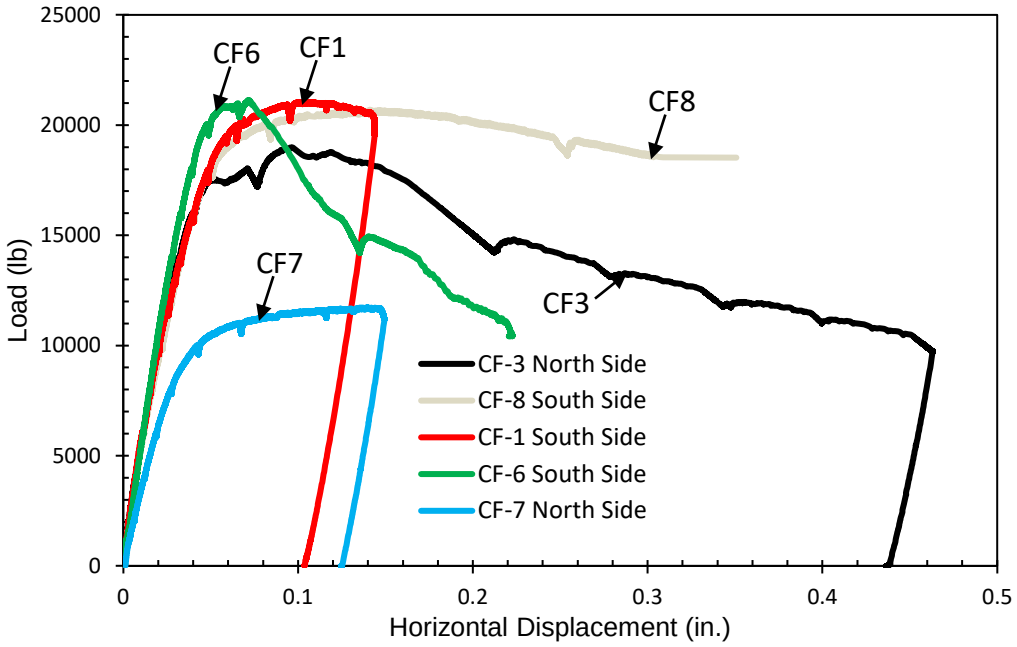

Figure 81. Load vs. horizontal displacement curves for specimens CF-1, CF-3, CF-6, CF-7 and CF-8

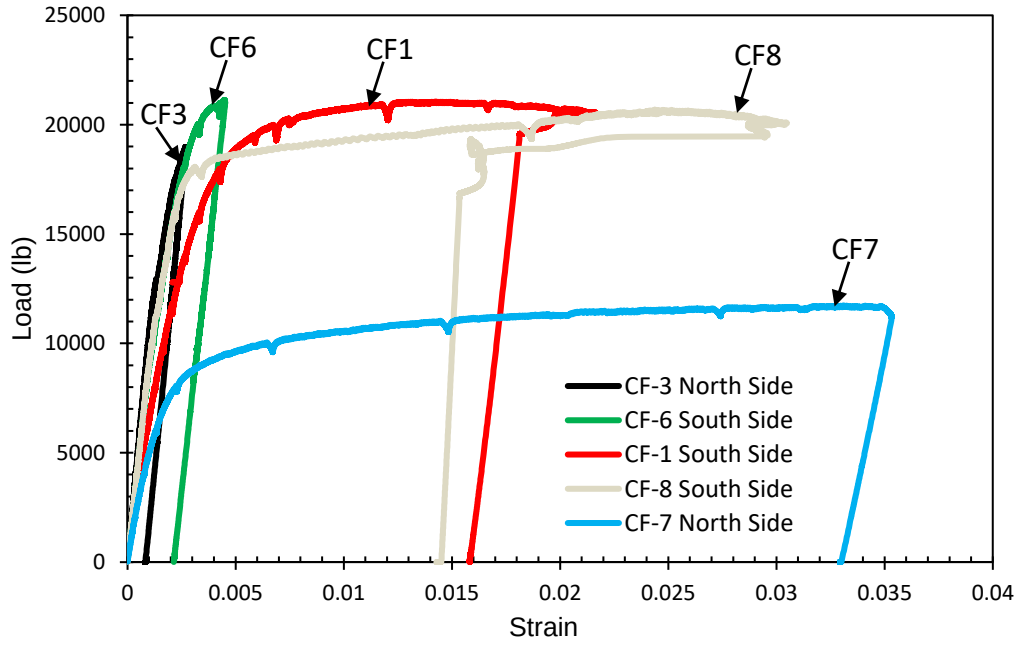

Figure 82. Load vs. strain curves for specimens CF-1, CF-3, CF-6, CF-7 and CF-8

5.4 Specimens CF-2, CF-4, and CF-9

This comparison presents the behavior of specimens CF-4, CF-2, and CF-9 cast with normal-strength concrete, high-strength concrete, and socketed connection using UHPC, respectively, at an embedment length of $1.8D_i$. As shown in Figure 83, all specimens showed a load-sustaining behavior after reaching the maximum load and failed due to local buckling in the steel pipe. Specimen CF-2 reached the highest peak load, but all three specimens exhibited a decrease in load and then sustained approximately 17.5 kips. No visible damage was observed to the footing for specimen CF-9, while specimens CF-2 and CF-4 exhibited minimal damage as cracks were detected in the footing.

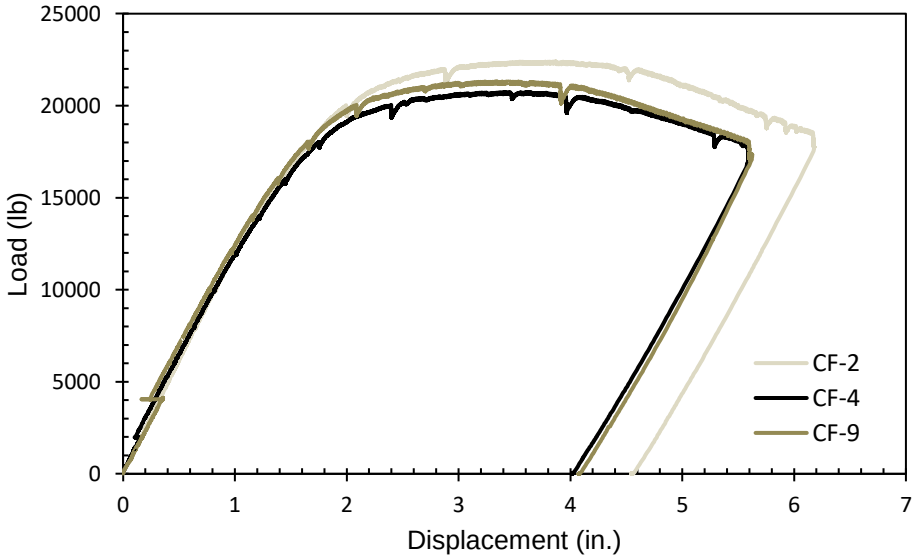

Figure 83. Load vs. displacement curves for specimens CF-2, CF-4, and CF-9

In terms of horizontal displacement, the behavior of the three specimens was similar, where they experienced a linear increase in horizontal displacement up to 14 kips followed by a nonlinear increase, as shown in Figure 84. The magnitude of the horizontal displacement was the highest in specimen CF-2 compared to the other two specimens potentially due to the higher maximum load. In terms of the strain, specimens CF-4 and CF-2 exhibited similar maximum strain, but the

decrease in strain after reaching the peak load was more significant for specimen CF-2. This indicates a more noticeable loss of bond leading to slippage of the steel pipe relative to the footing. The strain behavior of specimen CF-9 did not follow the trend of the other two specimens, as shown in Figure 85. This could potentially be due to damage of the strain gauge placed on the south side of the specimen. Although there may have been a loss of bond in the three specimens, the steel pipes on the failure sides exhibited yielding of the steel and local buckling at failure. This indicates that the embedment length of $1.8D_i$ for the steel pipes was sufficient to develop the full flexural strength of the steel pipe for each of the three concrete types.

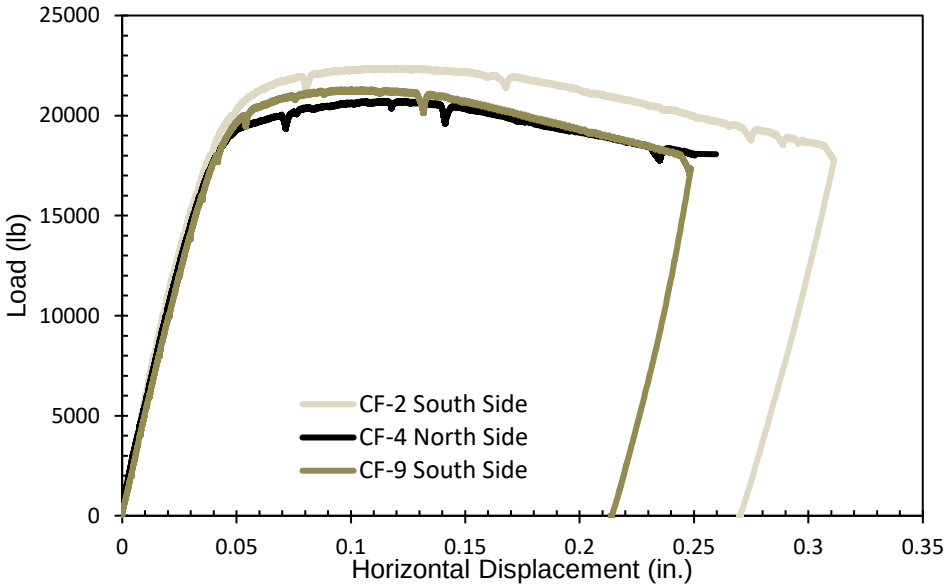

Figure 84. Load vs. horizontal displacement curves for specimens CF-2, CF-4, and CF-9

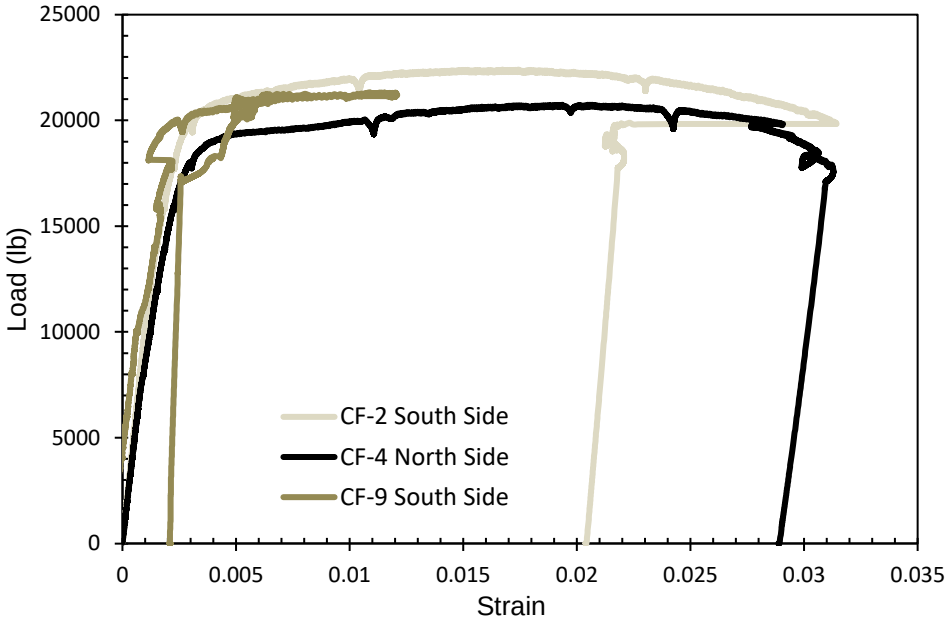

Figure 85. Load vs. strain curves for specimens CF-2, CF-4, and CF-9

6. Conclusion/Recommendations

6.1 Conclusion

Full development of the column footing connection for the HC-FCS column design was achieved after making a few modifications to the connection design. Parameters such as embedment length, diameter-to-thickness ratio, a series of lugs welded to the ends of the steel pipes, the use of socketed connection with UHPC, and compressive strength of the concrete footing can potentially change the behavior of the connection. Based on the results, the short embedment lengths ($1.6D_i$ and $1.68D_i$) were not sufficient to develop the steel pipe flexural strength with a normal-strength concrete footing. However, the use of socketed connection with UHPC, a high-strength concrete footing, and welding a series of lugs prevented the steel pipe from pulling out to some extent, and local buckling occurred in the steel pipe at moment greater than the calculated capacity of the steel pipe. The socketed connection with UHPC had the shortest embedment length ($1.4D_i$) but outperformed the other specimens with $1.6D_i$ and $1.68D_i$ embedment lengths.

The $1.8D_i$ embedment length prevented the steel pipe from pulling out whether using the socketed connection with UHPC, high-strength concrete, or normal-strength concrete. The specimens exceeded the flexural strength of the steel pipe, and local buckling failure occurred at failure. This supports the conclusion that the column footing connection with a $1.8D_i$ embedment length is sufficient on its own to develop full capacity of the steel pipe.

Using a smaller diameter-to-thickness ratio changed the nature of the failure of the connection. However, further investigation of this parameter is needed to evaluate its effect on the connection between the column and footing.

6.2 Recommendations

Based on the column-footing connection testing for HC-FCS columns, the following recommendations and future research work are suggested:

i) Measure the vertical deflection from the interface of the footing and steel pipe on each side of the specimen. This would give a more accurate deflection measurement for each side of the footing.

ii) Construct additional socketed connection specimens with high-strength grout to compare with UHPC socketed connection specimens.

iii) Since using a smaller diameter-to-thickness ratio changed the nature of the failure of the connection, further investigation of this parameter is needed to evaluate its effect on the connection between the column and footing. In this research, both the diameter and thickness of the steel pipe were different than the control specimen (CF-3). It would be better to have a different thickness of the same pipe diameter to get a better comparison between specimens and have a better understanding of the effect of the parameter on the performance of the connection.

iv) Evaluate the connection of half-scale HC-FCS column-footing specimens instead of having the column portion of the specimen in the form of only a steel tube. This could potentially help investigate the effect of the concrete shell and FRP tube on the connection between the column and footing. This could also help examine the confinement of concrete and FRP on steel tube and its effect on the connection.

v) Further investigation of the socketed connection design is desired since the steel pipe in both socketed connection specimens (CF-8 and CF-9) surpassed its theoretical flexural strength, and local buckling failure occurred in the pipe at failure. Studying the

effect of the space between the embedded steel pipe and the footing could help optimize the socketed connection design.

vi) Testing the specimens vertically with axial and lateral cyclic loading could achieve more realistic results. Thus, evaluating the suggested embedment lengths for half-scale HC-FCS column-footing specimens with that loading condition would help further understand the behavior of the connection and effect of axial load on the connection.

7. References

AASHTO LRFD Bridge Design Specifications, 8th Edition, 2017.

Albitar, M., Ozbakkaloglu, T., and Fanggi, L., Behavior of FRP-HSC and FRP-HSC-Steel Double-Skin Tubular Columns under Cyclic Axial Compression. Journal of Composites for Construction, 2015.

Alkaysi, M., and El-Tawil, S., Factors affecting bond development between Ultra High Performance Concrete (UHPC) and steel bar reinforcement, Construction and Building Materials, ScienceDirect, DOI.org/10.1016/j.conbuildmat.2017.03.091, Vol. 144, P. 412-422, 2017.

Al-Madani, M., Al-Osta, M., Ahmad, S., Khalid, H., and Al-Huri, M., Interfacial bond behavior between ultra high performance concrete and normal concrete substrates, Science Direct, Construction and Building Materials, DOI.org/10.1016/j.conbuildmat.2021.126229, 2022.

Building Code Requirements for Structural Concrete (ACI 318-19): An ACI Standard ; Commentary on Building Code Requirements for Structural Concrete, 2019.

Cheng, Z., and Sritharan, S., Side Shear Strength of Preformed Socket Connections Suitable for Vertical Precast Members, The American Society of Civil Engineers, Journal of Bridge Engineering, DOI:10.1061/(ASCE)BE.1943-5592.000139, Vol. 24, Issue 5, 2019.

ElGawady, M., Gheni, A., Anumolu, S., and Abdulazeez, M., Seismic Performance of Innovative Hollow-Core FRP–Concrete–Steel Bridge Columns. Journal of Bridge Engineering, 2015: p. 04016120.16.

ElGawady, M., and Abdulazeez, M., Column-Footing Connection Evaluation of Hollow-Core Composite Bridge Columns. Missouri University of Science and Technology, 2018.

Feng, S., Xiao, H., Liu, R., and Liu, M., The bond properties between ultra-high-performance concrete and normal strength concrete substrate: Bond macro-performance and overlay transition zone microstructure, Science Direct, Cement and Concrete Composites, DOI.org/10.1016/j.cemconcomp.2022.104436, Vol. 128, 104436, 2022.

FHWA, "UHPC: A Robust Solution for Highway Infrastructure," U.S. Department of Transportation Federal Highway Administration, Available at https://highways.dot.gov/research/structures/ultra-high-performance-concrete/ultra-high-performanceconcrete#:~:text=Ultra%2Dhigh%20performance%20concretes%20have,connection%20of%20multiple%20prefabricated%20elements [Cited December 2023]

FHWA, "Ultra-High Performance Concrete," U.S. Department of Transportation Federal Highway Administration, Available at https://highways.dot.gov/research/structures/ultra-highperformance-concrete/ultra-high-performance-concrete [Cited March 2022]

Fu, T., Hou, J., Zhu, Z., Meng, L., Sun, Z., Wang, K., and Ren, X., Experimental Study on UHPC-Based Grouting Materials and Mechanical Performance of Grouted Splice Sleeve Joints, Frontiers, Structural Materials, DOI:10.3389/fmats.2022.912509, Vol. 9, 2022.

Graybeal, B., "Design and Construction of Field-Cast UHPC Connections," FHWA-HRT-14- 084, Federal Highway Administration, McLean, VA, 2014.

Graybeal, B., "Tech Note | Ultra-High Performance Concrete," FHWA-HRT-11- 038, Federal Highway Administration, McLean, VA, 2011

Han, L., Tao, Z., Liao, F., and Xu, Y., Tests on cyclic performance of FRP–concrete–steel double-skin tubular columns. Fuzhou University, 2010.

Haraldsson, O., Janes, T., Eberhanrd, M., and Stanton, J., Seismic Resistance of Socket Connection between Footing and Precast Column, The American Society of Civil Engineers, DOI:10.1061/(ASCE)BE.1943-5592.0000413, 2013.

He, Z., et al., Review on Seismic Behavior of Precast Bridge Column with Socket Connections, Journal of Physics: Conference Series, 1838 012043, 2021.

Idris, Y., and Ozbakkaloglu, T., Seismic Behavior of FRP-High-Strength Concrete–Steel Double-Skin Tubular Columns. American Society of Civil Engineers, 2014.

Khaleghi, B., et. al, Accelerated Bridge Construction in Washington State: From Research to Practice, PCI Journal, Fall 2012.

Milner, J., C., Performance of multi-hazard-resistant hollow-core FRP-concrete-steel columns with high-strength SCC or UHPC, MS Thesis, The University of Oklahoma Norman, Ok, 2023.

Moon, J., Lehman, D., Roeder, C., and Lee, H., Evaluation of embedded concrete-filled tube (CFT) column-to-foundation connections. University of Washington, Seattle, 2013.

Munoz, M., Harris, D., Ahlborn, T., and Froster, D., Bond Performance between Ultrahigh-Performance Concrete and Normal-Strength Concrete, American Society of Civil Engineers, DOI.org/10.1061/(ASCE)MT.1943-5533.0000890, 2013.

Looney, T., McDaniel, A., Volz, J., and Floyd, R., Development and Characterization of Ultra-High Performance Concrete with Slag Cement for Use as Bridge Joint Material, British Journal of Civil and Architecture Engineering, Vol. 1, No. 2, pp. 1-14, 2019.

Pantelides, C., and Neupane, S., Analysis of ABC Bridge Column-to-Footing Joints with Recessed Splice Sleeve Connectors, Mountain-Plains Consortium, Report No. MPC-638, 2022.

Roeder, C., and Lehman, D., An economical and efficient foundation connection for concrete filled steel tube piers and columns. International conference on composite construction in steel and concrete, 2008.

Soliman, A., Heard, W., Williams, B., and Ranade, R., Effects of the tensile properties of UHPC on the bond behavior, Construction and Building Materials, ScienceDirect, DOI.org/10.1016/j.conbuildmat.2023.131990, 2023.

Stephens, M., Lehman, D., Roeder, C., Concrete-Filled Tube Bridge Pier Connections for Accelerated Bridge Construction, Department of Civil and Environmental Engineering, University of Washington, Report No. CA15-2417, 2015.

Teng, J.G., Yu, T., Wong, Y.L., Dong, S.L., Hybrid FRP–concrete–steel tubular columns: Concept and behavior. Construction and Building Materials, 2007.

Valikhani, A., Jahromi, A., Mantawy, I., and Azizinamini, A., Experimental evaluation of concrete-to-UHPC bond strength with correlation to surface roughness for repair application, Construction and Building Materials, ScienceDirect, DOI.org/10.1016/j.conbuildmat.2019.117753, 2019.

Varbel, J., Flores, E., Toledo, W., Newtson, C., and Weldon, B., Structural Testing of Ultra-High Performance Concrete Shear Keys in Concrete Bridge Superstructures, The American Society of Civil Engineers, Tran-SET, 2020.

White, S., and Palermo, A., Quasi-Static Testing of Posttensioned Nonemulative Column-Footing Connections for Bridge Piers, The American Society of Civil Engineers, DOI:10.1061/(ASCE)BE.1943-5592.0000872, Vol. 21, Issue, 6, 2016.

Williams, T., Experimental investigation of high strength concrete filled steel tubes in embedded column base foundation connections. a thesis submitted in partial fulfillment of the degree of Master of Science in Civil Engineering, University of Washington, Seattle, WA.2006.

Yuan, J., and Graybeal, B., Bond Behavior of Reinforcing Steel in Ultra-High Performance Concrete, Federal Highway Administration, FHWA-HRT-14-090, McLean, VA, 2014.

Zhang, B., Yu, T., and Teng, J., Behavior of hybrid double-skin tubular columns subjected to combined axial compression and cyclic lateral loading. University of Wollongong, 2012.

Zhang, G., Su, S., Han, Q., Xu, K., Li, Z., and Du, X., Experimental and numerical Investigation of Seismic Performance of Prefabricated Double-Column Piers Used in Accelerated Bridge Construction, Engineering Structures, DOI:10.1016/j.engstruct.2023.116688, 2023.

Zhang, G., Su, S., Han, Q., Xu, K., Li, Z., Du, X., and He, W., Experimental Investigation of Seismic Behavior of UHPC-filled Socket Precast Bridge Column-Foundation Connection with Shear Keys, Engineering Structures, DOI:10.1016/j.engstruct.2020.111527, 2020.